3-20-2017

Electrochemical Methods to Characterize Drilled Shaft Deficiencies

Sarah Jo Mobley
University of South Florida, sarahmobley@mail.usf.edu

Electrochemical Methods to Characterize Drilled Shaft Deficiencies

by

Sarah J. Mobley

A thesis submitted in partial fulfillment
of the requirements for the degree of
Master of Science in Civil Engineering
Department of Civil and Environmental Engineering
College of Engineering
University of South Florida

Major Professor: A. Gray Mullins, Ph.D.
Alberto A. Sagüés, Ph.D.
Michael J. Stokes, Ph.D.

Date of Approval:
March 10, 2017

Keywords: Corrosion, Mineral Slurry, Polymer Slurry,
Viscosity, Concrete

DEDICATION

To Matthew, my whole entire heart.

ACKNOWLEDGEMENTS

I am forever grateful to Dr. Gray Mullins and Dr. Alberto Sagüés, for without your patience, guidance and support this would not be possible. I am in your debt. Thank you for the experience and knowledge that I have gained throughout this process. Dr. Michael Stokes, for your eager willingness to help and your infectious love of learning.

Additional credit goes to the amazing structures research group, with special thanks to Kelly Costello. Most importantly, the Florida Department of Transportation for funding this research.

TABLE OF CONTENTS

LIST OF TABLES

LIST OF FIGURES

ABSTRACT

In recent years drilled shafts have become the preferred foundation method for marine bridges. Typically, the drilled shaft is selected over traditional driven piles due to soil strata encountered, construction economy, increased lateral stiffness requirements, and/or vibration control considerations. The most critical component in drilled shaft construction is borehole stabilization. Wall sloughing or groundwater inclusion can have devastating effects on the strength of the finished shaft however recent research has shown that the materials, more specifically the slurry, used to accomplish stabilization may be having a negative impact on the durability of the finished product. This thesis investigates the durability of drilled shaft specimens as it relates to the slurry type and viscosity.

Electrochemical corrosion potential test results from 23 lab cast specimens showed that the shafts cast using bentonite slurry were 54% more likely to exhibit corrosion potential crossing the ASTM threshold of -350mV. The laboratory setting allowed for visual inspection of each shaft. This inspection showed reflective quilting on all bentonite cast shafts, this quilting was visible to a lesser degree on select polymer cast shafts and not present on shafts cast in water. This creasing appears to be directly related to the slurry used and the resulting decrease in durability.

While current construction practice favors the use of bentonite slurry, the study indicates that both polymer slurry and the casing method are more advantageous from a durability standpoint.

CHAPTER 1: INTRODUCTION

1.1 Overview

Drilled shafts are cylindrical, cast-in-place, concrete, deep foundation elements that commonly range from 2 to 10 feet in diameter and can reach 300 feet in depth. Typically, the drilled shaft is selected over traditional driven piles due to soil strata encountered, construction economy, increased lateral stiffness requirements, and/or vibration control considerations. The process of constructing drilled shafts consists of three basic steps: (1) creation of a deep cylindrical void through the drilled excavation of rock and soil reaching to a depth of competent bearing capacity, (2) installation of necessary reinforcing steel, and (3) placement of concrete into the excavation (Figure 1.1). The primary concern during this process is maintaining the stability of the excavation walls. The walls act as the formwork for the drilled shaft in the absence of steel casing thereby allowing the in situ soil structure to determine the final shape of the shaft.

The stability of an excavation is customarily maintained through a combination of mechanical and hydrostatic methods. Mechanical stabilization relies on the use of a steel casing to support the walls of the excavation throughout the construction process. This casing may be partial or extend to the full excavation depth, either way it is removed all or in part after concrete placement but before the concrete cures. As the casing is extracted, the wet concrete flows out to push against the excavation walls.

Hydrostatic stabilization is the process of filling an excavation with a fluid to a level above the surrounding water table. This fluid provides constant pressure that forces flow of out of the

excavation into the soil preventing wall collapse. The types of fluids permitted for this application vary from state to state but general practice prescribes the use of a slurry formed from mineral or polymer additives. Most prevalently, the slurry will consist of bentonite clay combined with water.

Slurry is continuously added to the excavation throughout the construction process to maintain hydrostatic pressure, and is then displaced during concreting operations. When concrete is placed via tremie, a thin interface forms between the rising concrete level and the displaced slurry commonly referred to as laitance. However, the concrete also flows radially out of the reinforcing cage which presses through the cage openings between the reinforcement and a separation occurs whereby two separately contaminated faces. As these faces, recombine the laitance presses together creating a grid of channels in the concrete between the reinforcement and the surrounding environment. (Figure 1.2). These channels prevent the concrete from being contiguous and compromise the integrity of the concrete cover.

In the case of laboratory specimens cast in a bentonite environment, the side of the shaft surface exhibited reflective creases (quilting) that coincided with the reinforcing steel (Figure 1.3). In field applications, channels may be visible on the surface of the shaft but visual inspection is rarely conducted due to the fact that these structures are both underground and below the water table. Quality control during construction is often completely reliant on calculations that compare the volume of concrete poured to the theoretical volume required.

Chloride-induced corrosion will occur in reinforcing steel if it is exposed to oxygen, moisture and chlorides. The absence of any one of those elements will stall the chemical reactions until such time that they all exist again. Current design consensus assumes that concrete cover provides the necessary protection to isolate the reinforcing steel and inhibit chloride and oxygen exposure. In an idealized concrete shaft, the time required for chloride ions to penetrate the

concrete and reach the reinforcing steel can be calculated using a simple set of variables including the apparent diffusion coefficient of the concrete and the thickness of the concrete cover. Anomalies in concrete flow and the introduction of laitance channels can create direct pathways for the transmission of environmental chlorides into the network of reinforcing steel, negating the protective qualities of the concrete cover.

1.2 Objective Statement

The objective of this study is to employ electrochemical methods to determine the existence of deficiencies in the concrete cover of 23 lab-cast, drilled shaft specimens and classify whether those deficiencies have an effect on structural service life. The results will be sorted by construction type in order to identify any correlations between method of construction, concrete cover deficiencies and structural service life.

1.3 Organization of Thesis

The organization of this thesis is broken down into the five following chapters.

Chapter 2 defines the use of shafts and rationale for choosing drilled shafts over driven piles, the construction process, quality control procedures, concrete flow issues and slurry products. Additionally, this chapter covers fundamental corrosion theory and life span analysis, highlighting the application of corrosion potential mapping as a diagnostic tool for detecting concrete deficiencies.

Chapter 3 details the testing processes used to characterize each shaft specimen. The full testing prescription and all initial data is stated along with the identified variables and equipment used. Additional discussion on the electro-connectivity of the reinforcing steel is also included.

Chapter 4 discusses the outcome of the initial electro-connectivity screening along with the full results of the testing prescription outlined in chapter 3. Pre-testing evaluation of the test

specimens is also discussed as it pertains to the integrity of the shaft constructed using the wet/ slurry method.

Chapter 5 provides a narrative and summary of the results as well as recommendations for limitations on slurry materials and future testing that may further the overall understanding of the phenomena observed.

Chapter 6 consists of a succinct list of research conclusions and reiterates specific future testing recommendations.

Figure 1.1 Drilled shaft construction. excavation (left) reinforcement placement (middle), concreting (right)

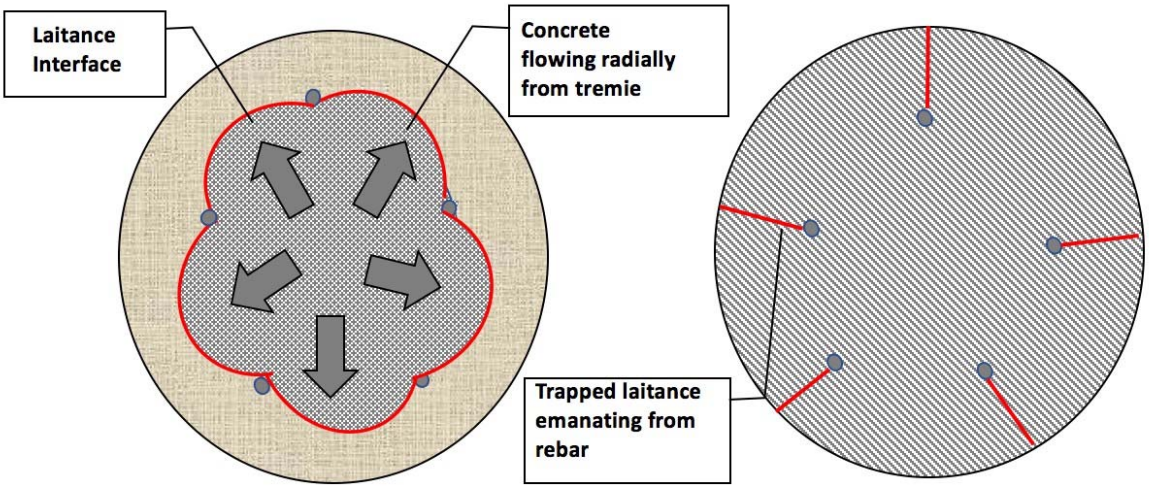

Figure 1.2 Laitance formation

Figure 1.3 Quilting in a drilled shaft experimental specimen

CHAPTER 2: LITERATURE REVIEW

This chapter provides a brief history of drilled shafts, and the role that corrosion testing plays in diagnosing possible concrete anomalies developed during drilled shaft construction.

2.1 Drilled Shafts

Deep foundation systems are principally used to transfer structural loads and moments through weak overlying soil strata to stronger, load bearing soil or rock at depth. The loads are most often the result of large buildings with increased wind load considerations or bridges that span considerable distances which necessitate foundations capable of resisting substantial dynamic and static loading. The two main types of deep foundations are driven piles and drilled shafts. Driven piles are steel, timber or pre-cast concrete elements that are driven to an appropriate depth based on calculated bearing resistance. The pile lengths are predetermined based on shipping limitations, installation method constraints or capacity requirements. Drilled shafts are defined by the The Federal Highway Administration (FHWA) as a "*cast-in-place deep foundation element constructed in a drilled hole that is stabilized to allow controlled placement of reinforcement and concrete*" (Brown, 2010). Drilled shaft technology was pioneered in major American cities in the early 1900s as a means to construct the deep foundations required to accommodate advancements in building and infrastructure design (Brown, 2010).

Prior to the inception of drilled shafts, caisson foundation systems were primarily used. Caissons are concrete foundation elements from the early 1800s. They were either precast and sunk in place to obtain necessary bearing capacity or cast in place in a hand dug excavation that

was shored up with timbers and braces to provide lateral support as the hole became progressively deeper. The first motorized, truck mounted boring machines began to appear in the early 1930s in Texas. These machines were originally developed for digging shallow holes but were later used for drilled shaft excavation. The basic technique for drilled shaft construction has remained the same since initial mechanization, but technological advancements over the decades have allowed the process to become more efficient and cost effective, making it a favorable option for various construction applications.

Drilled shafts have been proven as a cost effective alternative to driven piles due to the increased performance and minimal footprint. When a drilled shaft is installed to bear on or within rock, immense axial resistance values can be obtained in a small footprint. This allows for fewer foundation elements and the reduction in size or total elimination of the pile cap as well as the associated excavation.

The absence of a pile driving hammer makes drilled shaft construction a comparatively low noise, low vibration application. This allows for installation in urban areas and near existing structures where noise and vibration may be restricted.

The many advantages of drilled shafts can be easily negated by improper construction practices.

2.2 Methods of Construction

The principle of drilled shaft construction is simple: drill a hole into the ground and fill that hole with concrete. Varying site conditions and design consideration add complexities to construction in practice. As such, drilled shaft construction is broken into three subcategories: dry method, casing method, and wet or slurry method. Design may necessitate the use of more than

one construction method in the same site, and in some instances more than one method in the same borehole.

This thesis focuses on the wet or slurry construction method that presupposes work will occur below the ground water table. There are four basic steps to the wet method of drilled shaft construction: (1) excavation, (2) stabilization, (3) placement of reinforcement, and (4) concreting. This process demands the use of drilling equipment capable of drilling to the design depth and diameter. Soil is extracted using a rotary auger tool. As the tool advances to depth, it must be periodically removed from the hole to clear the soil spoils for later removal. Once the tip elevation is reached, a clean out bucket can be used to remove any remaining debris from the bottom of the excavation.

Throughout the excavation process is it of tantamount importance that the walls remain stable. Any caving or sloughing of soil into the excavation can compromise the structural properties of the finished shaft. This stabilization can be achieved by two means: mechanical and/or hydrostatic. Mechanical stabilization is achieved by inserting a steel casing into the excavation and then drilled inside of that casing. The casing can remain in place or be removed after concrete placement. The wet method is premised on the introduction of a fluid into the hole to maintain hydrostatic pressure on the excavation walls and prohibit the introduction of ground water (Figure 2-1). This reduces the likelihood of caving substantially. In many cases, a combination of the mechanical and wet method is used to ensure stability. The FHWA goes so far as to recommend that a temporary surface casing be used for all construction methods as soils near the surface are more likely to cave regardless of type.

The fluid used in the wet method is commonly referred to as slurry, meaning a water-based fluid which is often a mixture of water and some substance to reduce flow into the surrounding

soil. Slurries come in three categories: mineral, polymer or natural. Mineral slurries combine water with a dry clay powder, most commonly bentonite, attapulgite or sepiolite. Polymer slurries refer to a combination of some proprietary form of polyacrylamide and water. Natural slurries are formed through the combination of water with the existing soil. When a full length casing is in place, it is possible to use plain water in place of slurry to maintain the integrity of the base of the excavation.

Slurries are described using the material type, viscosity and density. Viscosity is a measurement of a fluids ability to resist flow under shear stress. This can be measured by a viscometer in the lab, but a Marsh funnel is used for field verification. The Marsh funnel determines the time required to empty one quart of slurry (passing a No. 12 sieve) through a standard orifice. The longer the time to empty the funnel, the higher the viscosity of the material. The slurries examined in this study range from 40-120 seconds.

Once the excavation is complete, the hole is clean and inspected. If the foundation element is required to resist tensile stresses, then a steel reinforcement cage will have to be installed in the hole prior to concreting. The slurry should be clean prior to the installation of the rebar cage. Additionally, the rebar must be clean and not come in contact with the soil during installation, with special care being taken to ensure that the rebar does not touch the base of the excavation. Direct contact between the steel and the underlying soil could lead to corrosion and undermine the effectiveness of the foundation element.

The time between the installation of rebar and pouring concrete should be kept to a minimum. Concrete is placed from the bottom of the shaft up to the top in a single pour using a tremie system. The initiation of concreting is the most critical step in the process as the first load must be separated from the slurry fluid. Once concrete flow is initiated, the outflow of the tremie

pipe remains embedded within the rising concrete level that has already been poured. This embedment depth must be sufficient to maintain a continuity but not so much as to resist the flow. Excessive embedment can lead to levels of resistance that lift the rebar cage. When the depth of embedment reflects the hydrostatic balance point, concrete should flow freely from the tremie without need of surging (rapid raising and lowering of the tremie) (DFI, 2016). As the concrete level rises the slurry is expelled (Figure 2-2). Once concreting operations are complete, all temporary casing is removed and the concrete flows out to fill the entirety of the excavation.

2.3 Natural Slurry

Natural slurry consists of naturally occurring groundwater or fresh or salt water placed in the vacant shaft. Water can serve as a drilling slurry when the excavation is permeable but stable and the sidewalls are not eroded. The unit weight of the groundwater and the natural slurry are often identical. Therefore, when using a natural slurry, importance lies in the maintenance of the head differential above the piezometric surface to guarantee the absence of inflow.

2.4 Mineral Slurry

Mineral slurry is the combination of water and a dry clay powder (sodium or calcium montmorillonite). The most commonly used clay is known as bentonite, though attapulgite, sepiolite and other naturally occurring clay minerals are also used. Bentonite is the common name for packaged, processed, clay powder made primarily of sodium montmorillonite. Bentonite slurry works three-fold to maintain the boring. While the slurry is providing lateral stabilization for the excavation, loose sands and fine cuttings become suspended in the liquid and are discharged with the slurry during the concreting process.

When bentonite slurry is introduced into an excavation, the suspended clay particles permeate the walls of the excavation and form a filter cake that aids in wall stabilization by

reducing outflow into the soil. This process begins immediately and works in conjunction with the hydrostatic pressure to prevent ground water intrusion. Though generally beneficial, the filter cake can have negative effects on the side shear of the shaft if the bentonite sits in the excavation for more than eight hours prior to concrete placement (Brown, 2010).

2.5 Polymer Slurry

Polymer slurry is the combination of water and a proprietary blend of polyacrylamides. These slurries are comprised of long, hair-like, chain molecules that are negatively charged promoting molecular repulsion (Reese and O'Neill, 1999). Like bentonite slurry, polymer requires a head differential sufficient to overcome the force of the groundwater inflow. The molecular structure of polymer slurries prohibits the formation of a filter cake, so it continuously permeates the excavation walls but at a lower rate due to the increase in viscosity. Polymer slurries are lower in density than mineral slurries, so a higher differential fluid level relative to the ground water is needed to provide the same outward lateral force on the excavation walls.

2.6 Concrete Quality

In order for concrete to be effective in a slurry supported drilled shaft application, it must possess certain basic characteristics: high workability, self-weight compaction, resistance to segregation and leaching and controlled setting time. Workability is of key importance because it is essential that the concrete be able to flow through the tremie, to flow out laterally through the reinforcement cage, and to impose lateral stress against the sides of the borehole. This is best accomplished with a highly fluid mix design. Self-weight compaction eliminates the need for mechanical vibration, which is impractical and could lead to undesirable mixing between the drilling slurry and the concrete. Additionally, drilled shaft concrete should maintain its fluid state throughout the depth of the excavation for the full time required to complete placement, while also

attaining an acceptable strength within a reasonable time after placement (Reese and O'Neill, 1999). The Florida Department of Transportation requires the concrete slump be between 7 and 9 in at the beginning of pour and must retain at least a 5in slump at all times throughout the pour (FDOT, 2016).

2.7 Anomaly Formation

An anomaly is a deviation from the perfect quality of the cast in-situ drilled shaft element. Anomalies can be, but are not necessarily defects. The marks left in the concrete surface during casing extraction is technically an anomaly, but should not be considered defects unless they compromise the structural integrity of the shaft. Most defects fall into three categories: inclusions, channeling, and quilting (DFI, 2016).

2.7.1 Inclusions

The term inclusion refers to any foreign material trapped within the concrete shaft outside of the design (Figure 2.3). It can be in-situ material, segregated concrete, or uncemented materials mixed with slurry. These can be detected during the construction process through indirect, non-destructive inspection methods such as cross-hole sonic logging or thermal integrity profiling (Johnson, 2016).

2.7.2 Channeling

Channeling refers to systems of vertical narrow lanes with loose aggregates or lightly cemented material or excess water. They are customarily in a longitudinal network near the surface of the pile (Figure 2.4). Channels are only considered defects if they are of significant depth and frequency to compromise the structural stability or durability of the shaft (DFI, 2016).

2.7.3 Quilting (Mattressing, Shadowing)

Quilting describes vertical or horizontal linear features emanating primarily from reinforcing bars. Concrete is always placed inside the cage such that flow must go outward through the reinforcement cage into the cover region. As the concrete flows around the reinforcement, a separation occurs whereby two separately contaminated faces, commonly referred to as laitance interfaces, must recombine outside the case by pressing these interfaces together. This creates creases that extend to the side of shaft surface in the form of a quilted grid pattern (Figure 2.5). The depth of the creases can span the entire thickness of the concrete cover. This presents significant durability issues, as the opening facilitates the corrosion process through the application of environmental chlorides.

2.8 Quality Control

The primary means of quality control for drilled shaft construction in the United States is visual inspection (Hertein, 2016). This involves physically observing every step of the process and comparing actual conditions to theoretical/design plans. This can prove impractical during wet construction applications as a majority of the structure is below both water and ground. The traditional method for assuring that concrete was placed properly, is to plot a curve that shows the column of the concrete actually placed as compared to the theoretical volume in increments of depth. These plots give a real time presentation of the stages of concrete placement and can be helpful in detecting large defects (Reese and O'Neill, 1999). Modern technologies such as gamma/gamma logging and thermal integrity profiling give a more accurate depiction of the final shaft shape (Hertein, 2016). All of these methods lack the ability to detect quilting and channeling anomalies as they do not drastically change the shaft shape, bulk density, or volume of energy producing concrete.

2.9 Corrosion

Corrosion is most often defined as the destruction of a metallic material due to a reaction with its environment. Practically all environments are corrosive to some degree, but this research focuses on corrosion in wet environments. Uniform corrosion in wet environments accounts for a large majority of all corrosion and usually involves aqueous solutions or electrolytes. Uniform corrosion is characterized by a chemical or electrochemical reaction that occurs over a large area. This reaction thins the metal to a point of eventual failure. Overall corrosion represents the greatest destruction of metal on a tonnage basis but this does not raise major industry concerns because uniform corrosion is both predictable and preventable in most instances (Fontana, 1967).

2.9.1 Corrosion Rate Expressions

Corrosion rates have been expressed by several means throughout literature; such as milligrams per square centimeter per day, grams per square inch per hour and percent weight loss. None of these give any indication of penetration. Mils per year (mpy) is the expression most commonly used in engineering to illustrate the rate in terms of weight loss or thinning of a structural piece. The formula is as follows:

$$mpy = \frac{534W}{DAT}$$

where W weight loss (mg)
D density of specimen (g/cm^3)
A area of specimen (in^2)
T exposure time (hr)

This expression uses whole number, which are easily handled and it can be used to predict the lifespan of a given structural component.

2.9.2 Corrosion Lifespan Analysis

To remain active, the corrosion process requires oxygen, moisture and a conductive electrolyte. Commonly, this electrolyte is saltwater which leads to chloride- induced corrosion (sulfates can also induce corrosion but the effect is comparatively insignificant when chlorides are present). If one of the three corrosion components is absent, the chemical reaction will stall until all elements are present. Consequently, the serviceability of a drilled shaft and the resultant life expectancy is dependent on the surrounding environment, isolation (concrete cover thickness), concrete quality and the ability of the encased reinforcement to withstand aggressive environments. These parameters can be defined as:

C_s Concentration of chloride ions at the concrete surface (environment)
x_{cover} Concrete cover (isolation)
D Apparent diffusion coefficient (concrete quality)
C_T Chloride threshold at which corrosion initiates (steel type dependent)

The amount of cementitous material in the concrete mix design, known as the cement factor (CF) should also be included along with the presence of any cracks. For the case of drilled shafts, quilting or laitance induced channeling should also be considered.

In a salt water environment, chlorides accumulate on the surface of a structure. Recall, the corrosion process requires that chlorides, moisture and oxygen coexist. When a structure is new, chlorides are not available to the process, time must pass as chlorides diffuse through the concrete to finally reach the surface of the encased reinforcement. This diffusion time can be calculated using the parameters defined above (Sagüés, 2002; Mullins, et al, 2009). The period during the diffusion process is known as the corrosion initiation time (t_i) and it represents the most critical designable aspect of corrosion control. Once corrosion begins, corrosion products begin forming on the surface of the reinforcing steel, increasing the volume. This volume increase can initiate

cracking that may propagate to the concrete surface and compromise the integrity of the structural element.

The traditional school of thought assumes that structures in a fully submerged environment are sufficiently separated from an oxygen source as to prohibit corrosion, recent studies have shown that this is not always the case and that under water structures can show signs of highly localized corrosive behavior (Walsh, 2016). Conservatively and for the sake of simplicity, the corrosion free lift expectancy of all reinforced concrete structures can be simply determined using $\boldsymbol{t_i}$.

2.9.2.1 Corrosion Initiation Time

The corrosion initiation time is commonly computed using an error function wherein $\boldsymbol{C_s}$, x_{cover}, D, and C_T are all input.

$$C_T = C_s(1 - erf\frac{x}{2\sqrt{Dt_i}})$$

A convenient method of solving for $\boldsymbol{t_i}$ is to plot the function (Figure 2.6), plotting the ratio $\boldsymbol{C_T/C_s}$ (dimensionless) on the y-axis and reading down to determine the x-axis value. The x-axis is expressed in the following form:

$$x - axis\ value = t_i 4D/x^2$$

2.9.2.2 Chloride Threshold

Chloride threshold (C_T) for a plain steel rebar can be approximated to be 0.004 times the Cement Factor. For a typical drilled shaft concrete mix design there is a minimum of 600pcy of cementitious material (CF=600), which results in the following calculation for the chloride ion concentration needed to initiate corrosion at the surface of the steel:

$$C_T=0.004(600)=2.4pcy$$

2.9.2.3 Surface Chloride Concentration

The driving force for chloride diffusion into the concrete is dictated by the chloride concentration at the concrete surface, C_s. For a soil with a chloride content of 1200 ppm (2.0pcy) the C_T/C_s ration would be greater than one, which is out of the range of the chart (Figure 2.6) and therefore non-corrosive. When the C_T/C_s is that high, the $t_i 4D/x^2$ expression can be conservatively assumed to be 100.

2.9.2.4 Apparent Diffusion Coefficient

Laboratory studies has shown that the apparent diffusion coefficient (D) for concrete mixes containing flyash ranges from 1E-8 cm/s to 7E-8cm/s with an average value of 2E-8 cm/s (Sagüés, 2002). Assuming worst case scenario values of D=1E-8cm/s and a concrete cover of 7.5 cm (3in), the resulting time to initial corrosion works out to be 450 years. This is well outside of the anticipated design life of a structure (50-100 years.) This value corresponds to dry structures with mild soil conditions. Placing the structure in a salt water marine environment reduces the C_T/C_s value to 0.1 which results in an initiation time of 16 years for 3 inches of cover. If the cover thickness were doubled to 6 inches the initiation time would be resultantly quadrupled to 64 years.

2.9.3 Anomalies and Corrosion Potential

Design lifespan computations assume a contiguous concrete cover. Field and laboratory observation has shown reflective quilting (laitance channel formation) in shaft specimens constructed in wet conditions, where concrete is placed into slurry using a tremie. Quilting introduces the possibility of direct ground or sea water access to the reinforcing cage, thus negating the afforded protection that the above calculations represent, along with the calculations themselves. This thesis aims to diagnose the condition of the concrete cover as it relates to the type

of slurry used in construction in order to determine the applicability of standard corrosion lifespan calculations.

2.10 Previous Data Collection

The specimens examined in this thesis were constructed during two previous University of South Florida research projects. The process used in constructing shafts 1-18 can be found in "Defining the Upper Viscosity Limit for Mineral Slurries Used in Drilled Shaft Construction" (Mullins, 2014). The purpose of this study was to test the current upper viscosity limit for mineral slurries. During this research, 18 miniature test shafts were prepared. Each shaft measures 42in in diameter and 24in in height. Shaft specifics can be found in Table 2.1 (Figure 2.7-2.30).

Examination of Table 2.1 reveals that mineral slurry, polymer slurry and water were used during the casting process. Water shafts were used to replicate mechanical stabilization and act as a control group. Six additional shafts were cast during another University of South Florida study conducted for KB International. Of particular note are shafts 22 and 23 which were cast using self consolidating concrete. The shaft specifics can be found in Table 2.2.

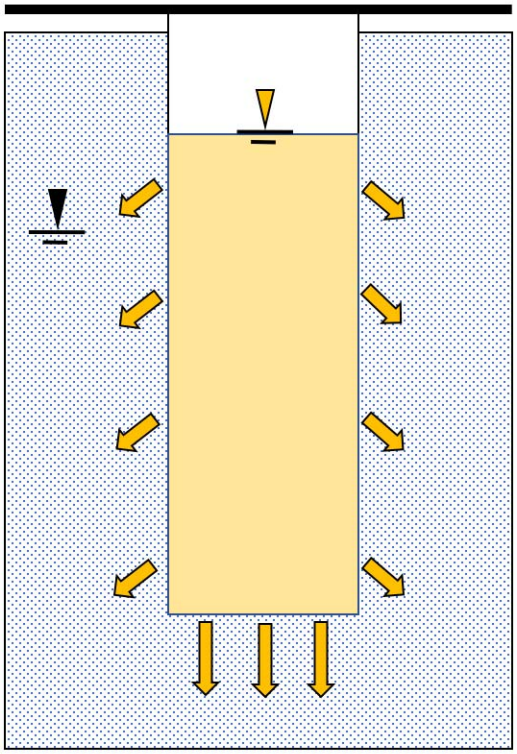

Figure 2.1 Hydrostatic force

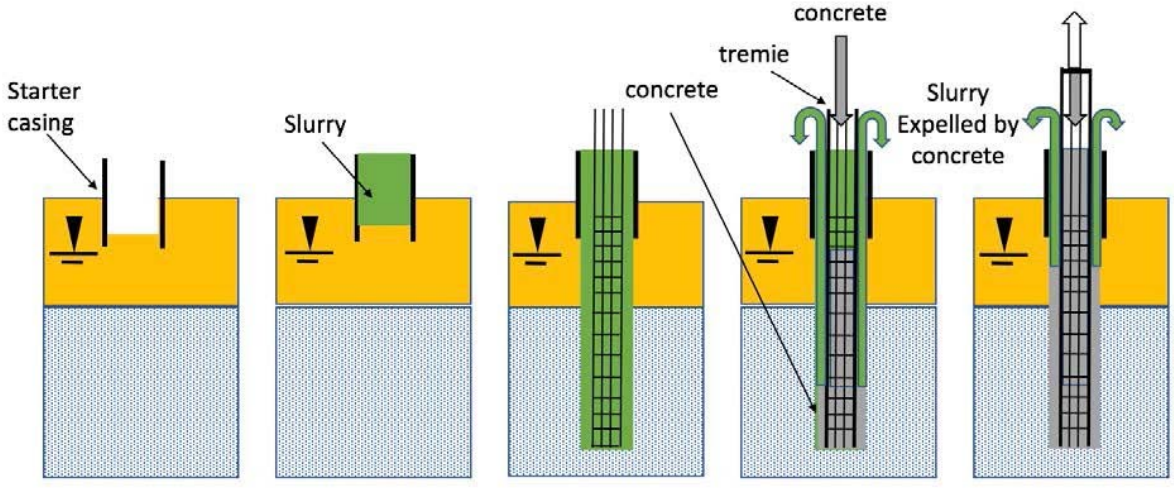

Figure 2.2 Wet construction

Figure 2.3 Inclusions (DFI, 2016)

Figure 2.4 Channeling (DFI, 2016)

Figure 2.5 Quilting

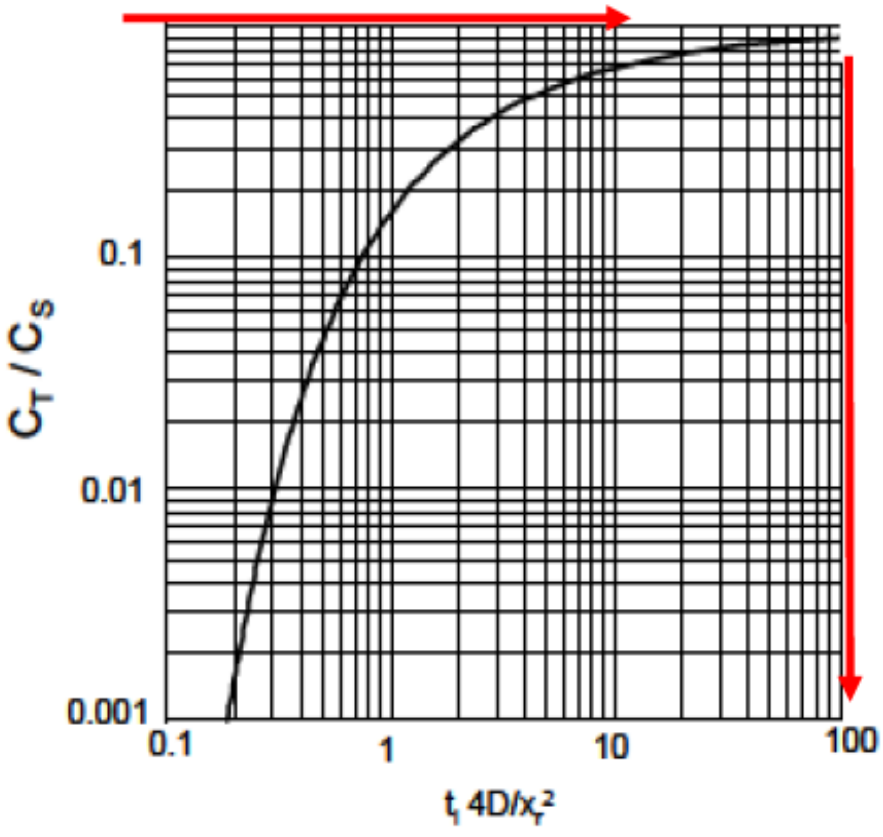

Figure 2.6 Solving for t_i

Table 2.1. Summary of miniature shaft properties

Shaft #	Pour Date	Concrete Mix	Slurry Type	Viscosity	Average Pullout Strength (kips)	Average Concrete Compressive
1	2/20/2013	4KDS	Bentonite	40	57.234	6150
2	2/20/2013	4KDS	Bentonite	90	49.704	6150
3	5/8/2013	4KDS	Bentonite	40	36.894	4358
4	5/8/2013	4KDS	Bentonite	50	32.697	4358
5	5/8/2013	4KDS	Bentonite	90	38.094	4358
6	5/8/2013	4KDS	Water	26	54.304	4358
7	5/8/2013	4KDS	Bentonite	30	28.754	4530
8	6/18/2013	4KDS	Bentonite	40	24.212	4530
9	6/18/2013	4KDS	Bentonite	50	20.524	4530
10	6/18/2013	4KDS	Bentonite	90	23.139	4530
11	6/18/2013	4KDS	Polymer	60	32.338	4530
12	6/18/2013	4KDS	Polymer	60	33.941	4530
13	9/20/2013	4KDS	Bentonite	30	25.636	4753
14	9/20/2013	4KDS	Bentonite	30	27.641	4753
15	9/20/2013	4KDS	Bentonite	50	19.804	4753
16	9/20/2013	4KDS	Polymer	90	24.077	4753
17	9/20/2013	4KDS	Polymer	90	26.247	4753
18	9/20/2013	4KDS	Water	26	34.042	4753

Table 2.2. Summary of miniature shaft properties for KBI study.

Shaft #	Pour Date	Concrete Mix	Slurry Type	Viscosity	Average Pullout Strength (kips)	Average Concrete Compressive Strength (psi)
19	5/3/2015	4KDS	Polymer	60	20.9	4100
20	5/3/2015	4KDS	Polymer	130	19.3	4100
21	5/3/2015	4KDS	Bentonite	40	20.7	4100
22	5/3/2015	4KDS	Water	26	21.8	4100
23	5/3/2015	SCC	Water	26	Not Tested	Not Tested
24	5/3/2015	SCC	Bentonite	40	Not Tested	Not Tested

Figure 2.7 Shaft 1: f'c 6150psi; drilled shaft mix; 44 sec/qt bentonite; rough with creases

Figure 2.8 Shaft 2: f'c 6150psi; drilled shaft mix;105sec/qt bentonite; coarse with well-defined creases

Figure 2.9 Shaft 3: f'c 4358 psi; drilled shaft mix; 40 sec/qt bentonite; coarse with well-defined creases.

Figure 2.10 Shaft 4: f'c 4358 psi; drilled shaft mix; 55 sec/qt bentonite; coarse with well-defined creases.

Figure 2.11 Shaft 5: f'c 4358 psi; drilled shaft mix; 90 sec/qt bentonite; coarse with well-defined creases.

Figure 2.12 Shaft 6: f'c 4358 psi; drilled shaft mix, water cast, smooth with minor channeling

Figure 2.13 Shaft 7: f'c 4530 psi; drilled shaft mix, 30 sec/qt bentonite; coarse.

Figure 2.14 Shaft 8: f'c 4530 psi; drilled shaft mix, 40 sec/qt bentonite; rough with defined creases

Figure 2.15 Shaft 9: f'c 4530 psi; drilled shaft mix, 50 sec/qt bentonite; rough with defined creases

Figure 2.16 Shaft 10: f'c 4530 psi; drilled shaft mix, 50 sec/qt bentonite; rough with defined creases

Figure 2.17 Shaft 11: f'c 4530 psi; drilled shaft mix, 65 sec/qt polymer; smooth

Figure 2.18 Shaft 12: f'c 4530 psi; drilled shaft mix, drilled shaft mix, 66 sec/qt polymer, rough

Figure 2.19 Shaft 13: f'c 4753 psi; drilled shaft mix, 30 sec/qt bentonite, rough

Figure 2.20 Shaft 14: f'c 4753 psi; drilled shaft mix, 30 sec/qt bentonite, rough

Figure 2.21 Shaft 15: f'c 4753 psi; drilled shaft mix, 56 sec/qt bentonite, rough with defined creases

Figure 2.22 Shaft 16: f'c 4753 psi; drilled shaft mix, 85 sec/qt polymer, smooth light creases

Figure 2.23 Shaft 17: f'c 4753 psi; drilled shaft mix, 85 sec/qt polymer, smooth light creases

Figure 2.24 Shaft 18: f'c 4753 psi; drilled shaft mix, water cast, smooth minor channeling

Figure 2.25 Shaft 19: f'c 4100 psi; drilled shaft mix, 63 sec/qt polymer, smooth

Figure 2.26 Shaft 20: f'c 4100 psi; drilled shaft mix, 121 sec/qt polymer, smooth

Figure 2.27 Shaft 21: f'c 4100 psi; drilled shaft mix, 42 sec/qt bentonite, coarse with well-defined creases

Figure 2.28 Shaft 22: f'c 4100 psi; drilled shaft mix, water cast, smooth minor channeling

Figure 2.29 Shaft 23: self consolidating concrete, water cast, smooth minor channeling

Figure 2.30 Shaft 24: self consolidating concrete, 40 second bentonite slurry, rough disintegrating

CHAPTER 3: LABORATORY EQUIPMENT AND TESTING

This chapter discusses the initial screening of lab cast specimens as well as the electro-chemical methods used to determine corrosion potential in encased reinforcement.

3.1 Connection Quality

In order to determine the quality of the electrical connections in the reinforcement system, mutual potential and mutual resistance tests were performed on all vertical reinforcement for each shaft. Each shaft specimen included seven vertical steel reinforcing bars (rebar). Prior to testing, the exposed end of each rebar was tapped and a stainless steel screw was installed to establish a connection point (Figure 3.1). The metal was brushed prior to connection to ensure a bright metal to bright metal contact. The rebar on each shaft were lettered A-G counterclockwise and testing was completed to identify all rebar relationships.

Mutual potential was measured by setting a standard multimeter on the 2000mV setting, and then using alligator clips to attach the positive line to one rebar connection port and the negative line to another rebar connection port. This wiring arrangement causes one rebar to serve as a working electrode and the other to serve as a reference electrode, the reading on the multimeter is the difference in potential between the two connection points.

Mutual resistance was measured using a Nilsson meter. A Nilsson meter is a four pin, alternating current, null balancing ohmmeter customarily used to measure resistivity in soils. For the purpose of this test, the meter was used in a two pin configuration (Figure 3.2). Wires with

alligator clips are used to establish a connection between the established stainless steel ports and the rebar being tested. The Nilsson meter works by generating a low voltage current between the C1 and C2 posts. The detector senses a voltage drop between the two posts, compares it to internal resistors, and indicates a difference on the null detector. When the null detector is balanced using the range switch and the dial, the resistance in ohms is the dial reading multiplied by the range switch position (Nilsson, 1984) (Figure 3.3).

Mutual potential and mutual resistance tests were conducted in immediate succession to ensure similarity in testing conditions (Figure 3.4). After determining the connection quality for each shaft, stainless steel, solid-core wire was used to physically connect the seven rebar ports. This physical connection eliminates any error resulting from disparate connection quality. An example data collection sheet can be found in Appendix A.

The resistance that occurs when two sections of rebar have a passive connection was used as the baseline for connectivity resistance. In order to determine this, one section of rebar was laid on top of another on an inert surface. The amount of overhang was kept at 4 inches to keep the force between the bars consistent. Hose clamps were used to establish a connection port on each bar and then alligator clips were used to connect those ports to the positive and negative inputs on a multimeter (Figure 3.5). A total of 30 resistance readings were taken at different locations along the bottom rebar.

3.2 Corrosion Potential

Two methods were used to collect corrosion potential data: instantaneous multi-point surface mapping and single point long-term data collection. The former gives the current corrosion distribution over a given area and the later gives trends in the corrosion rate over a given length of

time. Used in conjunction these methods provide a four dimensional analysis of the corrosion potential for each shaft specimen.

3.2.1 Multi-Point Surface Mapping

In order to map corrosion potential evenly over the surface of the shaft, a grid was created. The grid was made out of single piece of 28-inch by 42-inch plastic sheeting. A sharpened 2-inch diameter pipe was used to punch holes through the plastic (Figure 3.6) in rows with a 2.5 inch spacing in both directions (Figure 3.7). Testing was then conducted per ASTM C876-09: *Standard Test Method for Corrosion Potentials of Uncoated Reinforcing Steel in Concrete*, using a copper-copper sulfate reference electrode and a standard multimeter.

The saturated copper-copper sulfate reference electrode (Figure 3.8) was selected because it provides a stable and reproducible potential over a temperature range of 32º to 120ºF. A wet sponge was used to establish an electrical junction, by means of a low electrical resistance liquid bridge between the concrete surface and the porous tip of the reference electrode. To ensure electrical continuity, the sponge was wrapped around the tip of the reference electrode and secured with a rubber band. Having previously established secure electrical connection to the reinforcing steel, an alligator clip was used to connect the steel to the positive port on the volt meter. Similarly, the negative or COM port was attached to the cap of the reference electrode (Figure 3.9).

Prior to commencing testing, all shafts were saturated for 24 hours or until such time as a test measurement of corrosion potential reveals no change or fluctuation. Once saturated, measurements were taken systematically across the 80 grid positions with the multimeter set to 2000 millivolt range. The readings were recorded to the nearest millivolt. A sample data collection sheet can be found in Appendix A.

3.2.2 Open Cell Long Term Testing

The following testing procedure was developed in order to approximate long term corrosion potential in a laboratory setting. Acrylic tanks were affixed to the surface of the shafts and equipped with thermal sensors and titanium reference electrodes. The tanks were first filled with water and then a chloride solution and the potential difference was monitored for a total of 8 days.

Tanks were built out of 12-inch sections of 8-inch diameter clear acrylic pipe. A rotary machine was used to cope one end of each pipe section (Figure 3.10). This allowed the tanks to sit flush on the surface of the shaft (Figure 3.11). The tanks were sealed to the shafts using architectural grade silicon and allowed to cure for 24 hours prior to charging the system with water (Figure 3.12). Surface deterioration on nine of the 24 shafts prevented a watertight seal between the tank and the concrete resulting in their exclusion from this portion of the testing prescription. The filled tanks were left to sit for four days prior to initial data collection to allow for surface saturation.

Titanium reference electrodes were constructed for continuous potential difference data collection. Sections approximately four inches long were cut from a rod of activated titanium. The ends were then filed to reveal bare metal and create a level surface. Taking care to protect the surface coating, the rods were wrapped in cardboard and clamped into a lathe for drilling (Figure 3.13). A hole approximately ¼-inch deep was drilled into one end of each rod (Figure 3.14) using a $1/16^{th}$ inch cobalt coated drill bit.

Chromium-nickel alloy wire with a Teflon coated insulation was used to connect the electrode to the data logger (Figure 3.15). The properties of the metal in the wire and the metal in the electrode necessitated the use of a mechanical connection. The wire coating was stripped back

to reveal ½ inch of bare metal (Figure 3.16). The wire was then folded back on itself and inserted into the drilled end of the titanium rod and the connection was crimped using pliers to insure connection stability.

The reference electrodes were submerged in the tanks and suspended one inch from the shaft surface. Care was taken to ensure that the electrodes were parallel and in line with the incased vertical reinforcement. Shaft potential readings were taken with the positive lead attached to the interconnected exposed reinforcement and the negative lead attached to the titanium electrode as previously described. A thermocouple twisted wire pair was also placed in each tank taking care to separate the disparate wires and coat all exposed ends to prevent metallic deterioration (Figure 3.17). The electrode and the thermocouple wire for each shaft were attached to a Campbell Scientific CR1000 data collection system (Figure 3.18).

Each tank was calibrated daily using a copper-copper sulfate reference electrode (Figure 3.19). This was accomplished by attaching a voltmeter to the titanium reference electrode and the calibrating copper-copper sulfate electrode. The value was recorded along with the time of measurement.

After four days of continuous testing, the fresh water was exchanged for salt water. Salt water was simulated by adding aquarium salt to fresh water until the specific gravity exceeded 1.028 as measured by a hydrometer (Figure 3.20). Testing and daily calibration continued for four days after the introduction of salts.

Figure 3.1 Stainless steel port

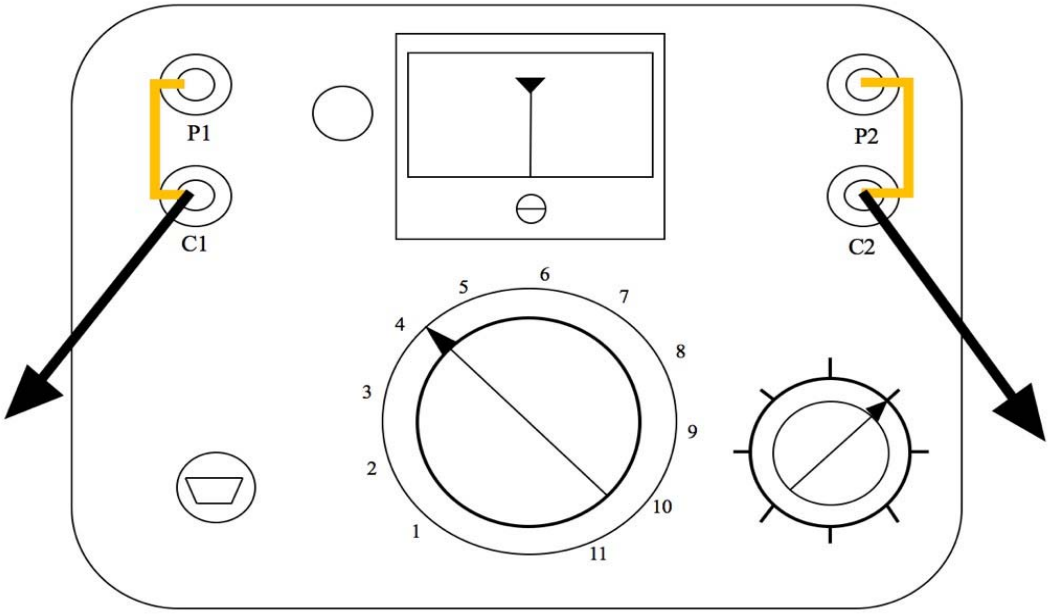

Figure 3.2 Nilsson meter configuration

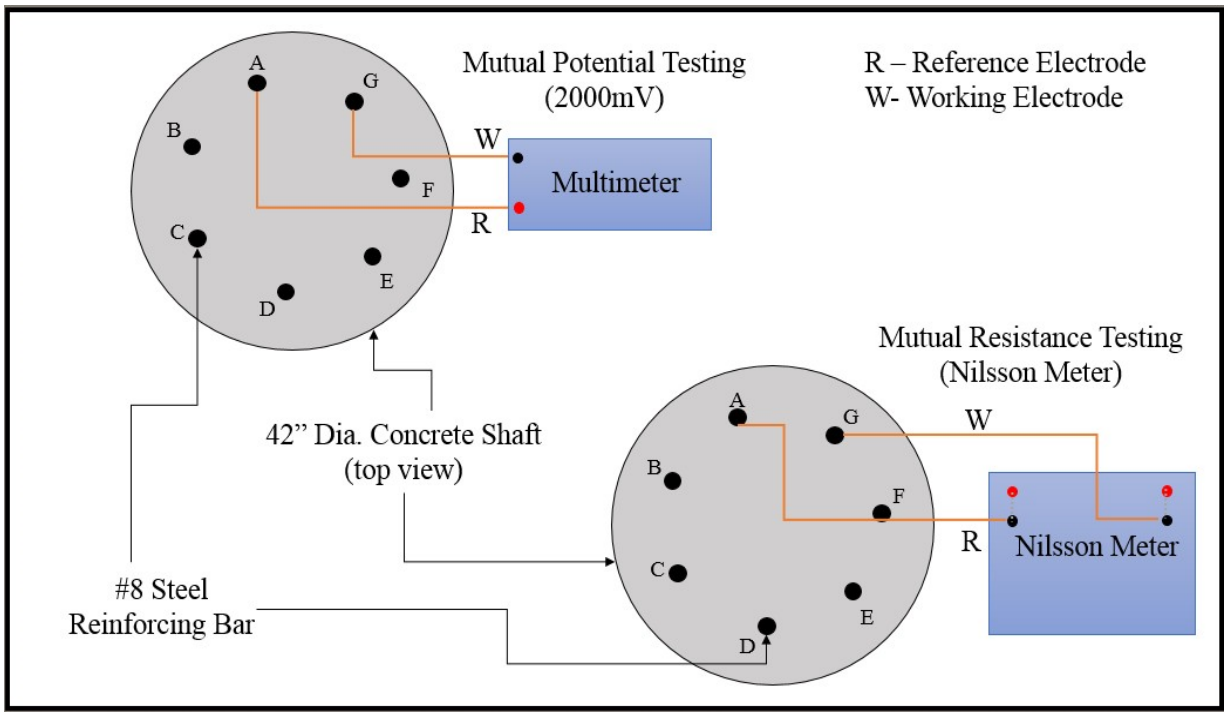

Figure 3.3 Mutual potential/ mutual resistance wiring diagram

Figure 3.4 Mutual potential / mutual resistance testing setup

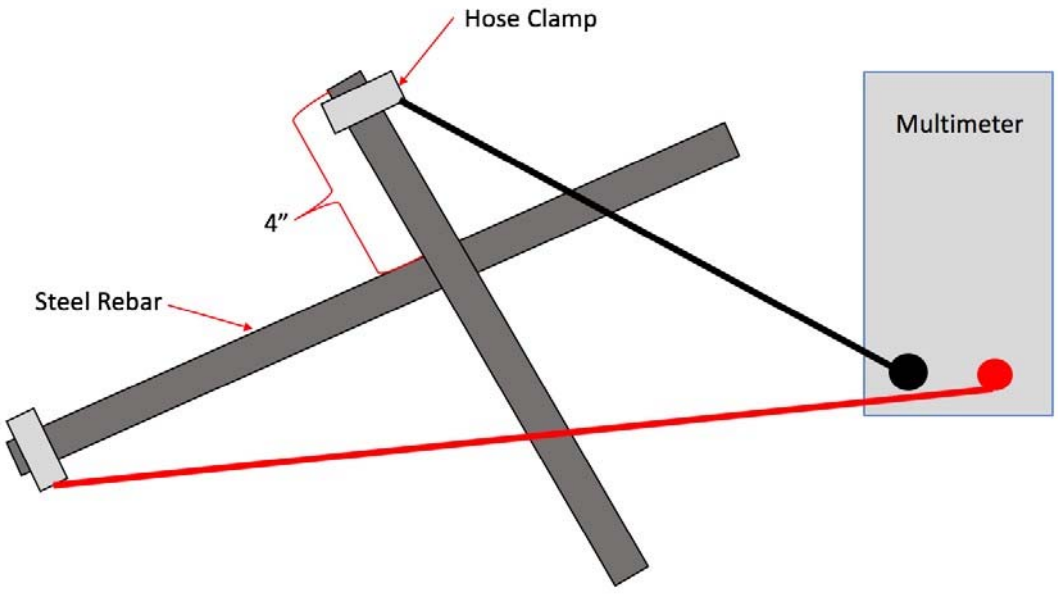

Figure 3.5 Rebar resistance wiring diagram

Figure 3.6 Template construction

Figure 3.7 Finished template

Figure 3.8 Copper- copper sulfate reference electrode

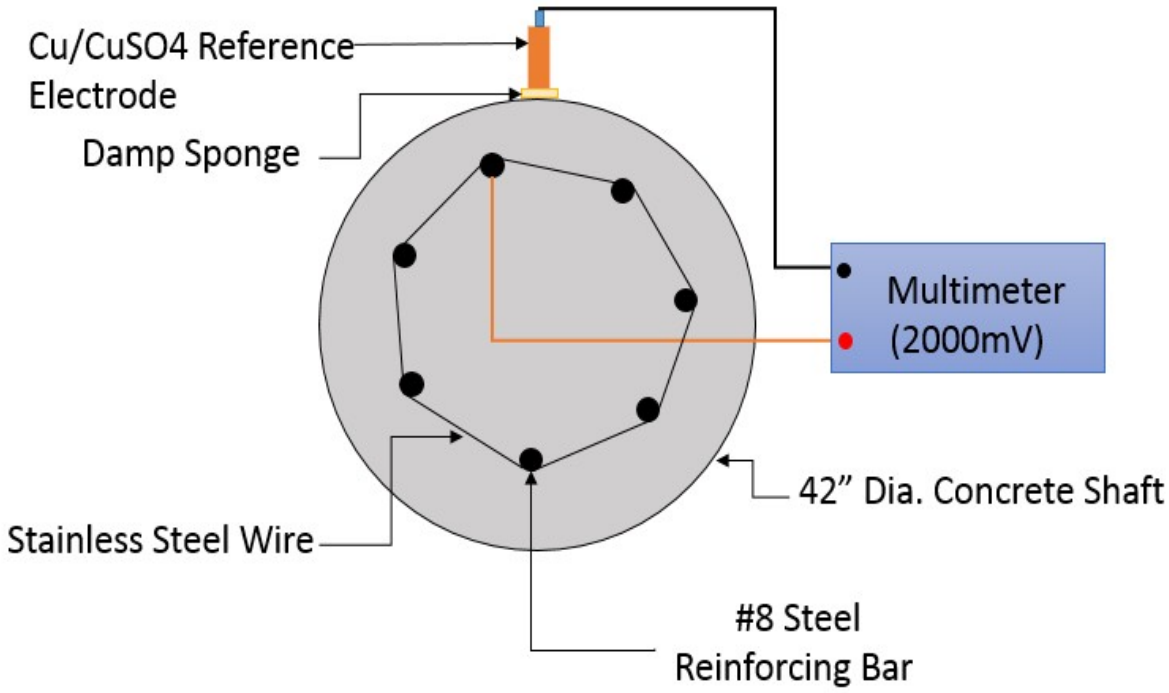

Figure 3.9 Surface mapping wiring diagram

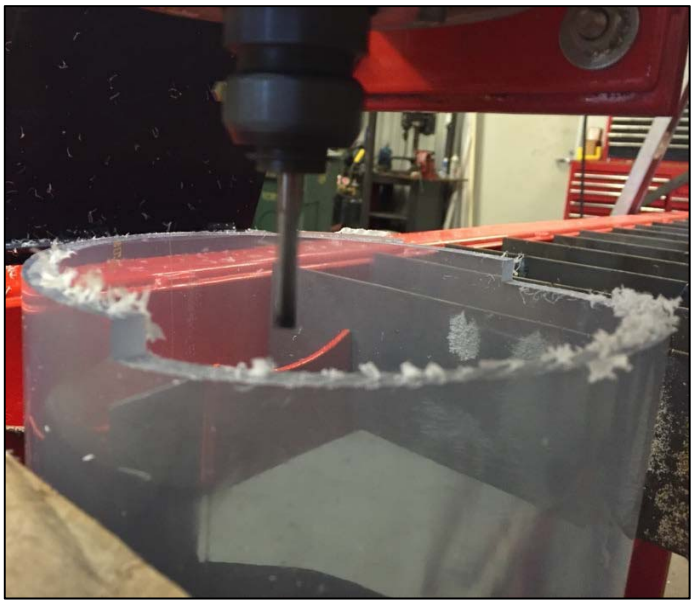

Figure 3.10 Rounding end of tank

Figure 3.11 Tank fit on shaft surface

Figure 3.12 Tanks installed on shafts

Figure 3.13 Drilled titanium rod

Figure 3.14 Drilled out titanium rod

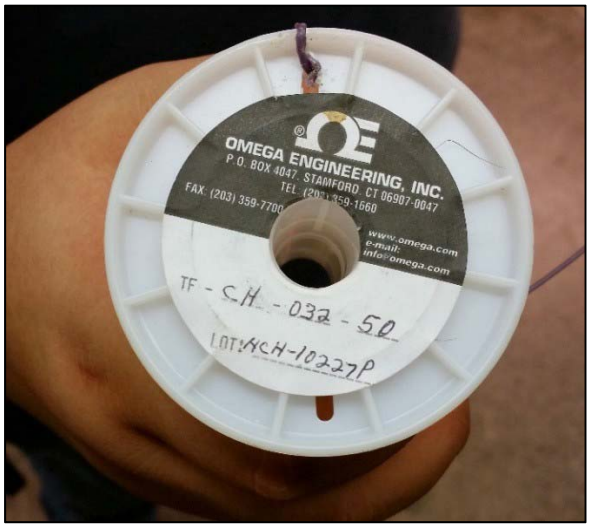

Figure 3.15 Connection wire

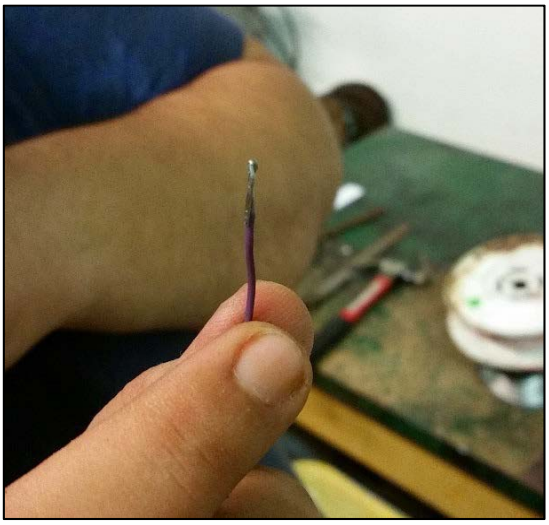

Figure 3.16 Wire pre installation

Figure 3.17 Testing tank

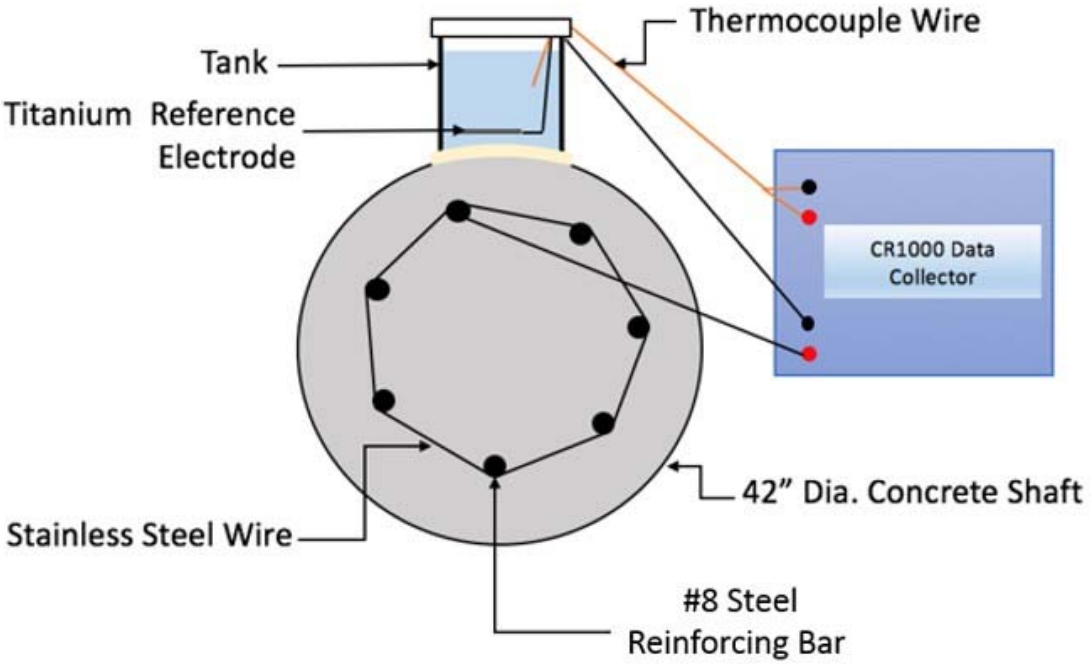

Figure 3.18 Open cell testing wiring diagram

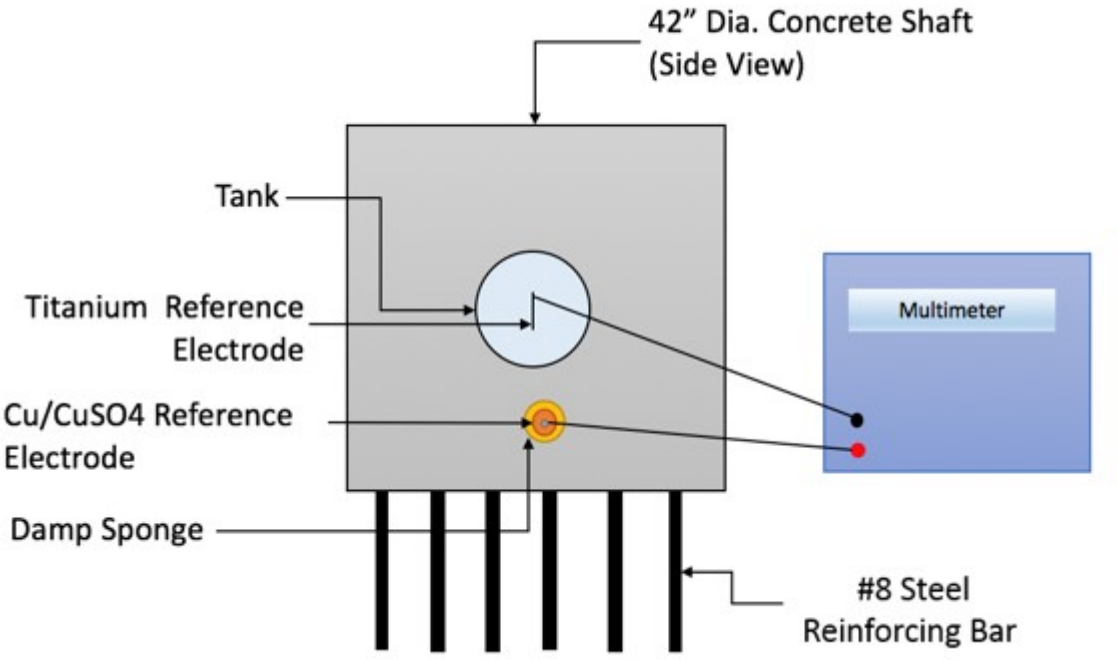

Figure 3.19 Cu-CuSo4 calibration wiring diagram

Figure 3.20 Hydrometer used to test specific gravity

CHAPTER 4: RESULTS

This chapter discusses the results of the testing outlined in chapter 3. This includes: mutual potential vs. mutual resistance, corrosion potential surface mapping and concludes with open cell corrosion potential.

4.1 Connection Quality

The mutual potential versus mutual resistance graph (Figure 4.1) consists of 460 points, representing 20 resistance and 20 potential measurements for 23 subject shafts. The data is color coded by slurry type: orange for bentonite, green for polymer and blue for water. The graph displays distinct banding on both the horizontal and vertical axis. The potential values for data points with a resistance of less than 100Ω are within 3mV of the zero excluding four statistical outliers. Above 100Ω the potential values form a vertical band between zero and 135mV. The data points of particular interest are the ones that exhibit near zero potential values above 100Ω resistance. A resistance value of 100Ω cannot be considered negligible, and if this resistance was the only method used for testing electro-connectivity, the point would be classified as poorly connected, if connected at all. However, a potential reading within 5mV of zero indicates a well-connected network

The rebar to rebar resistance readings varied from 0 to 105 Ω. A median resistance of 29 Ω was determined using a standard distribution curve (Figure 4.2). This value serves as the resistance baseline for the reinforcement system.

4.2 Corrosion Potential Surface Mapping

The copper-copper sulfate testing for each shaft included 80 data points. The 50th percentile (E_{50}) potential data for all shafts ranged from -508mV to -155mV with a standard deviation of 91mV. A total of 35% of the test shafts have a E_{50} potential below -350mV and all of that 35% were constructed using bentonite slurry (Table 4.1 and Figures 4.3-4.25). All of the data was graphed topographically using three dimensional mapping software. Using a color coding system and standardized contour spacing, the topographic surface maps illustrate the corrosion potential of each shaft.

4.3 Open Cell Corrosion Potential

The raw potential readings between the rebar and the titanium reference electrode were recorded over a ten day period and graphed as a function of time (Figure 4.26). The red line indicates the point when chlorides were introduced to the system. Additionally, the daily copper-copper sulfate calibration readings were graphed over time (Table 4.2 and Figure 4.27). From this graph it is possible to determine which reference electrodes malfunctioned during testing by their behavior after the introduction of chlorides. The shafts with malfunctioning reference electrodes were omitted from the remainder of the open cell analysis (Figure 4.28).

Linear interpolation was used in order to apply the daily copper-copper sulfate readings to the more frequent titanium electrode readings:

$$R'_c(t_i) = R_c(t_o) + [R_c(t_3) - R_c(t_0)] * \frac{t_i - t_o}{t_3 - t_0}$$

- $R'_c(t_i)$ is the $Cu/CuSO_4$ reading at the time in question, mV
- $R_c(t_o)$ is the initial or previous $Cu/CuSO_4$ potential reading, mV
- t is the time in minutes
- $R_c(t_3)$ is the $Cu/CuSO_4$ potential reading taken after $R_c(t_o)$, mV
- t_i is bounded by the domain $t_0 \leq t_i \leq t$

After all of the copper-copper sulfate readings were interpolated, those values were added to the corresponding reading from the titanium reference electrode, resulting in the corrected potential reading.

$$P(t) = M(t) + R_c'(t)$$

- P(t) is the corrected potential reading
- M(t) titanium reference electrode reading
- $R'_c(t_i)$ is the $Cu/CuSO_4$ reading at the time in question, mV

The resulting corrected graph shows a distinct change in potential at the point of chloride introduction (Figure 4.29).

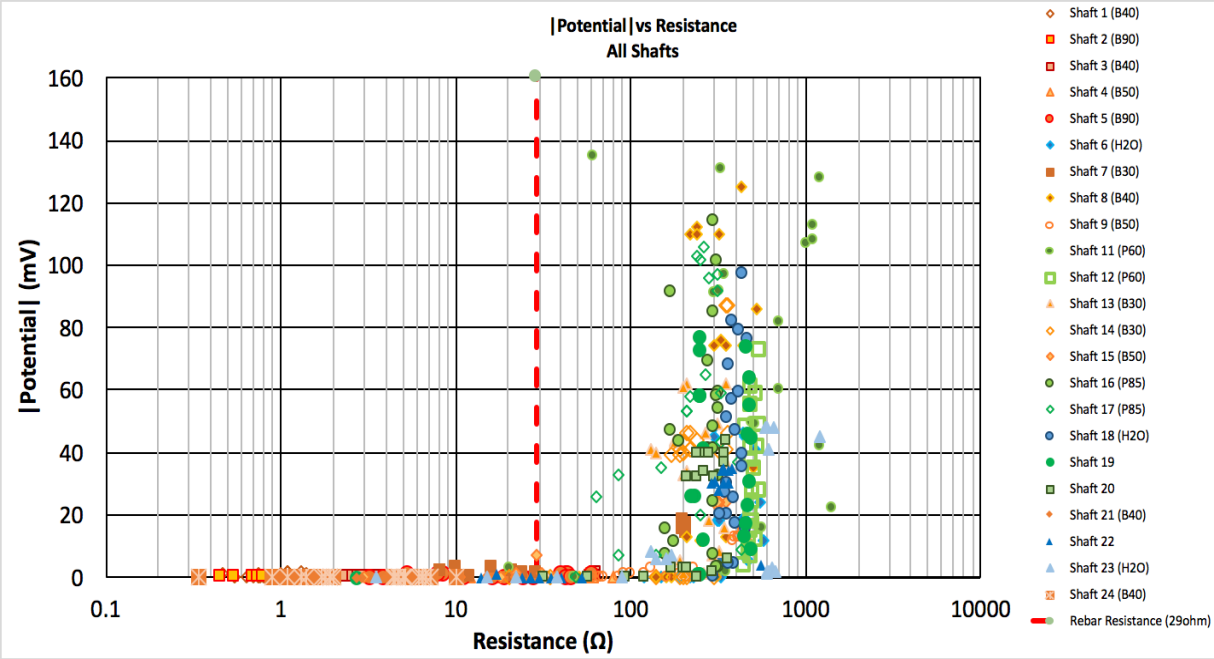

Figure 4.1 Mutual potential vs mutual resistance

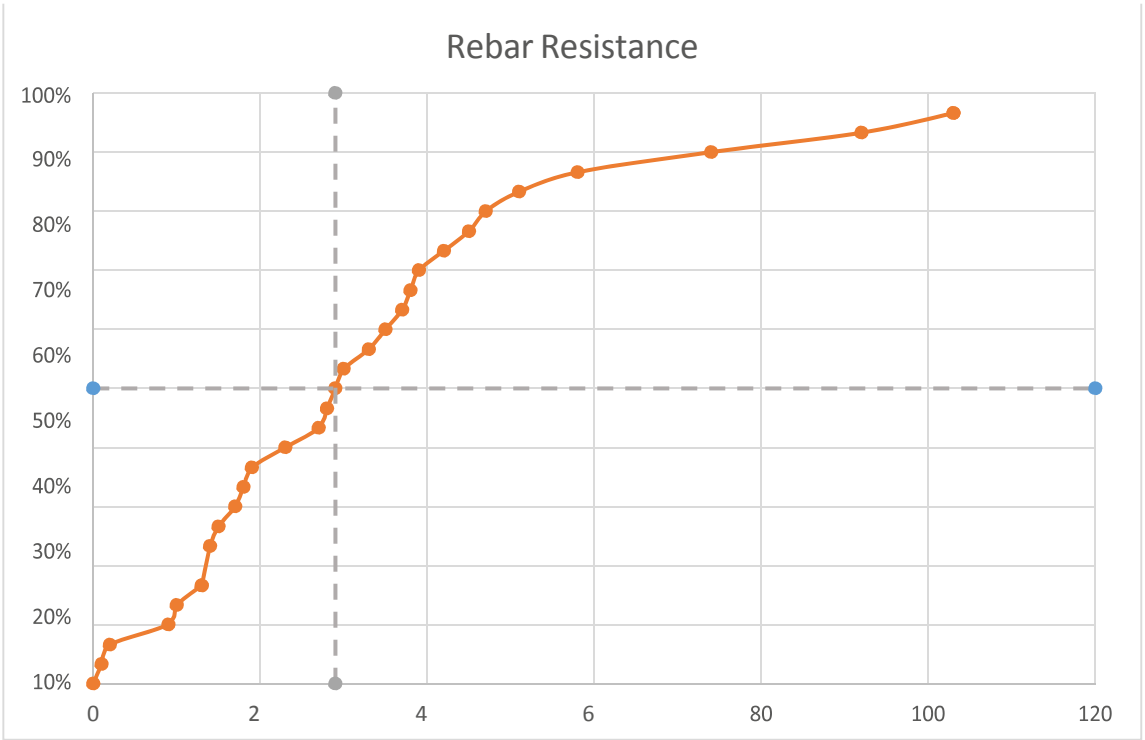

Figure 4.2 Rebar resistance standard distribution

Table 4.1. Cu-CuSO4 testing summary

Shaft #	Slurry	Mix	E50 (mV)	Shaft #	Slurry	Mix	E50 (mV)
1	B40 (44) 6K	4KDS	-317	14	B30	4KDS	-282
2	B90 (105)	4KDS	-449	15	B50 (56)	4KDS	-335
3	B40	4KDS	-373	16	P85	4KDS	-279
4	B50 (55)	4KDS	-443	17	P85	4KDS	-300
5	B90	4KDS	-447	18	water	4KDS	-293
6	Water	4KDS	-155	19	P60	4KDS	-243
7	B30	4KDS	-372	20	P130	4KDS	-242
8	B40	4KDS	-225	21	B40	4KDS	-508
9	B50	4KDS	-383	22	water	4KDS	-250
11	P60 (65)	4KDS	-285	23	water	SCC	-258
12	P60 (66)	4KDS	-190	24	B40	SCC	-425
13	B30	4KDS	-289				

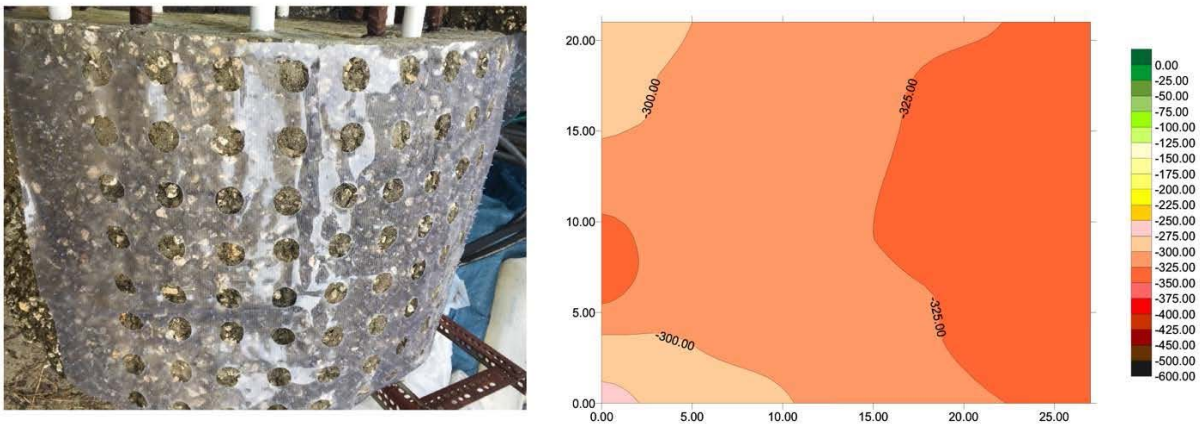

Figure 4.3 Shaft 1 testing template and corrosion potential map

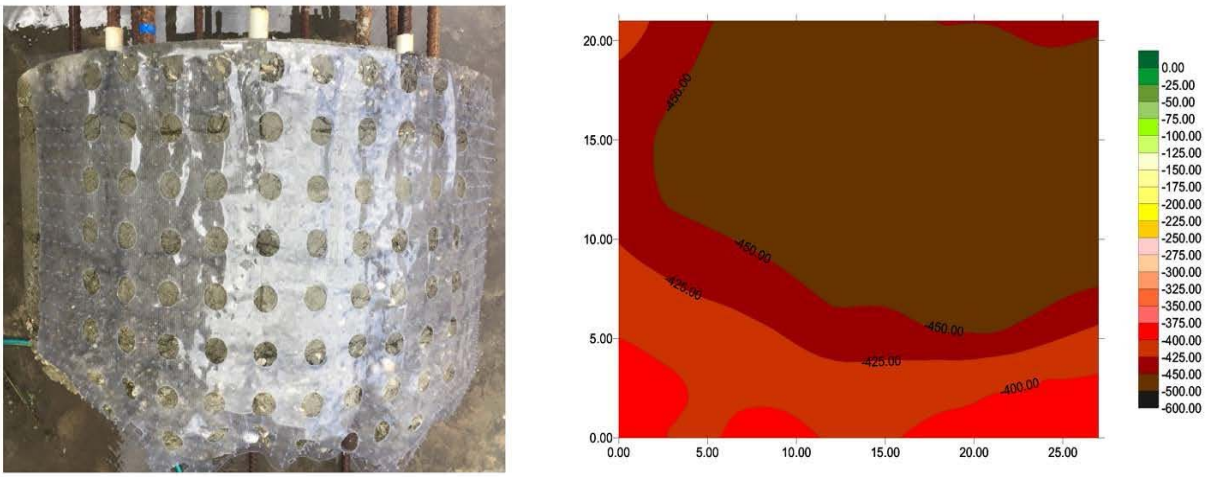

Figure 4.4 Shaft 2 testing template and corrosion potential map

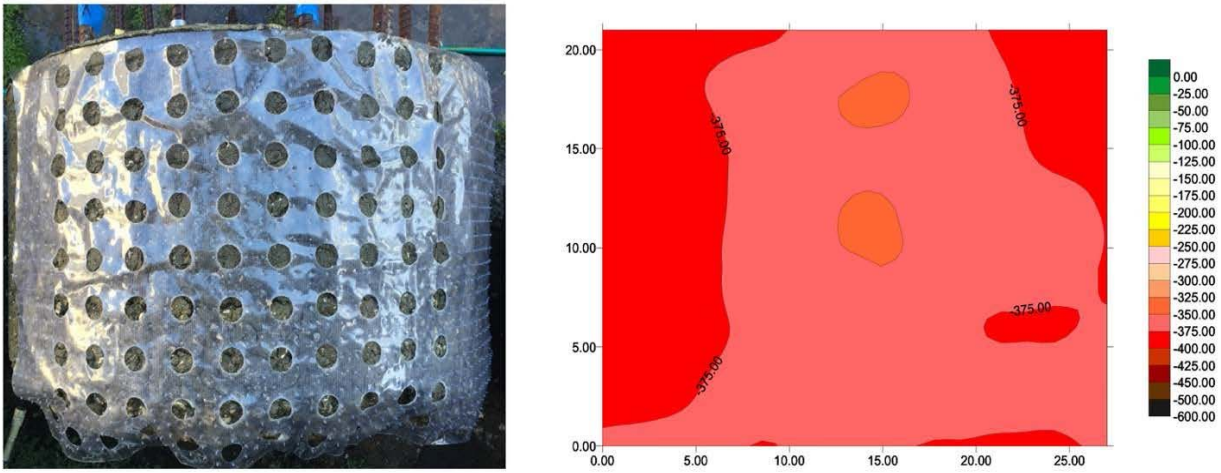

Figure 4.5 Shaft 3 testing template and corrosion potential map

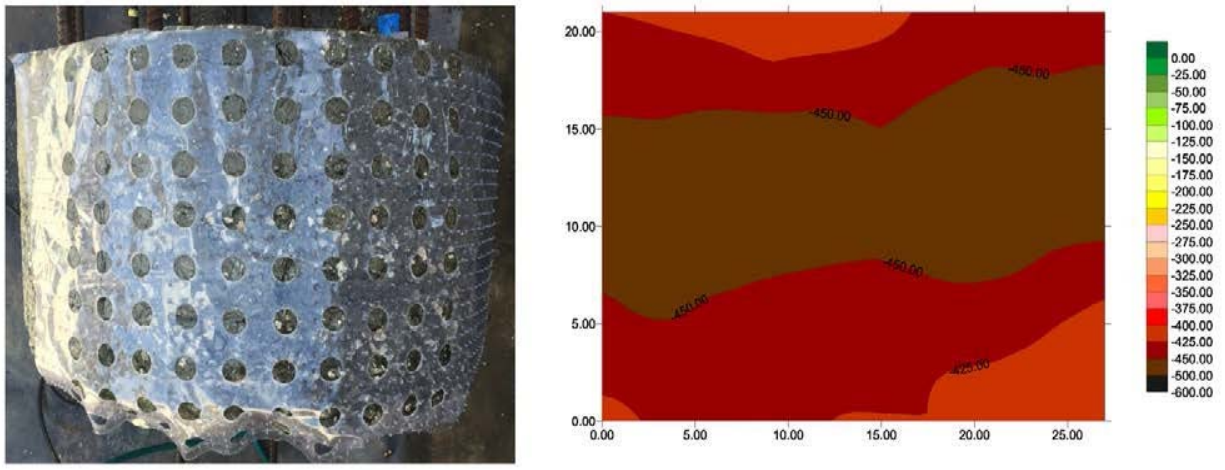

Figure 4.6 Shaft 4 testing template and corrosion potential map

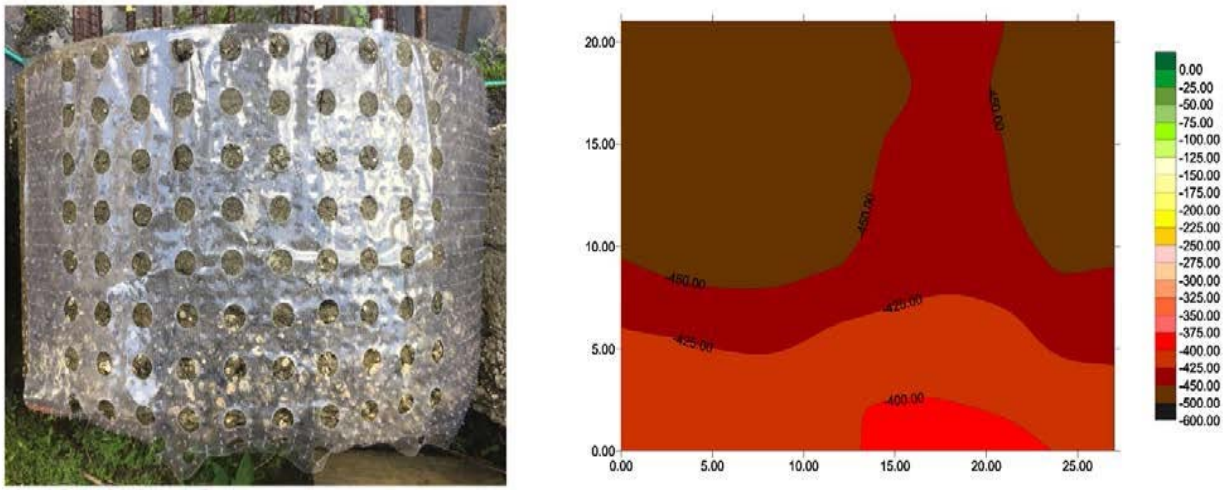

Figure 4.7 Shaft 5 testing template and corrosion potential map

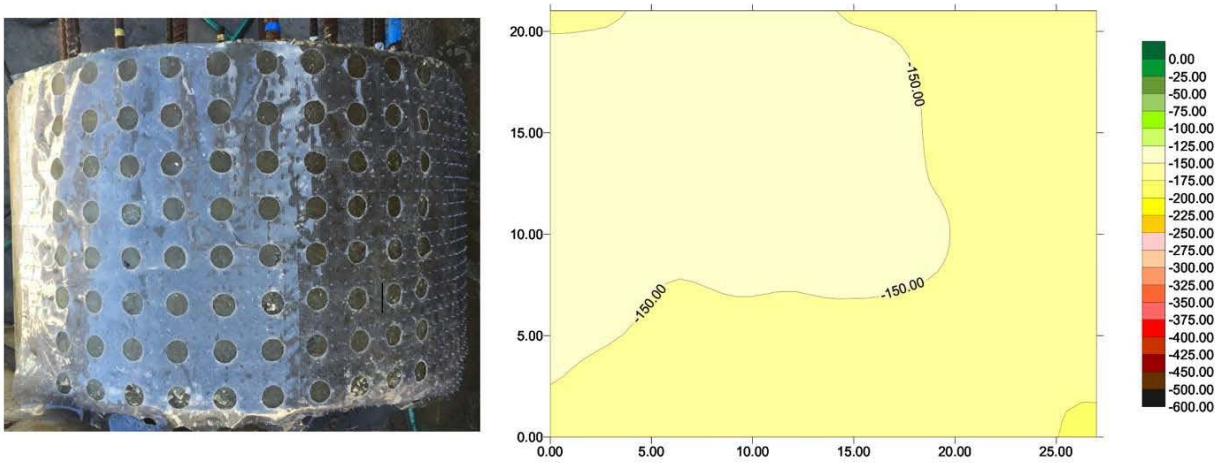

Figure 4.8 Shaft 6 testing template and corrosion potential map

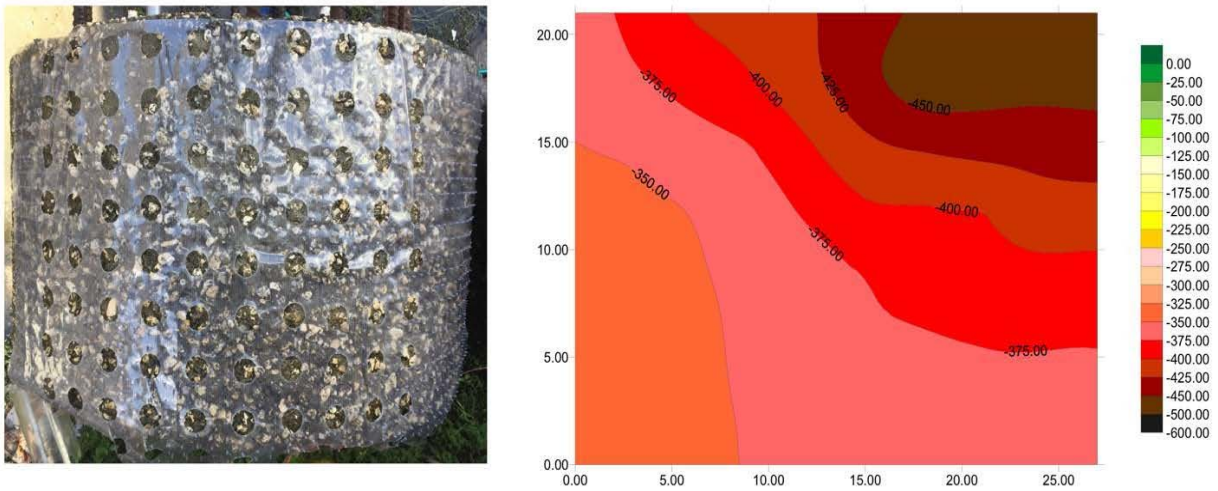

Figure 4.9 Shaft 7 testing template and corrosion potential map

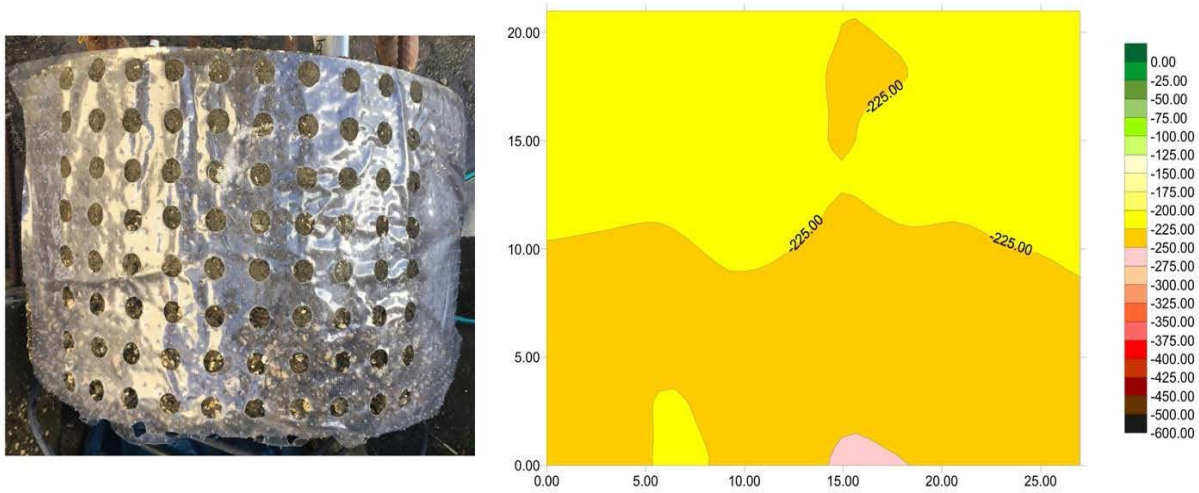

Figure 4.10 Shaft 8 testing template and corrosion potential map

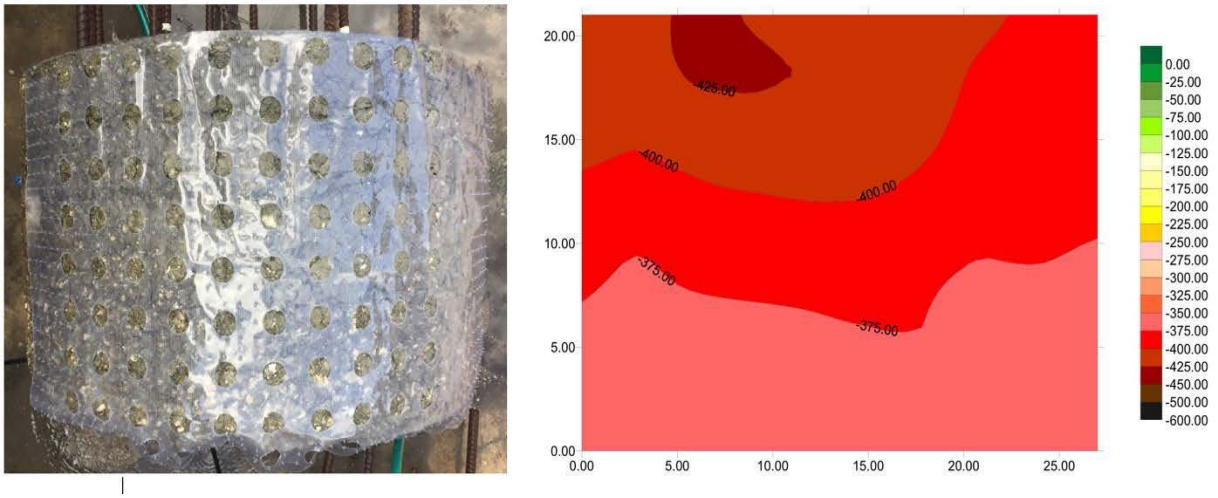

Figure 4.11 Shaft 9 testing template and corrosion potential map

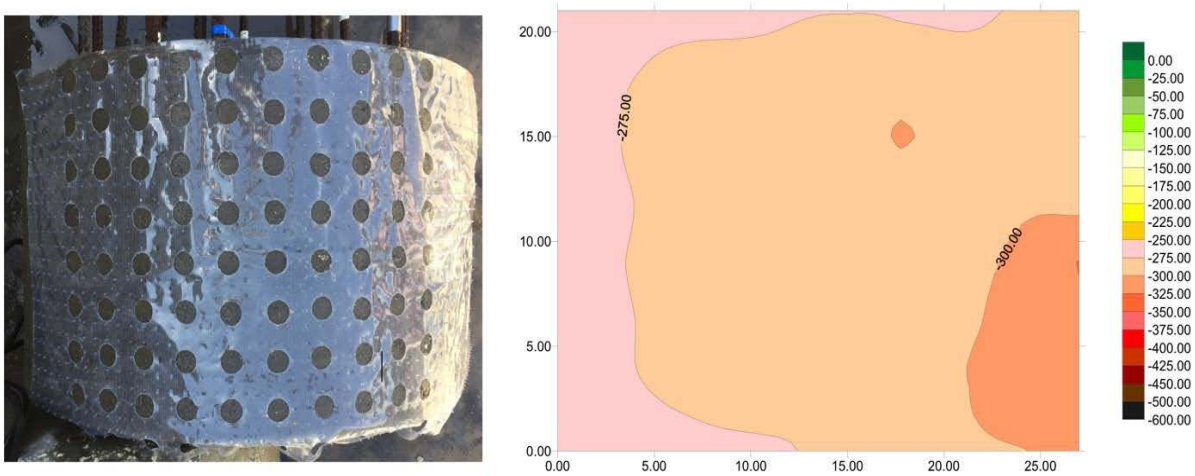

Figure 4.12 Shaft 11 testing template and corrosion potential map

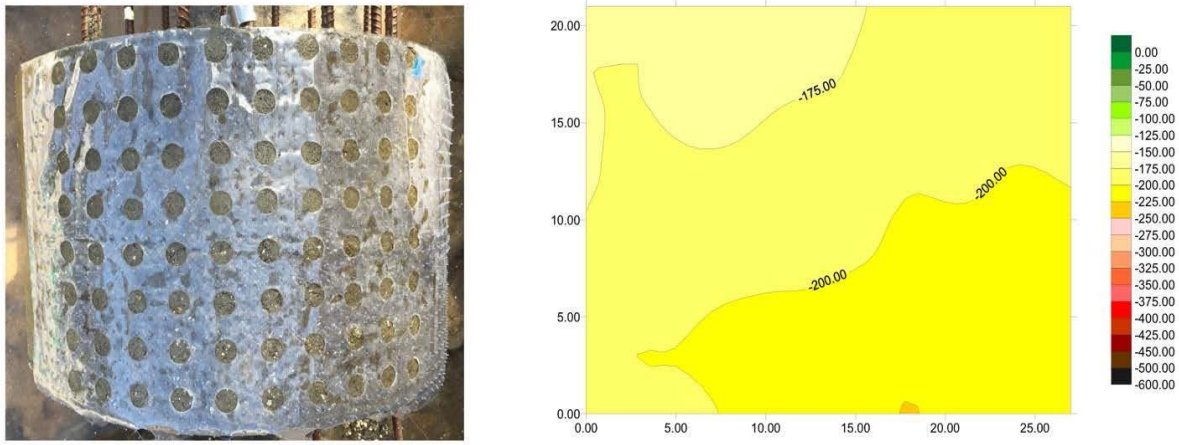

Figure 4.13 Shaft 12 testing template and corrosion potential map

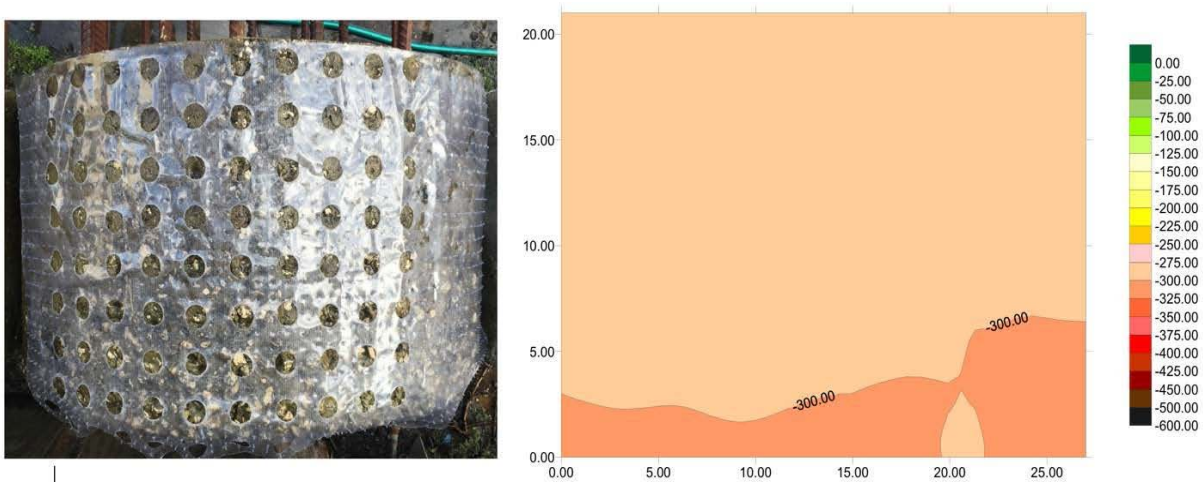

Figure 4.14 Shaft 13 testing template and corrosion potential map

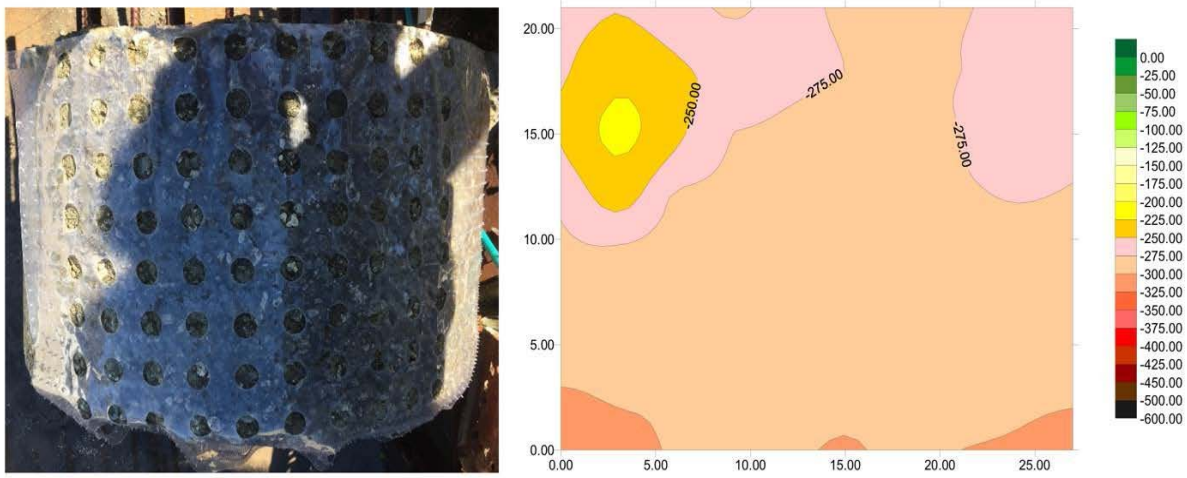

Figure 4.15 Shaft 14 testing template and corrosion potential map

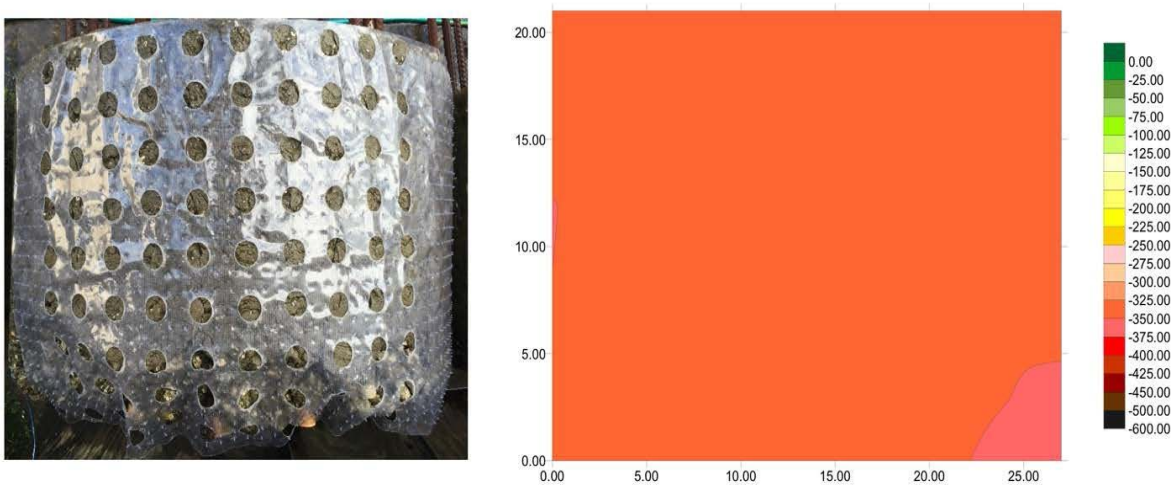

Figure 4.16 Shaft 15 testing template and corrosion potential map

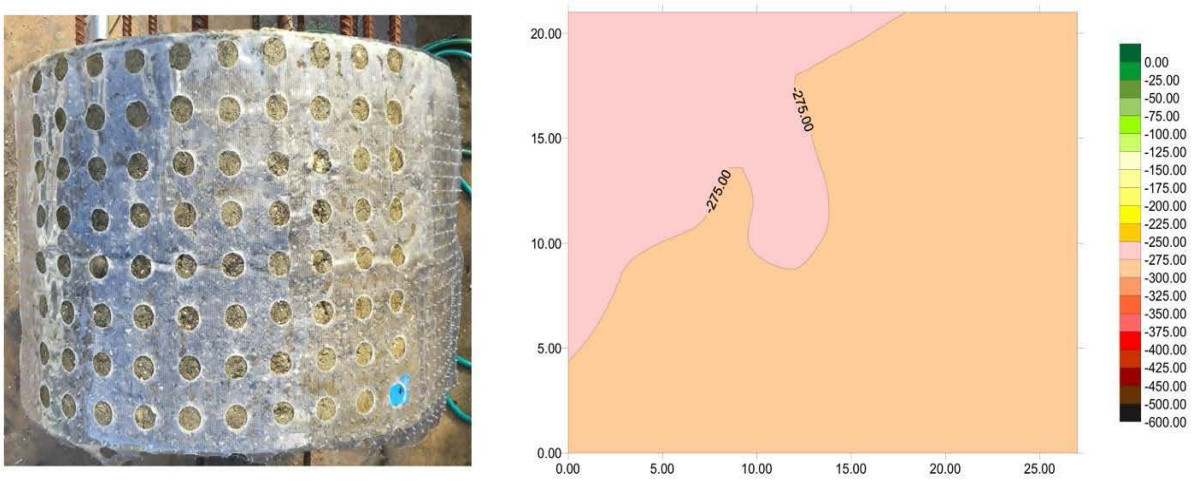

Figure 4.17 Shaft 16 testing template and corrosion potential map

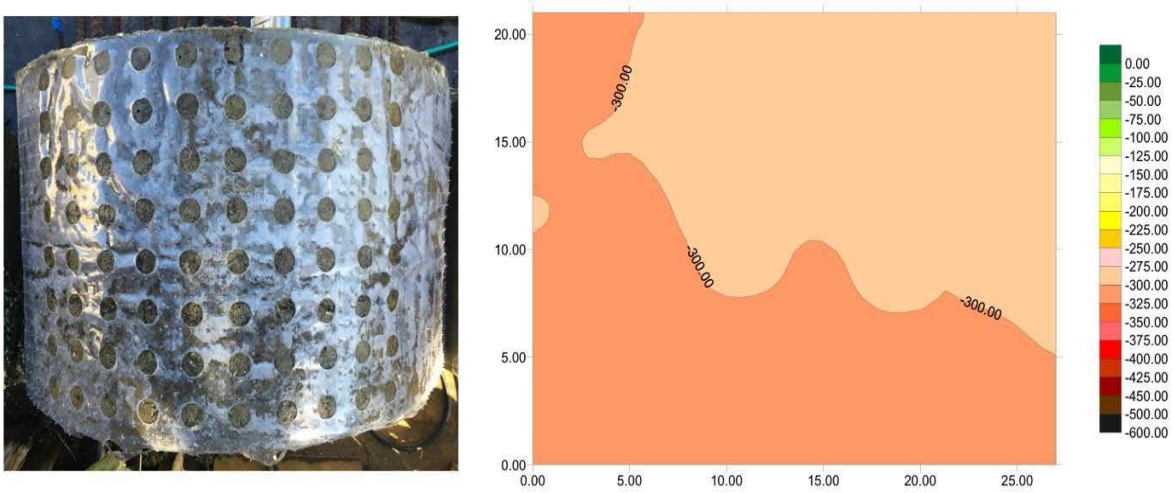

Figure 4.18 Shaft 17 testing template and corrosion potential map

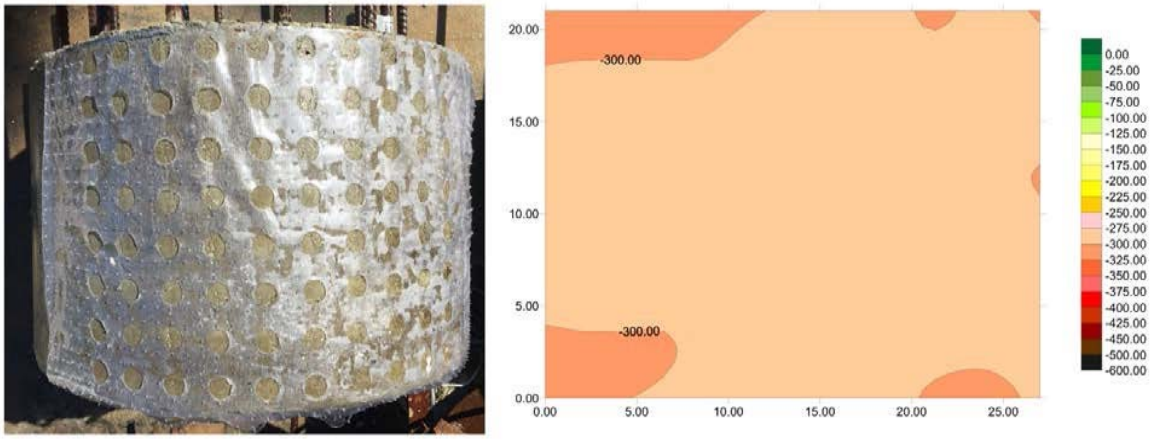

Figure 4.19 Shaft 18 testing template and corrosion potential map

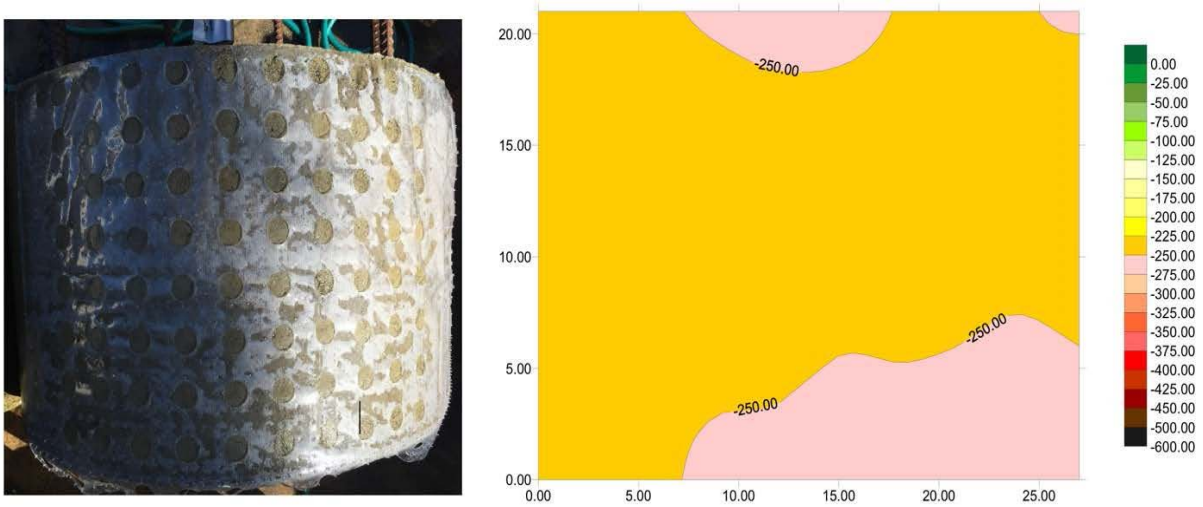

Figure 4.20 Shaft 19 testing template and corrosion potential map

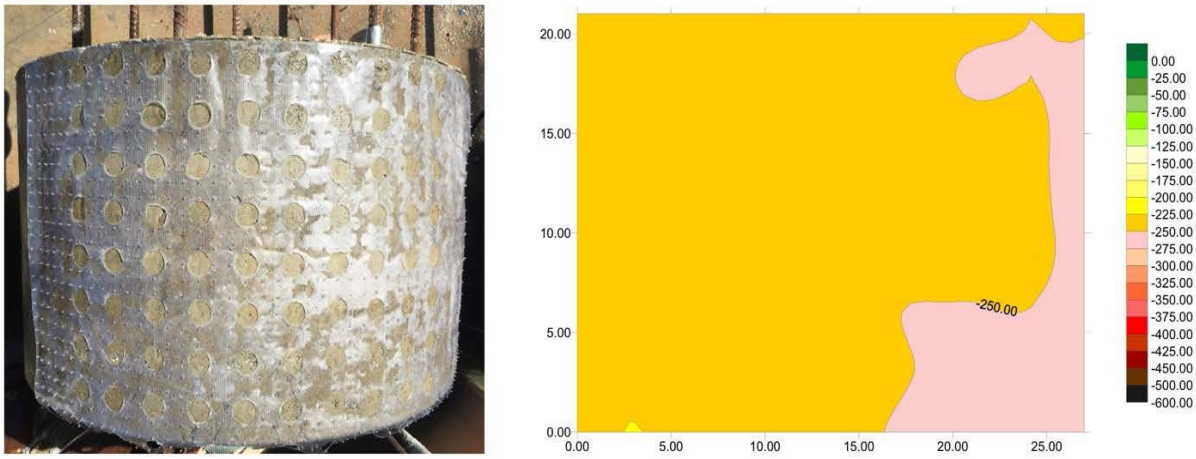

Figure 4.21 Shaft 20 testing template and corrosion potential map

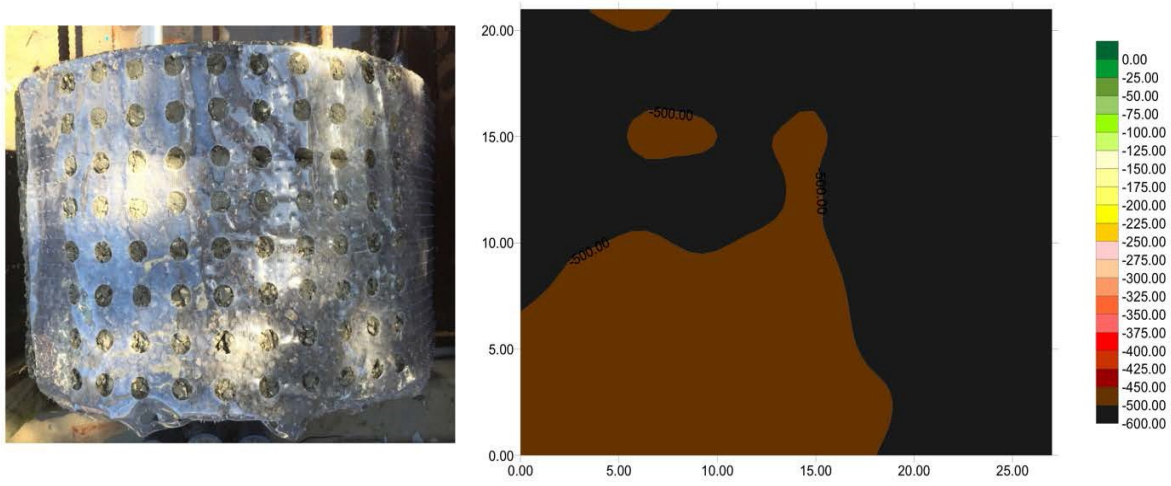

Figure 4.22 Shaft 21 testing template and corrosion potential map

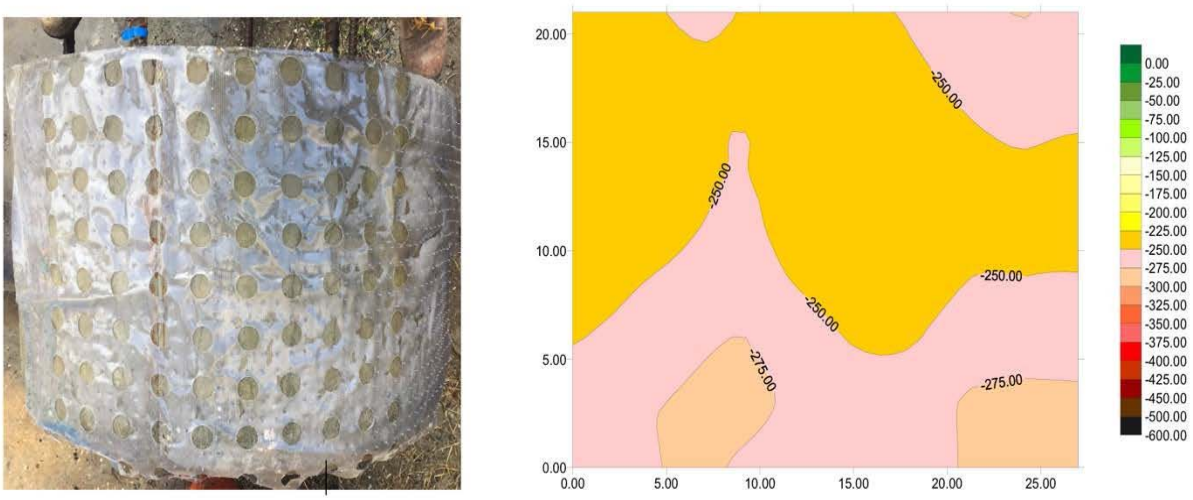

Figure 4.23 Shaft 22 testing template and corrosion potential map

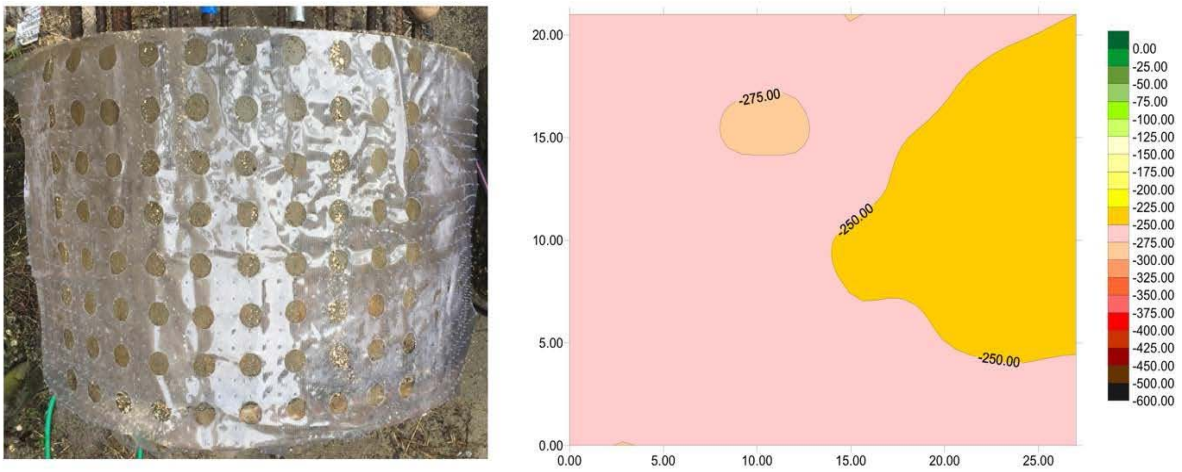

Figure 4.24 Shaft 23 testing template and corrosion potential map

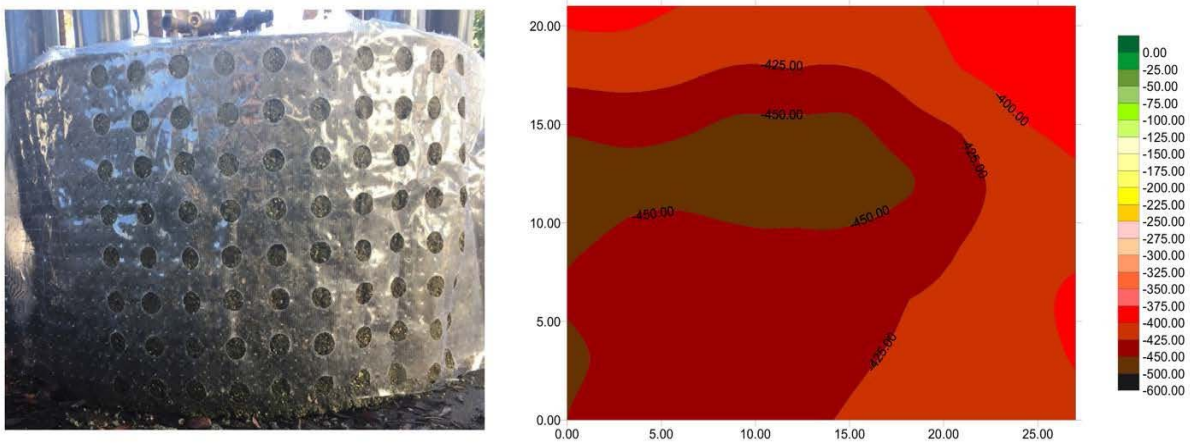

Figure 4.25 Shaft 24 testing template and corrosion potential map

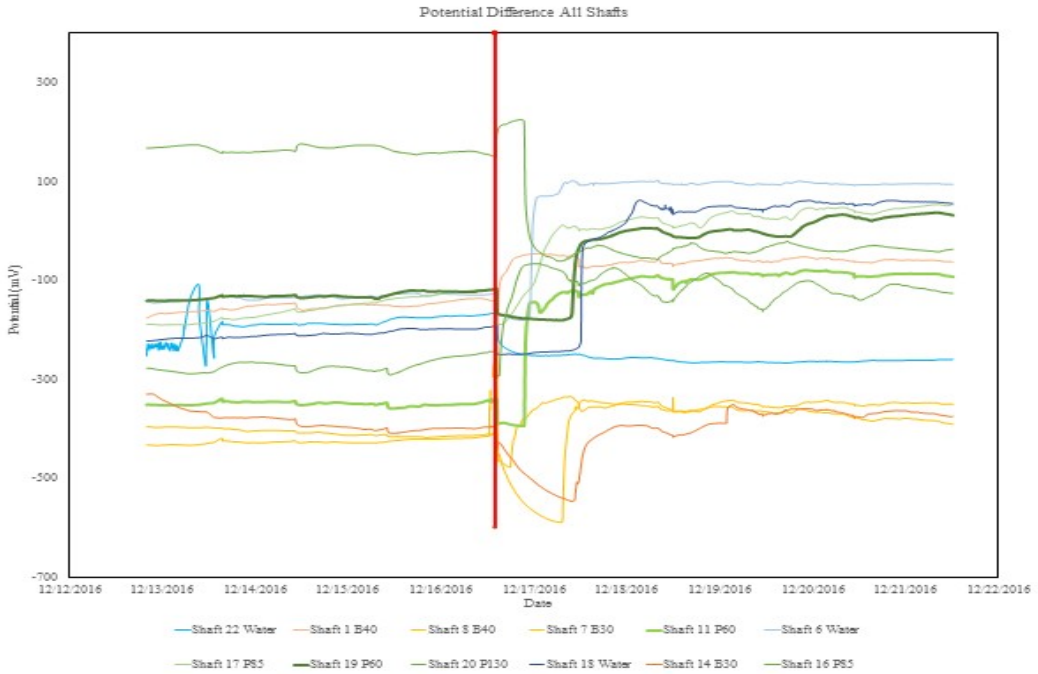

Figure 4.26 Raw potential difference data

Table 4.2. Correction data table

		Cu/CuSO4-Correction				Fresh	Salt Water	Salt Water Cu/CuSO4 Correction (mV)				
Shaft #	Slurry	12-Dec	13-De	14-Dec	15-Dec	16-Dec	16-	17-Dec	18-Dec	19-Dec	20-Dec	21-Dec
1	B40	234	238	222	225	218	218	274	254	258	258	254
6	Water	76	64	73	75	64	64	-143	-160	-163	-165	-160
7	B30	71	35	48	59	32	32	-46	-70	-98	-110	-115
8	B40	34	8	72	63	54	54	-109	-130	-146	-148	-148
11	P60	84	58	65	76	56	56	-108	-135	-173	-182	-175
12	P60	46	39	43	45	33	33					
13	B30	-25	-31	-31	-28		0					
14	B30	71	58	73	77	64	64	67	-66	-138	-145	-144
16	P85	83	58	65	77	57	57	-117	-139	-152	-159	-150
17	P85	37	18	3	-23	-29	-29	-169	-185	-210	-224	-231
18	water	73	55	53	115	54	54	100	-164	-181	-189	-189
19	P60	70	46	51	47	48	48	-30	-75	-89	-122	-122
20	P130	-122	-122	-110	-76	-99	-99	-99	-109	-123	-129	-123
22	water	86	71	78	67	63	63	208	152	146	142	1
23	water-SCC	57	45	53	20	35	35	145	109	107	72	103
	TIME	14:00	12:0	10:30	11:00	12:30	12:45	11:30	11:45	11:00	10:50	12:15

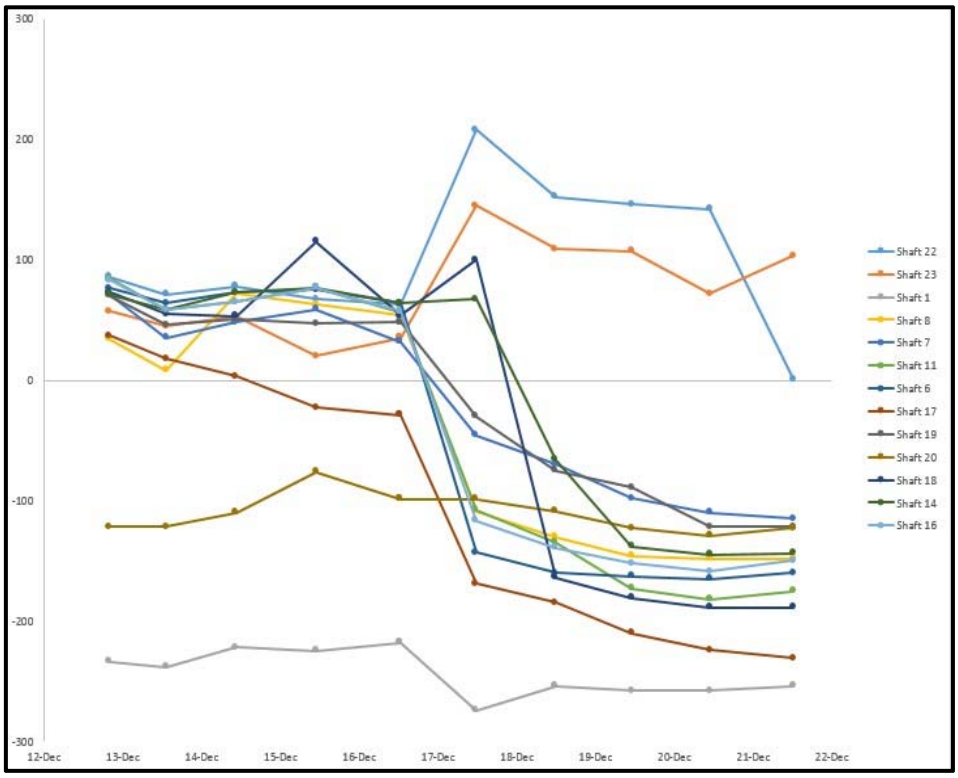

Figure 4.27 Correction data

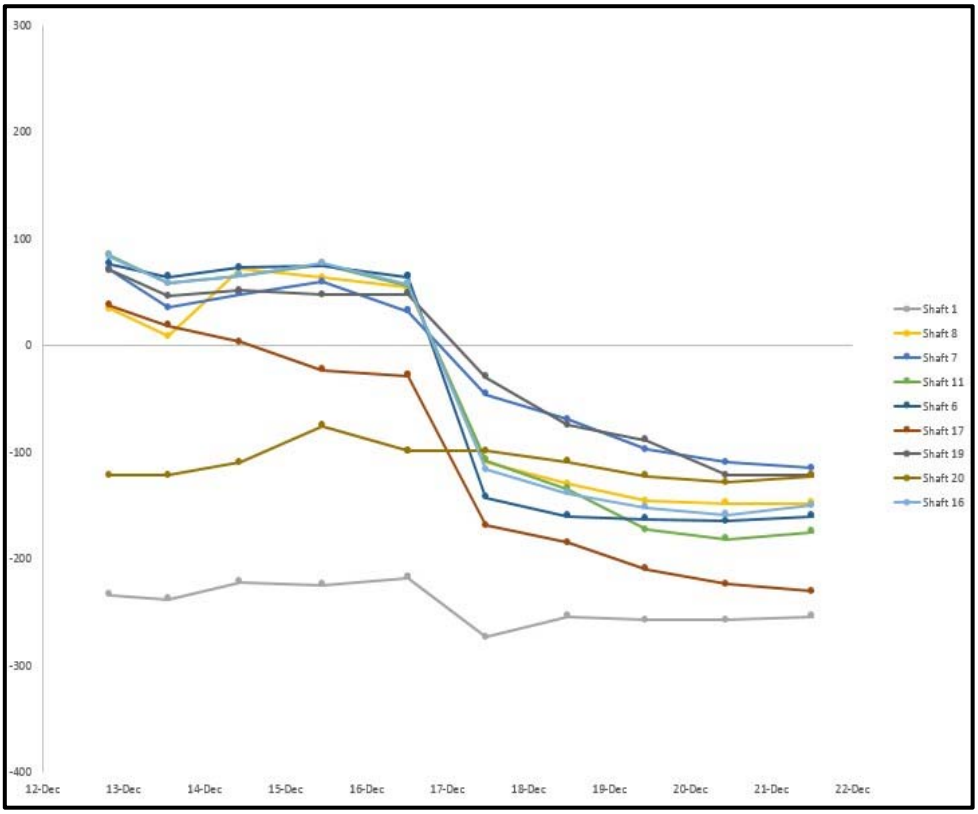

Figure 4.28 Edited correction data

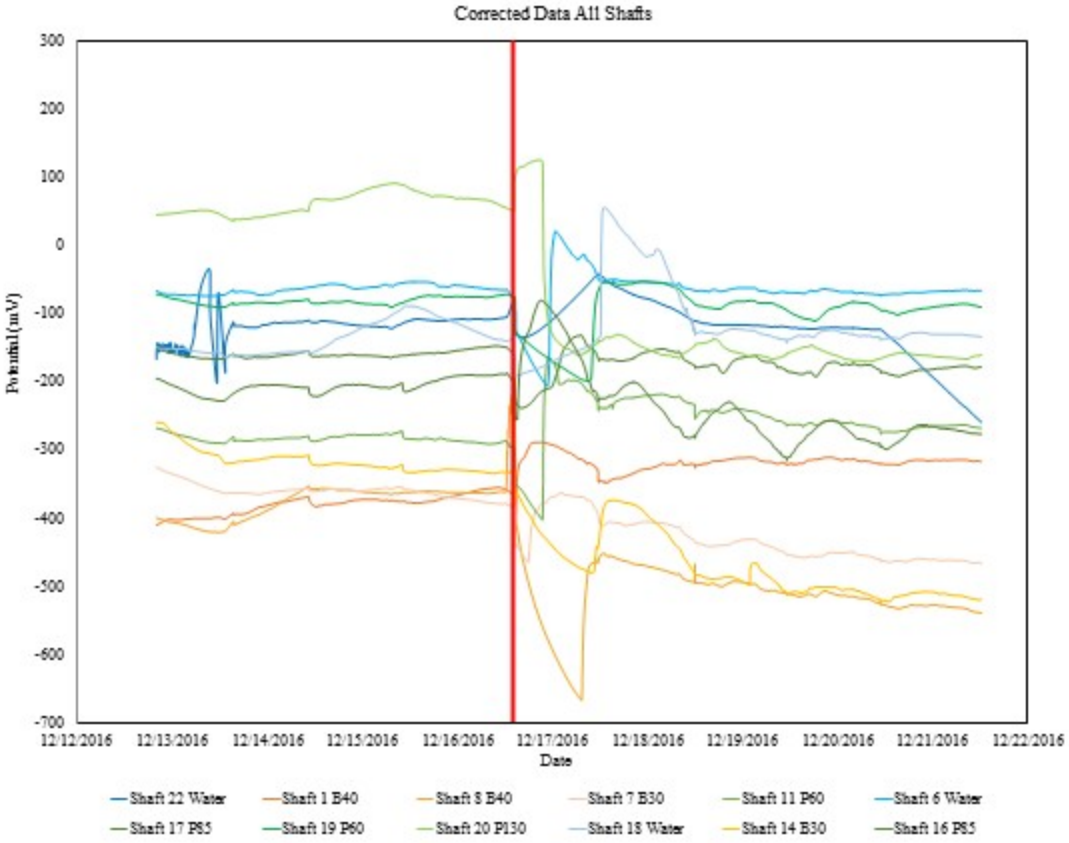

Figure 4.29 Corrected open cell potential data

CHAPTER 5: DISCUSSION AND RECOMMENDATIONS

The general school of thought in construction is that if all quality control and best management practices have been followed, the finished result will meet the design intention. In many instances this logic holds true, however drilled shaft construction is primarily completed both underwater and underground which introduces a level of uncertainty. The research in this thesis emerged from the initial recognition that current construction methods and materials may be having a negative effect on the durability of drilled shafts that has heretofore gone unnoticed.

Durability describes the ability of a material to resist wear and decay. One way to quantify durability in concrete in drilled shafts is to assess the quality of protection that the concrete is providing to the encased reinforcement. Certain materials used to stabilize the excavation during drilled shaft construction have been shown to cause a surface anomaly known as quilting (Figure 5.1). Quilting can create direct pathways for the transmission of environmental chlorides into the network of reinforcing steel, negating the protective qualities of the concrete cover. Final quantification of durability is achieved by correlating the stabilization material used with the corrosion potential of the encased steel.

Corrosion potential data was collected using two electro-chemical methods. The first employed a copper-copper sulfate electrode and data was collected on an eighty-point grid in order to map changes in potential across a portion of the surface. The second method consisted of a titanium reference electrode suspended in a water-filled tank on the surface of the shaft. This test was conducted over the course of eight to ten days and served the purpose of showing how the

corrosion potential varied with time and with the eventual introduction of chlorides. Prior to electro-chemical testing all shafts were tested using mutual potential and mutual resistance measurements to determine the quality of connection in the steel reinforcement system.

5.1 Connection Quality

When the mutual potential is graphed against the mutual resistance, the data is banded along the zero millivolt potential line horizontally and just past the 100-Ω resistance line vertically. The data points scattered along the potential axis between zero and five are generally indicative of a well-connected system as this reading reflects a negligible potential difference across the system. The data points above five millivolts that are also above 29 Ω would generally indicate a poorly connected system as they exceed the inherit resistance between two pieces of reinforcing steel and exhibit a loss in potential across the system. The points of particular interest are the ones positioned at the base of the vertical band in the data (Figure 5.2). These points have a resistance over 100-Ω but show negligible loss of potential.

The initial assumption that these high resistance, zero potential points were statistical scatter was disproven when the sample data distribution for all points over 100 Ω was plotted against the normal standard distribution curve for the same data range (Figure 5.3). The normal distribution curve shows a 5% occurrence of points within the -5mV to 5mV range. The sample data distribution shows that the actual percentage of points in that range is 15% (Figure 5.4). This is three times the expected distribution. As of yet it is uncertain what causes this phenomenon but further research is recommended. This work could have extended impacts into the diagnosis of system connection prior to the application of cathodic protection. Current common practice relies on the use of mutual resistance or mutual potential to determine connectivity; this data proves that using only one type of testing may be insufficient to conclusively make that determination.

Another key relationship identified through examination of the mutual potential versus mutual resistance graph is the correlation between bentonite slurry viscosity and electro connectivity. As the viscosity value increases from 30 seconds to 90 seconds, the average potential value decreases from 22.57mV to 0.17mV (Figures 5.5-5.9). This could indicate two things: 1) concrete more easily displaces high viscosity bentonite slurry leaving no residue between the reinforcing bars or 2) high viscosity bentonite slurry has enough inherent electrical conductivity to convey the induced charge through the residue without an identifiable potential difference. Both of these scenarios warrant further investigation.

5.2 Corrosion Potential Surface Mapping

The corrosion potential surface mapping data was analyzed for each specimen individually. Statistical methods were used to plot a distribution curve and determine the 50^{th} percentile corrosion potential for every shaft. Surface mapping summary sheets showing this work and the potential maps can be found in Appendix B.

ASTM C876 states that a potential reading below -350mV indicates a 90% chance of corrosion so it is generally used as the threshold for corrosion activity. When the 50^{th} percentile corrosion potential is plotted against the slurry viscosity distinct divisions become apparent (Figure 5.10); seven of the 13 shafts cast with bentonite slurry fell below the -350mV threshold where none of the shafts cast with polymer did. This is a clear indicator that shafts cast using bentonite slurry are more prone to corrosion than shafts casts using the subject polymer. Recall that the surface potential measurements were taken with a freshwater wetted surface and when no chlorides had been introduced. It is likely that in the presence of chlorides more of the shafts would have crossed the threshold.

5.3 Open Cell Corrosion Potential

Recalling from chapter 2, there are three necessary components required for chloride induced corrosion: oxygen, moisture and chloride. Open cell corrosion potential testing examines how well concrete cover inhibits the introduction of chlorides. For the first four days of testing the open cell tanks were filled with fresh water to establish a baseline corrosion potential for each shaft. On day five the fresh water was replaced with a chloride solution and the potential showed an immediate change (Figure 5.11). This change, if sustained in a downward trend can indicate a direct channel between the surface of the concrete and the encased reinforcement. The shafts constructed using water and polymer slurry showed no appreciable change in potential (Figure 5.12, 5.13). The shafts constructed using bentonite showed a distinct downward trend in corrosion potential after the introduction of chlorides, falling below the -350mV threshold (Figure 5.14). These data reinforce the result from the surface potential mapping and further supports the connection between increased propensity for corrosion and the use of bentonite slurry during construction.

5.4 Recommendations for Future Work

Further topics of study include the continued examination of low potential-high resistance readings in reinforcement systems in order to determine the mechanism causing the anomaly. Also, exploration into the physical and chemical properties of quilted concrete with an emphasis on the depth of influence and methods of prevention. This would further quantify the relationship between slurry and durability and assist the industry in making procedural or policy decisions moving forward.

Figure 5.1 Reflective quilting exhibited in a drilled shaft test specimen

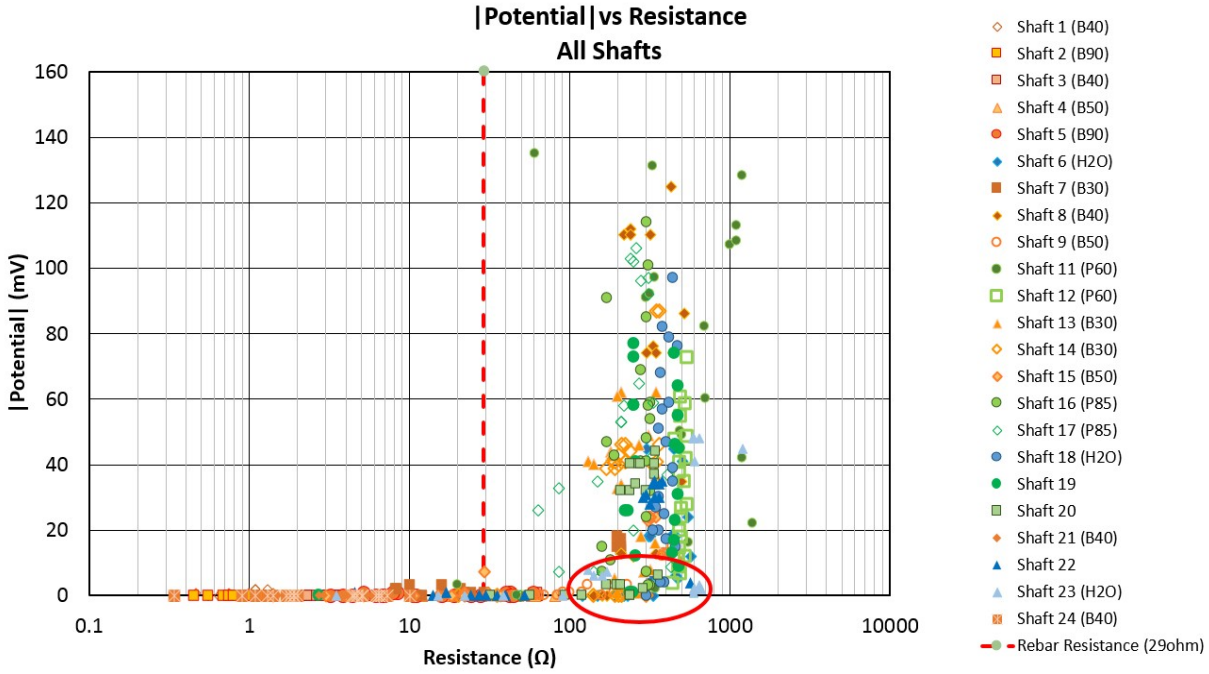

Figure 5.2 Mutual potential vs. mutual resistance area of interest

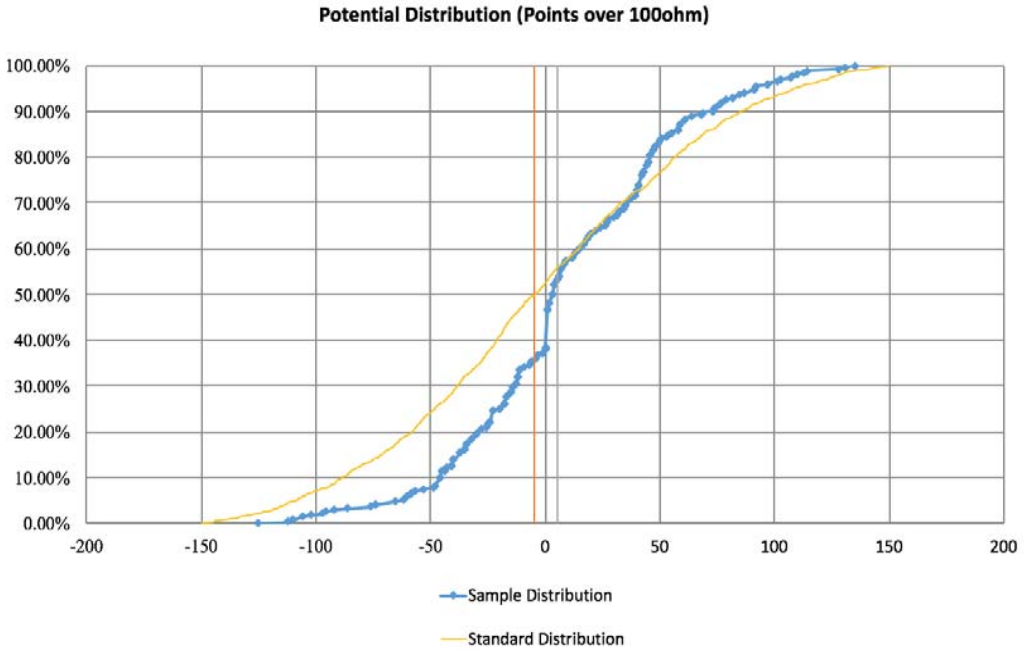

Figure 5.3 Potential distribution shown with standard distribution

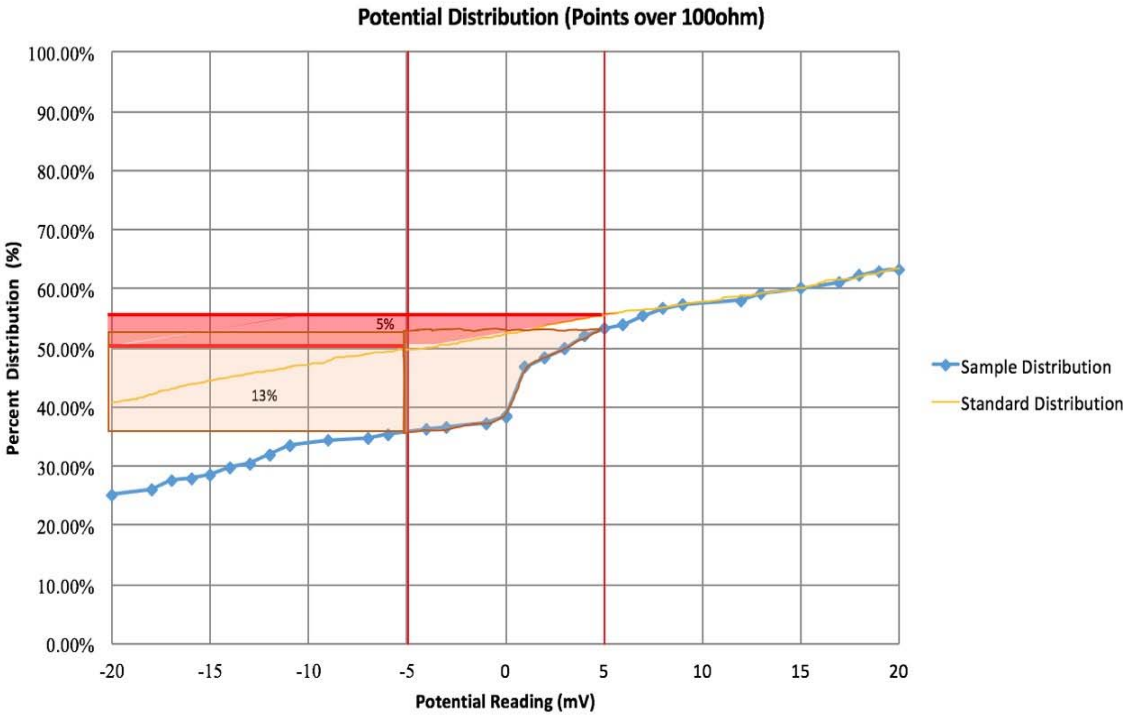

Figure 5.4 Area of interest detail

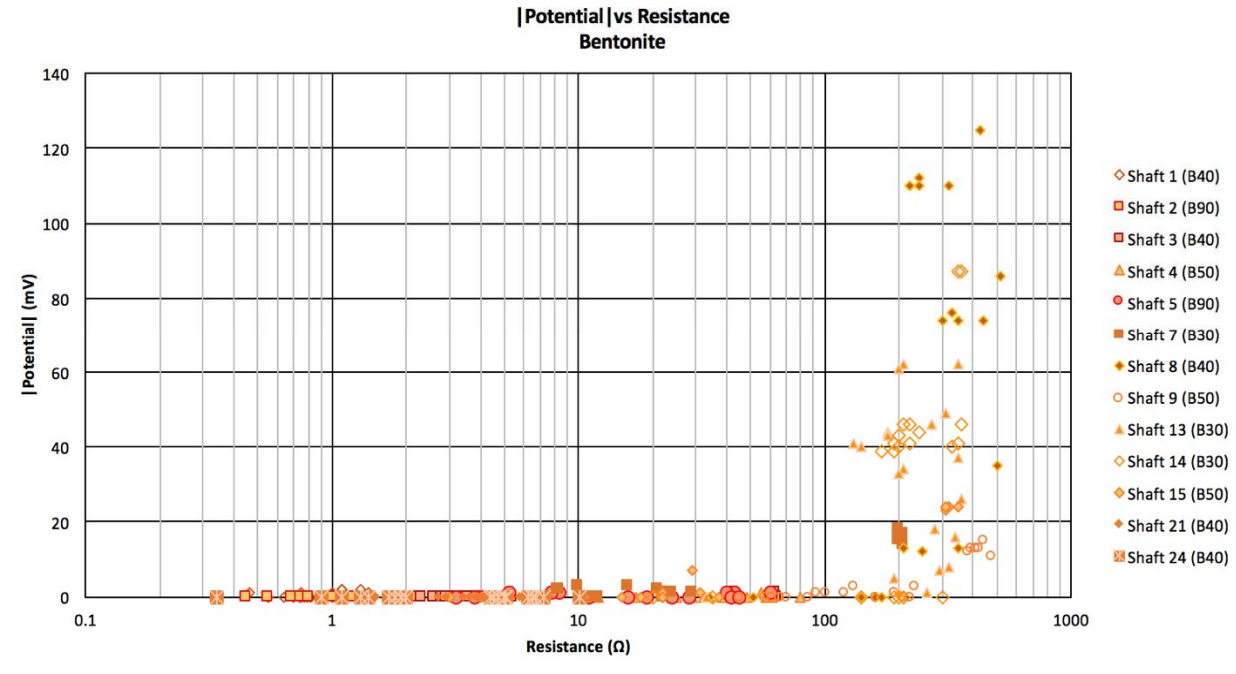

Figure 5.5 Data from all shafts cast in bentonite

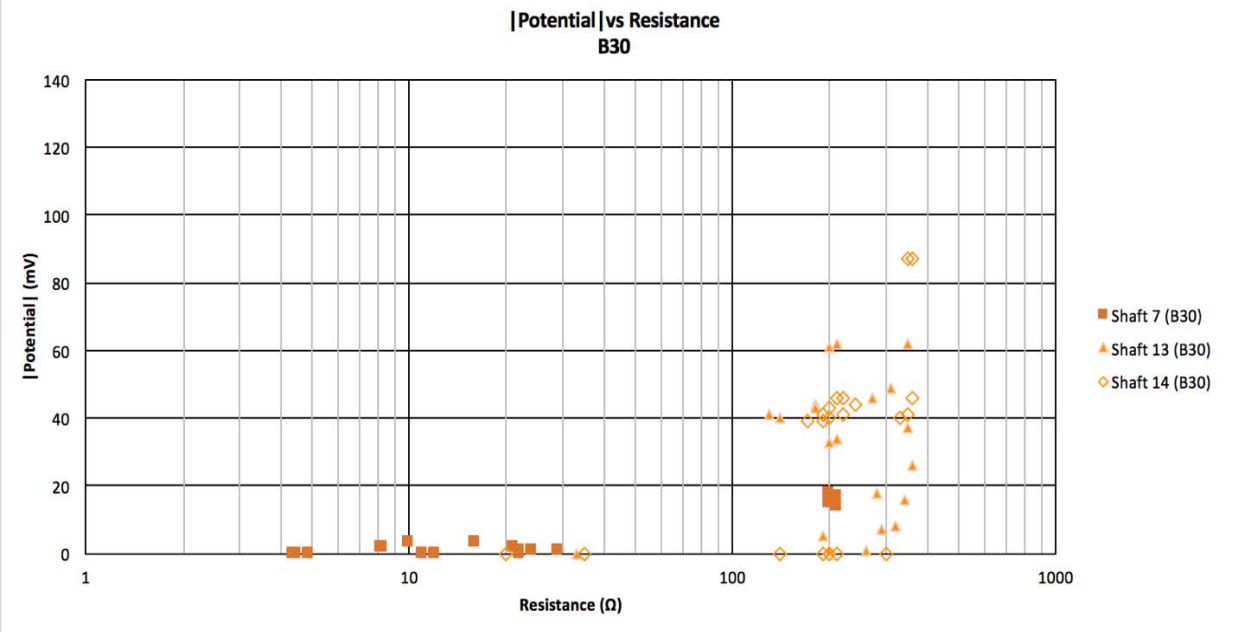

Figure 5.6 Data from shafts cast in 30 second bentonite

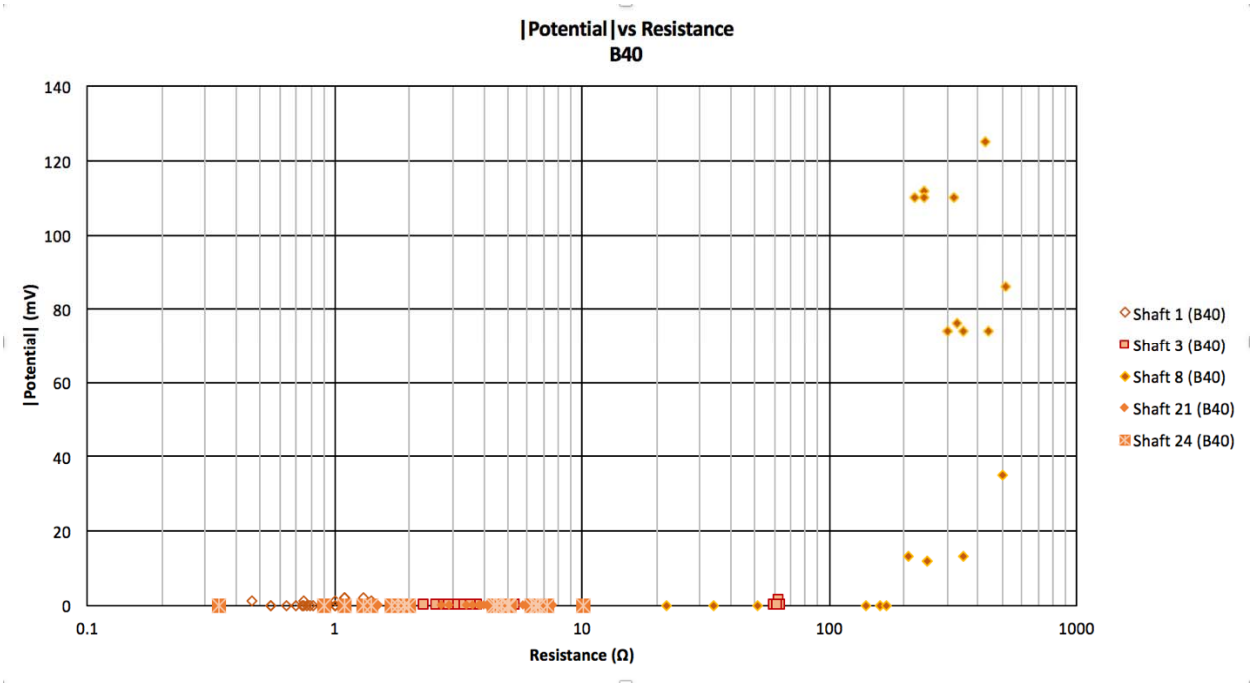

Figure 5.7 Data from shafts cast in 40 second bentonite

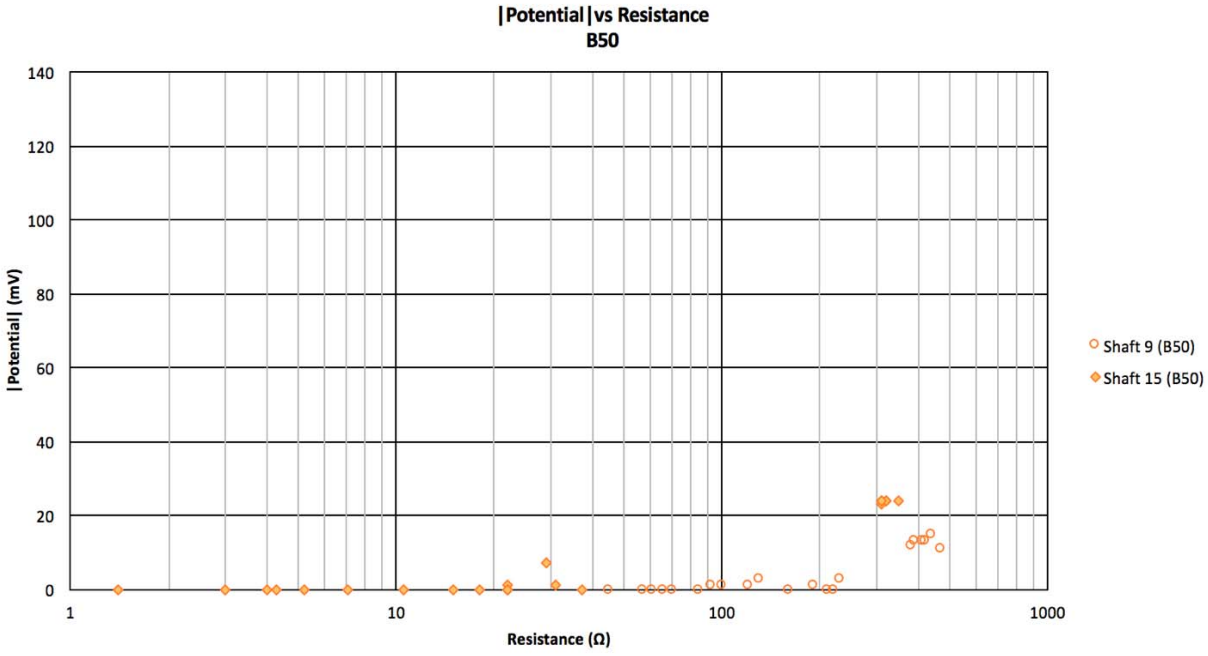

Figure 5.8 Data from shafts cast in 50 second bentonite

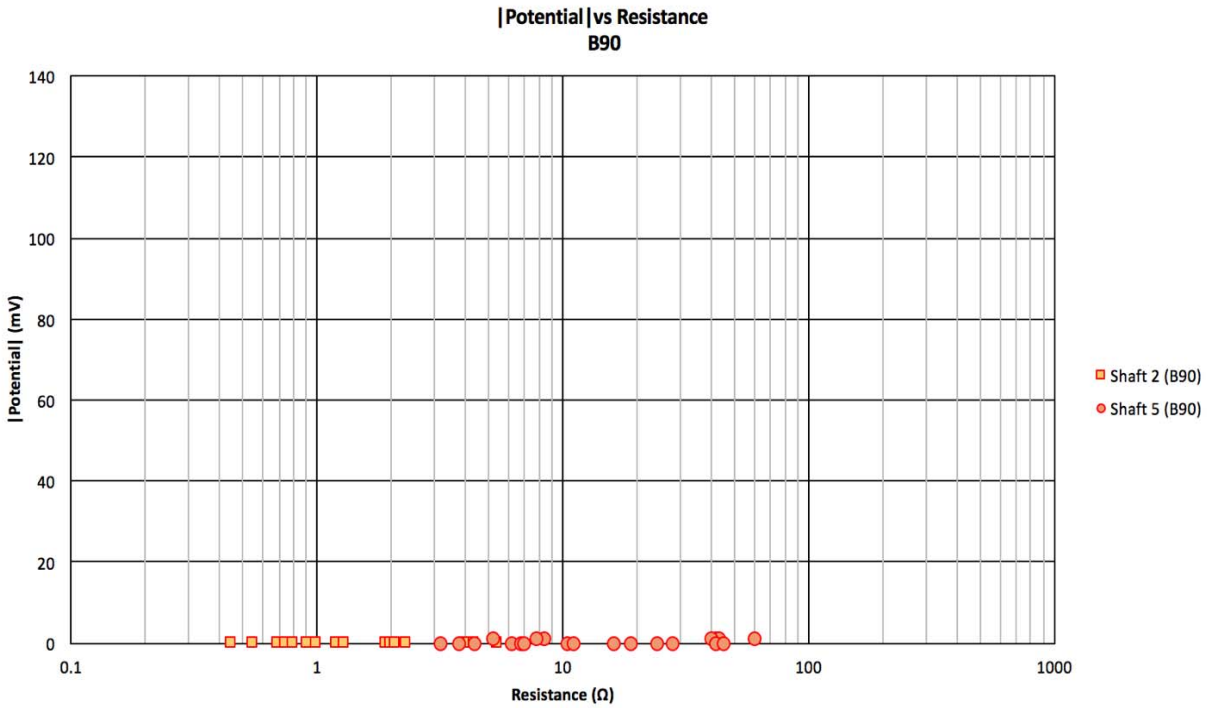

Figure 5.9 Data from shafts cast in 90 second bentonite

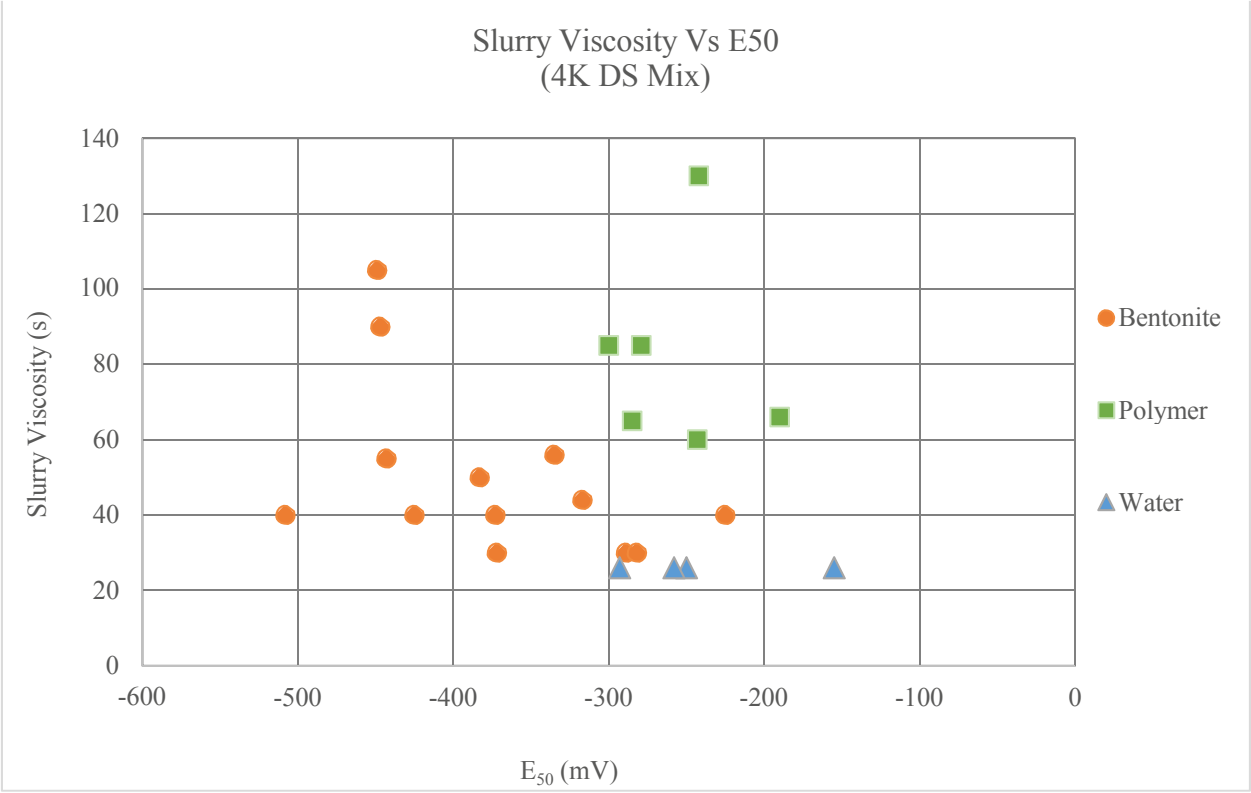

Figure 5.10 Slurry viscosity vs 50th percentile corrosion potential

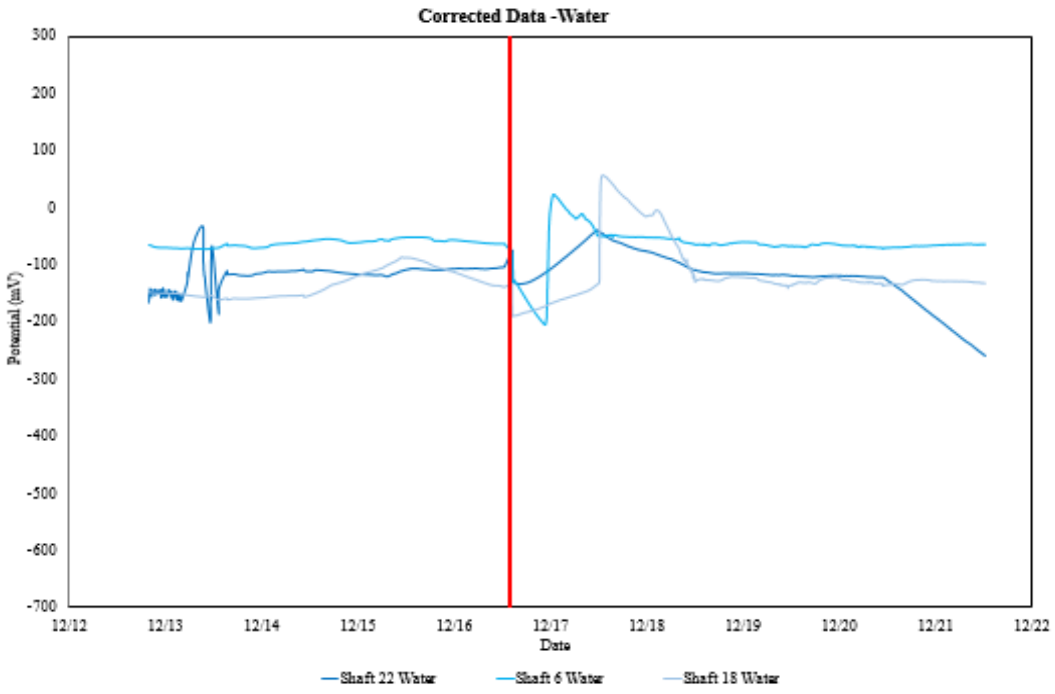

Figure 5.11 Open cell potential –no slurry

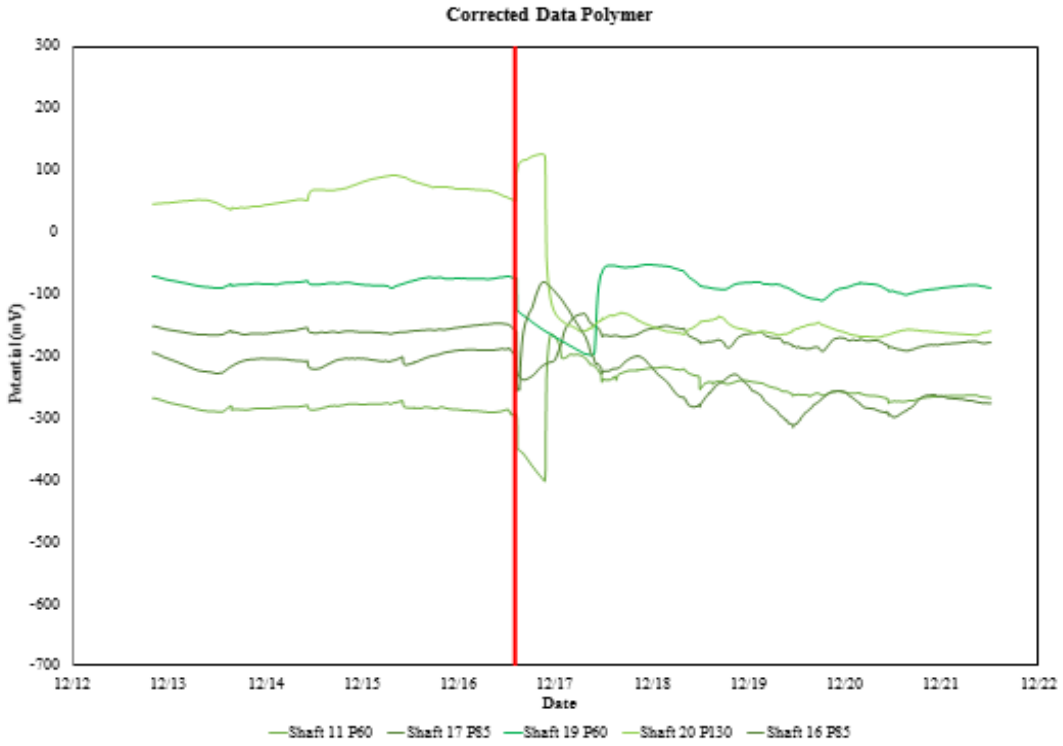

Figure 5.12 Open cell potential- polymer slurry

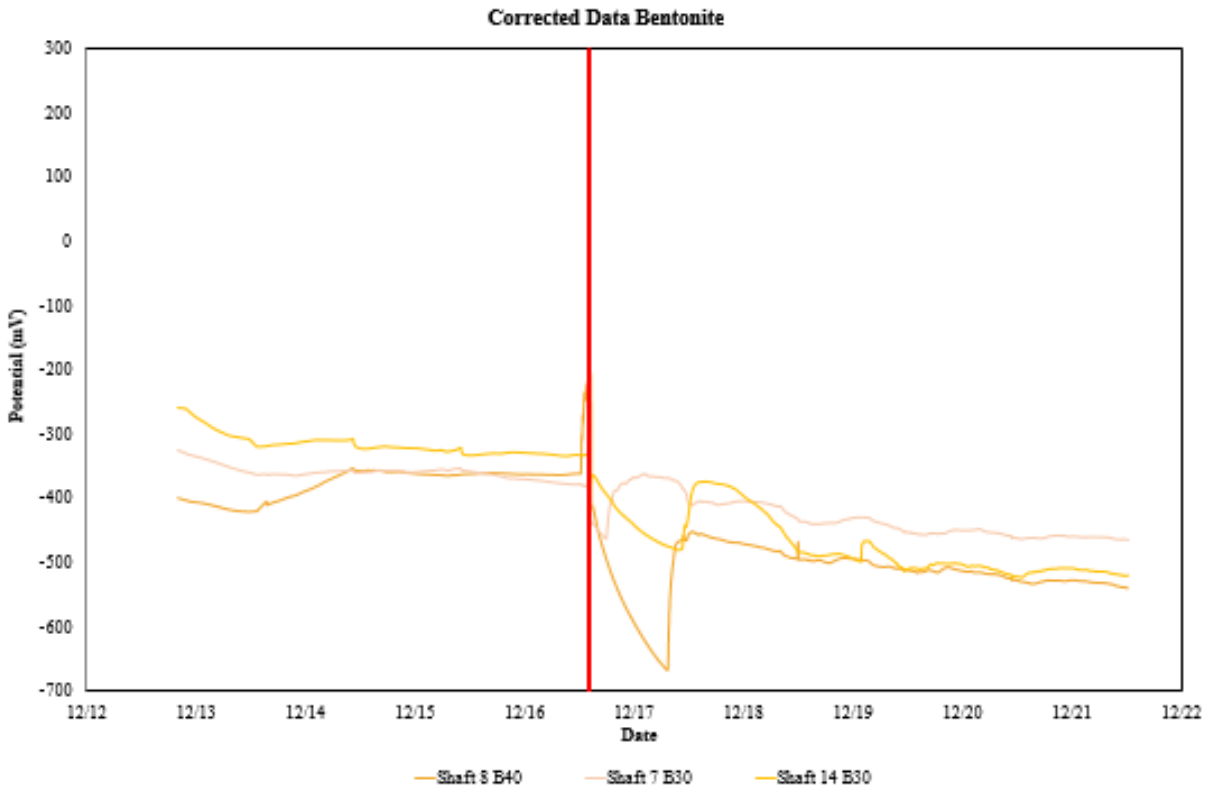

Figure 5.13 Open cell potential – bentonite slurry

CHAPTER 6: CONCLUSIONS

- Initial screening for electro-connectivity of the reinforcement systems in drilled shafts revealed areas with a high resistance that would indicate poor connection quality but a potential difference of zero. The occurrence of these high resistance/zero potential difference points was three times more likely than what might be expected for normally occurring statistical scatter. The source of this phenomena requires further investigation.
- When the 50th percentile corrosion potential is plotted against the slurry viscosity distinct divisions become apparent. Seven of the 13 shafts cast with bentonite slurry fall below the -350mV line in a freshwater environment where none of the shafts cast with polymer did. This is a clear indicator that shafts cast using bentonite slurry are more prone to corrosion than shafts casts using the subject polymer.
- Shafts constructed using bentonite show a distinct downward trend in corrosion potential after the introduction of chloride, falling and continuing to fall below the -350mV threshold (Figure 5.14). These data reinforce the result from the surface potential mapping and further support the connection between increased propensity for corrosion and the use of bentonite slurry during construction.

REFERENCES

ASTM C876-09: *Standard Test Method for Corrosion Potentials of Uncoated Reinforcing Steel in Concrete* Annual Book of ASTM Standards, ASTM International, West Conshohocken, Pennsylvania.

Beckhaus, K. (2016). *EFFC/DFI Best Practice Guide to Tremie Concrete for Deep Foundations* (1st ed.). Hawthorne, NJ: Deep Foundations Institute.

Brown, D. A., Turner, J. P., & Castelli, R. J. (2010). *Drilled shafts: construction procedures and LRFD design methods*. McLean, VA: U.S. Dept. of Transportation, Federal Highway Administration.

Carino, N.J. (1999). "Nondestructive Techniques to Investigate Corrosion Status in Concrete Structures." *Journal of Performance of Constructed Facilities. ,Vol. 13*(3), pp. 96-106.

Cicek, V. (2013). *Cathodic protection: Industrial solutions for protecting against corrosion*. Hoboken, NJ: John Wiley & Sons.

Florida Department of Transportation (2016). *Soils and Foundations Handbook.* State Materials Office, Gainesville, Florida.

Fontana, M.G. (1986). *Corrosion engineering*. New York: McGraw-Hill.

Mullins, G., Sosa, R., Sen, R., and Issa, M. (2009). "Seal Slab / Steel Pile Interface Bond from Full-Scale Testing," Deep Marine Foundations, A Perspective on the Design and Construction of Deep Marine Foundations, Deep Foundations Institute, ISBN: 978-0-9763229, 277-288.

Mullins, G. and Winters, D. (2014)."Defining the Upper Viscosity Limit for Mineral Slurries used in Drilled Shaft Construction", FDOT Project No. BDK84-977-24, Final Report, 264 pp.

O'Neill, M.W., and Reese, L.C. (1999). "Drilled Shafts: Construction Procedures and Design Methods," Publication No. FHWA-IF-99-025, Federal Highway Administration, Washington, D.C., 758 p.

Ribeiro, D., and Abrantes, J. (2016). "Application of electrochemical impedance spectroscopy (EIS) to monitor the corrosion of reinforced concrete: A new approach." *Construction and Building Materials,* Vol. *111*. pp. 98-104.

Sagüés, A. A. (2004). Corrosion of Metals in Concrete. *Galvanized Steel Reinforcement in Concrete,* 71-86. doi:10.1016/b978-008044511-3/50018-9

Sagüés, A. A., & Kranc, S. C. (2002). Decreased Corrosion Initiation Time of Steel in Concrete due to Reinforcing Bar Obstruction of Diffusional Flow. *ACI Materials Journal,99*(1). doi:10.14359/11316

Sagüés, A.A., Pech-Canul , M., and Al-Mansur, A.S. (2003). "Corrosion macrocell behavior of reinforcing steel in partially submerged concrete columns." *Corrosion Science. pp 45*(1), 7-32.

Walsh,V. and Sagüés, A. A. (2016). "Steel Corrosion in Submerged Concrete Structures - Part 1: Field Observations and Corrosion Distribution Modeling." *Corrosion,* 518-533.

APPENDIX A: DATA COLLECTION SHEET

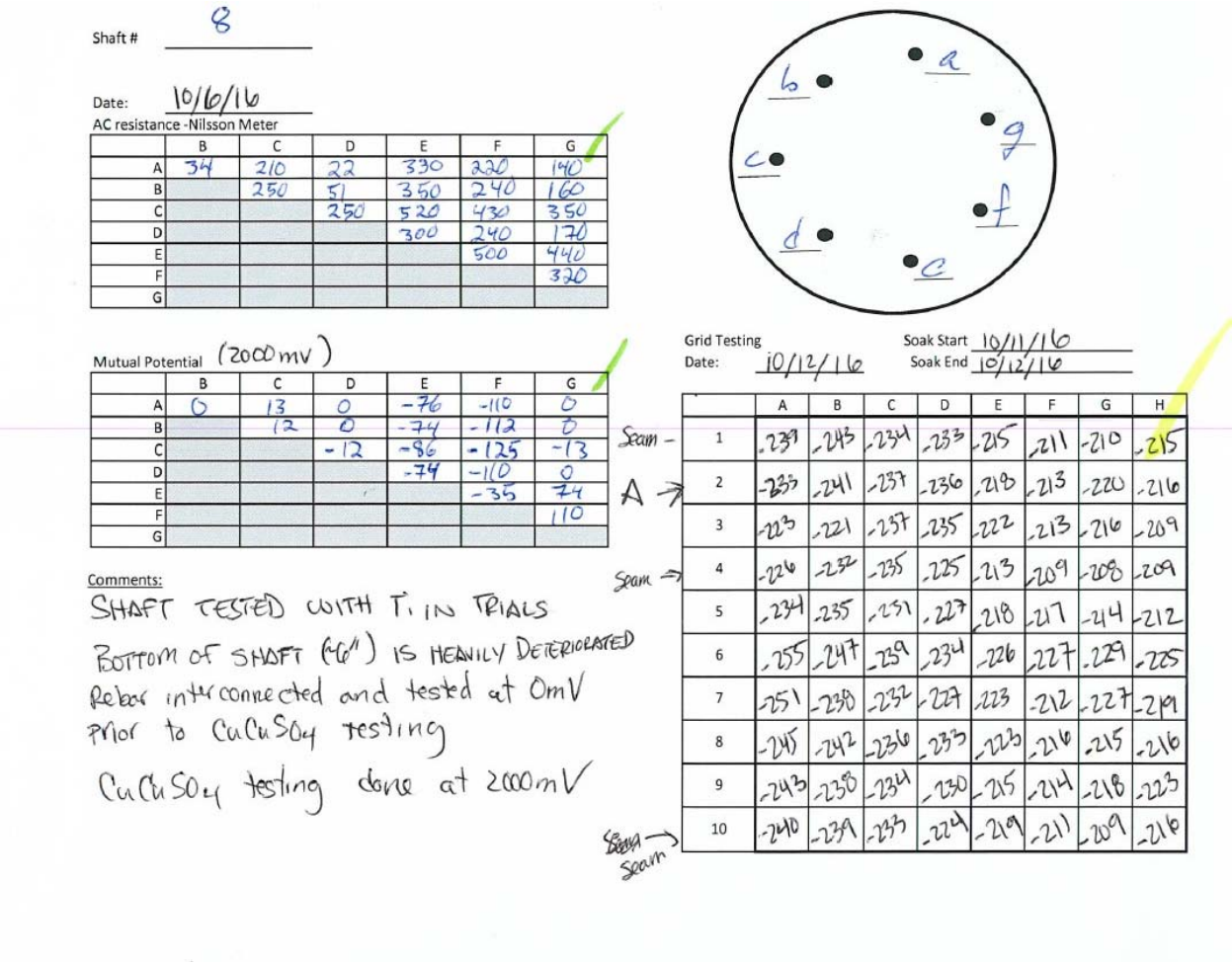

Shaft # 8

Date: 10/6/16

AC resistance -Nilsson Meter

	B	C	D	E	F	G
A	34	210	22	330	220	140
B		250	51	350	240	160
C			250	520	430	350
D				300	240	170
E					500	440
F						320
G						

Mutual Potential (2000mv)

	B	C	D	E	F	G
A	0	13	0	-76	-110	0
B		12	0	-74	-112	0
C			-12	-86	-125	-13
D				-74	-110	0
E					-35	74
F						110
G						

Comments:

SHAFT TESTED WITH Ti IN TRIALS

BOTTOM OF SHAFT (66") IS HEAVILY DETERIORATED

Rebar interconnected and tested at 0mV prior to CuCuSO4 testing

CuCuSO4 testing done at 2000mV

Grid Testing Date: 10/12/16

Soak Start 10/11/16

Soak End 10/12/16

	A	B	C	D	E	F	G	H
1	-239	-243	-234	-233	-215	-211	-210	-215
2	-235	-241	-237	-236	-218	-213	-220	-216
3	-223	-221	-257	-235	-222	-213	-216	-209
4	-226	-232	-235	-225	-213	-209	-208	-209
5	-234	-235	-251	-227	-218	-217	-44	-212
6	-255	-247	-259	-234	-226	-227	-229	-225
7	-251	-230	-232	-229	-223	-212	-227	-219
8	-245	-242	-236	-233	-223	-216	-215	-216
9	-243	-230	-234	-230	-215	-214	-218	-223
10	-240	-239	-233	-224	-209	-211	-209	-216

Seam – A → Seam → Seam

Figure A.1 Sample data collection sheet for mutual potential/ mutual resistance and surface map testing

APPENDIX B: MUTUAL POTENTIAL AND MUTUAL RESISTANCE DATA

Table B.1. Mutual potential and mutual resistance raw data shafts 1, 2, 3, and 4

	Shaft 1(B40)		Shaft 2 (B90)		Shaft 3 (B40)		Shaft 4 (B50)	
	Resistance (Ω)	|Potential| (mV)	Resistance (Ω)	|Potential| (mV)	Resistance (Ω)	|Potential| (mV)	Resistance (Ω)	|Potential| (mV)
AB	1	0	4	0	63	1	44	0
AC	1.3	0	4	0	5.3	0	25	0
AD	0.64	0	5.4	0	3.2	0	38	0
AE	0.75	0	4	0	2.6	0	32	0
AF	0.55	0	4.2	0	5.3	0	58	0
AG	1	0	4.4	0	3.4	0	80	0
BC	1.4	0	0.45	0	63	0	25	0
BD	0.74	0	2	0	62	0	24	0
BE	0.55	0	0.69	0	60	0	24	0
BF	0.7	0	0.94	0	64	0	41	0
BG	0.79	0	0.91	0	62	0	61	0
CD	1.1	2	1.9	0	4.8	0	17	0
CE	1.3	2	0.55	0	3.8	0	6.6	0
CF	1.1	2	0.75	0	6.6	0	34	0
CG	1.4	1	1	0	5.4	0	55	1
DE	0.75	1	2	0	2.3	0	12	0
DF	0.46	1	2.1	0	4.9	0	24	0
DG	1	1	2.3	0	2.8	0	43	0
EF	0.77	0	0.8	0	3.6	0	29	0
EG	0.82	0	1.2	0	2.9	0	48	0
FG	1	0	1.3	0	5.4	0	61	0

.

Table B.2. Mutual potential and mutual resistance raw data shafts 5, 6, 7, and 8.

	Shaft 5 (B90)		Shaft 6 (H2O)		Shaft 7 (B30)		Shaft 8 (B40)	
	Resistance (Ω)	|Potential| (mV)	Resistance (Ω)	|Potential| (mV)	Resistance (Ω)	|Potential| (mV)	Resistance (Ω)	|Potential| (mV)
AB	42	1	300	48	21	2	34	0
AC	4.4	0	340	6	200	18	210	13
AD	43	1	120	0	8.2	2	22	0
AE	10.5	0	220	0	16	3	330	76
AF	8.4	1	310	18	8.3	2	220	110
AG	5.2	1	230	0	10	3	140	0
BC	7.8	1	510	41	210	17	250	12
BD	60	1	300	45	22	0	51	0
BE	28	0	450	45	29	1	350	74
BF	24	0	550	24	22	1	240	112
BG	19	0	440	46	24	1	160	0
CD	40	1	320	6	200	15	250	12
CE	11	0	470	5	210	14	520	86
CF	6.2	0	570	12	210	14	430	125
CG	3.2	0	460	6	210	15	350	13
DE	42	0	150	0	11	0	300	74
DF	45	0	320	18	4.5	0	240	110
DG	3.8	0	190	0	4.5	0	170	0
EF	16	0	460	18	12	0	500	35
EG	6.8	0	330	0	4.4	0	440	74
FG	7	0	440	19	4.9	0	320	110

Table B.3. Mutual potential and mutual resistance raw data shafts 9, 10 (not available), 11, and 12

	Shaft 9 (B50)		Shaft 10		Shaft 11 (P60)		Shaft 12 (P60)	
	Resistance (Ω)	|Potential| (mV)	Resistance (Ω)	|Potential| (mV)	Resistance (Ω)	|Potential| (mV)	Resistance (Ω)	|Potential| (mV)
AB	92	1	0	0	47	3	470	12
AC	440	15	0	0	20	0	490	7
AD	230	3	0	0	310	107	500	27
AE	120	1	0	0	1000	50	480	41
AF	130	3	0	0	490	91	450	48
AG	100	1	0	0	300	135	490	55
BC	380	12	0	0	61	2	500	24
BD	160	0	0	0	350	113	530	42
BE	66	0	0	0	1100	49	520	59
BF	70	0	0	0	510	97	490	61
BG	45	0	0	0	340	131	540	73
CD	470	11	0	0	330	108	500	18
CE	410	13	0	0	1100	45	510	35
CF	420	13	0	0	500	92	480	38
CG	390	13	0	0	320	128	540	49
DE	210	0	0	0	1200	60	480	15
DF	220	0	0	0	710	16	480	20
DG	190	1	0	0	560	22	540	28
EF	85	0	0	0	1400	42	440	4
EG	57	0	0	0	1200	82	520	12
FG	61	0	0	0	700	36	470	9

Table B.4. Mutual potential and mutual resistance raw data shafts 13, 14, 15, and 16.

	Shaft 13 (B30)		Shaft 14 (B30)		Shaft 15 (B50)		Shaft 16 (P85)	
	Resistance (Ω)	|Potential| (mV	Resistance (Ω)	|Potential| (mV	Resistance (Ω)	|Potential| (mV	Resistance (Ω)	|Potential| (mV)
AB	190	5	200	0	29	7	300	48
AC	180	44	220	46	4.3	0	320	3
AD	210	34	200	43	7.1	0	320	59
AE	130	41	140	0	18	0	190	43
AF	210	62	35	0	3	0	320	32
AG	33	0	190	39	310	24	320	54
BC	310	49	360	46	22	1	280	41
BD	350	37	350	41	31	1	300	114
BE	270	46	190	0	37	0	170	91
BF	350	62	210	0	22	0	300	85
BG	200	1	330	40	350	24	310	101
CD	320	8	360	87	5.2	0	280	69
CE	260	1	210	46	15	0	170	47
CF	340	16	240	44	1.4	0	300	41
CG	180	43	350	87	310	23	310	58
DE	290	7	190	41	22	0	160	15
DF	360	26	220	41	4	0	300	24
DG	200	33	300	0	320	24	310	3
EF	280	18	20	0	10.5	0	160	7
EG	140	40	170	39	320	24	180	11
FG	200	61	200	40	310	24	300	7

Table B.5. Mutual potential and mutual resistance raw data shafts 17, 18, 19, and 20.

	Shaft 17 (P85)		Shaft 18 (H2O)		Shaft 19 (P60)		Shaft 20 (P130)	
	Resistance (Ω)	|Potential| (mV	Resistance (Ω)	|Potential| (mV	Resistance (Ω)	|Potential| (mV	Resistance (Ω)	|Potential| (mV)
AB	280	96	380	82	450	17	120	0
AC	430	9	440	39	470	55	240	0
AD	410	37	460	15	250	58	32	0
AE	310	92	470	76	470	31	240	32
AF	330	59	440	97	480	45	270	40
AG	310	97	370	68	250	58	200	3
BC	240	103	360	30	450	74	240	0
BD	210	53	380	57	250	77	57	0
BE	49	0	390	4	460	46	260	34
BF	64	26	360	20	470	64	280	40
BG	86	7	300	0	250	73	210	3
CD	330	43	390	25	240	1	94	0
CE	250	102	440	35	460	23	300	32
CF	270	65	400	47	480	9	340	40
CG	260	106	350	27	245	1	290	2
DE	210	53	420	59	230	26	210	32
DF	250	20	420	79	260	12	240	40
DG	220	58	360	51	2.7	0	170	3
EF	86	33	400	17	440	13	360	6
EG	140	7	370	4	220	26	340	37
FG	150	35	330	20	260	41	350	44

Table B.6. Mutual potential and mutual resistance raw data shafts 21, 22, 23, and 24.

	Shaft 21 (B40)		Shaft 22 (H2O)		Shaft 23 (H2O)		Shaft 24 (B40)	
	Resistance (Ω)	|Potential| (mV)	Resistance (Ω)	|Potential| (mV)	Resistance (Ω)	|Potential| (mV)	Resistance (Ω)	|Potential| (mV)
AB	3.9	0	4.5	1	140	6	10.1	0
AC	3.4	0	300	31	640	3	6.5	0
AD	4.6	0	17	1	130	8	7.2	0
AE	7.2	0	340	35	170	7	6.5	0
AF	7	0	27	0	610	41	6.2	0
AG	5.8	0	30	0	160	6	6.7	0
BC	0.34	0	290	30	600	1	4.7	0
BD	1.7	0	14	0	3.5	0	4.4	0
BE	4.1	0	330	34	10	0	5	0
BF	3.8	0	24	0	590	48	4.5	0
BG	2.9	0	27	0	22	0	5.1	0
CD	1.5	0	320	28	600	2	1.3	0
CE	4	0	560	4	610	2	1.9	0
CF	3.6	0	340	30	1200	45	1.4	0
CG	2.7	0	360	30	670	2	1.7	0
DE	5.2	0	340	34	15	0	1.1	0
DF	4.9	0	35	0	600	48	0.34	0
DG	3.9	0	40	0	90	0	2	0
EF	7.6	0	360	34	600	48	0.9	0
EG	6.4	0	380	35	38	0	1.8	0
FG	5.9	0	52	0	650	48	1.9	0

APPENDIX C: SURFACE MAPPING SUMMARY SHEETS

Summary Shaft #1	
Mix	4K DS
Slurry	B40
Avg. Pull out Strength	57.234 Kips
E_{50}	-317mV

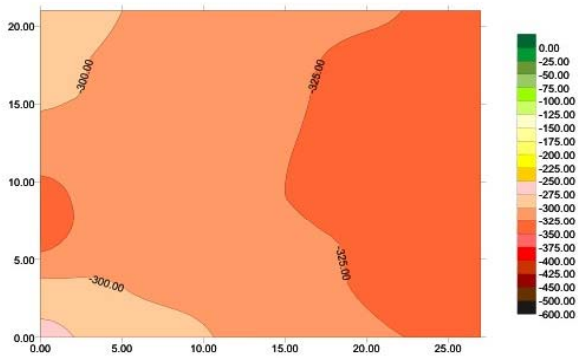

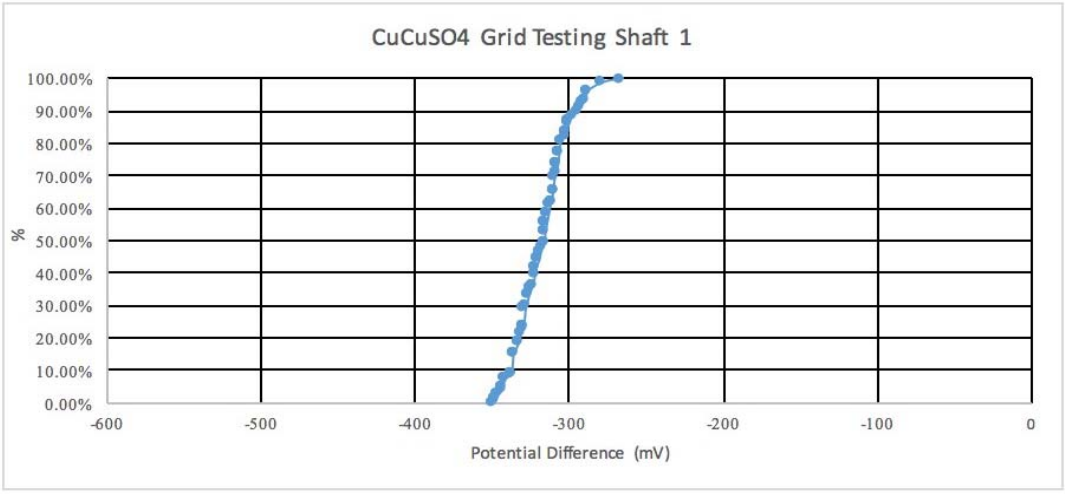

Figure C.1 Shaft 1

Summary Shaft #2	
Mix	4K DS
Slurry	B90
Avg. Pull out Strength	49.704 kips
E_{so}	-449mV

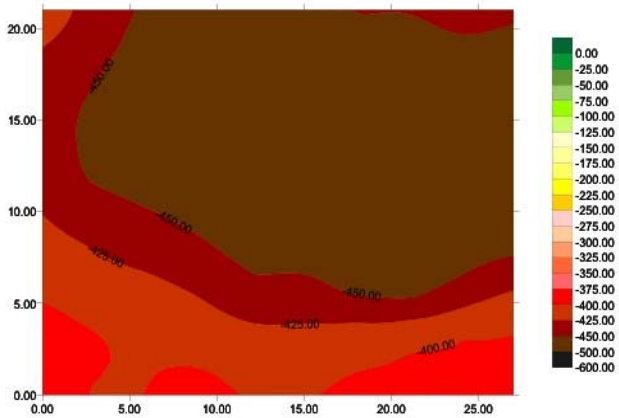

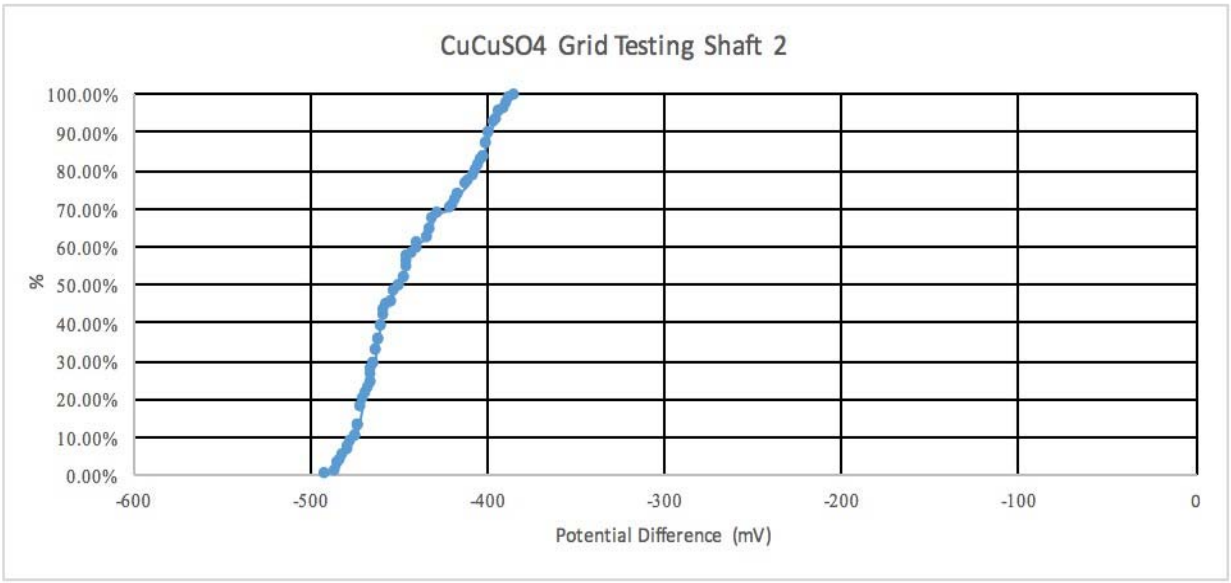

Figure C.2 Shaft 2

Summary Shaft #3	
Mix	4K DS
Slurry	B40
Avg. Pull out Strength	36.894 kips
E_{50}	-373 mV

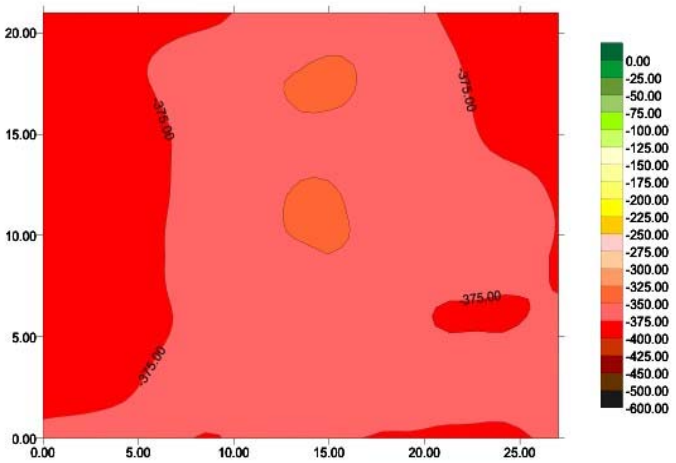

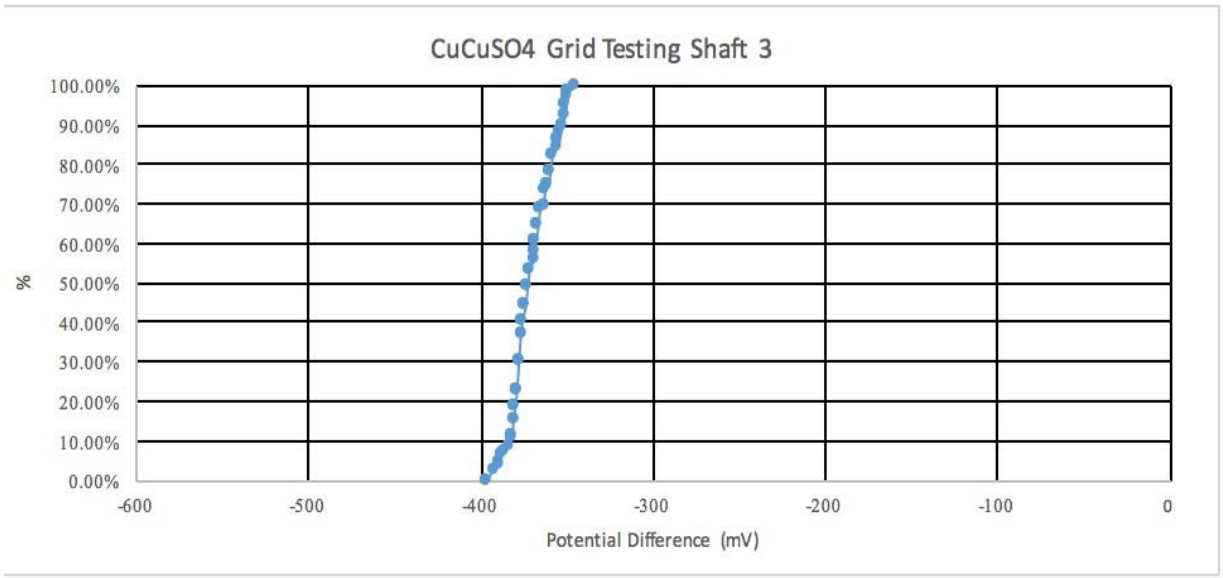

Figure C.3 Shaft 3

Summary Shaft # 4	
Mix	4K DS
Slurry	B50
Avg. Pull out Strength	32.697 kips
E_{so}	-443mV

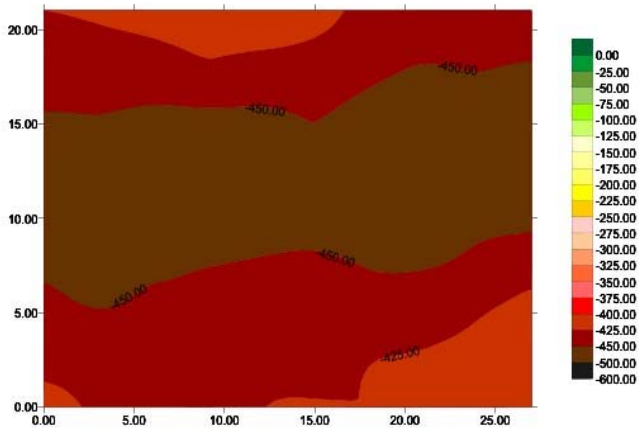

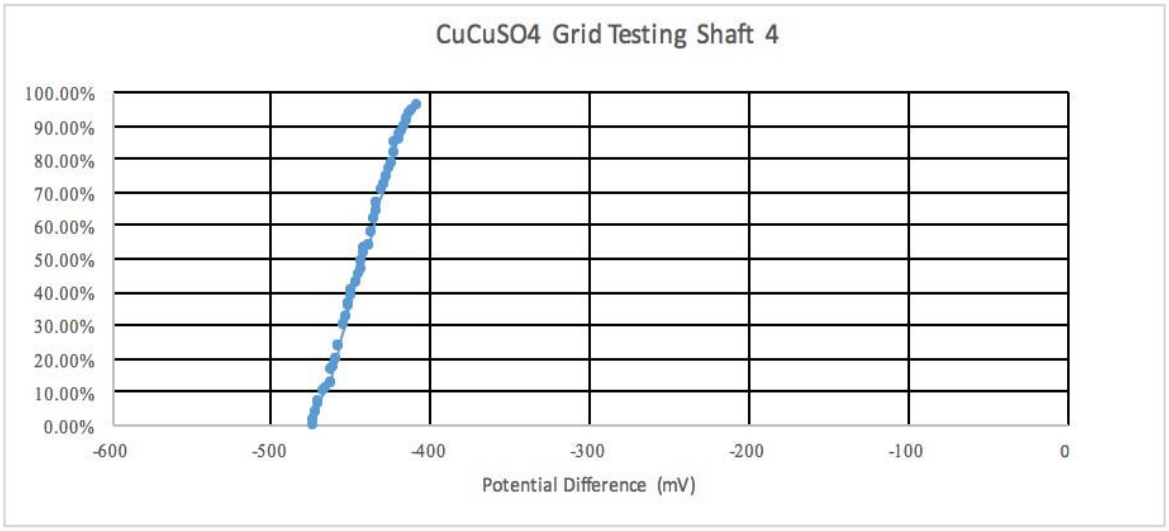

Figure C.4 Shaft 4

Summary Shaft #5	
Mix	4KDS
Slurry	B90
Avg. Pull out Strength	38.094
E_{50}	-447mV

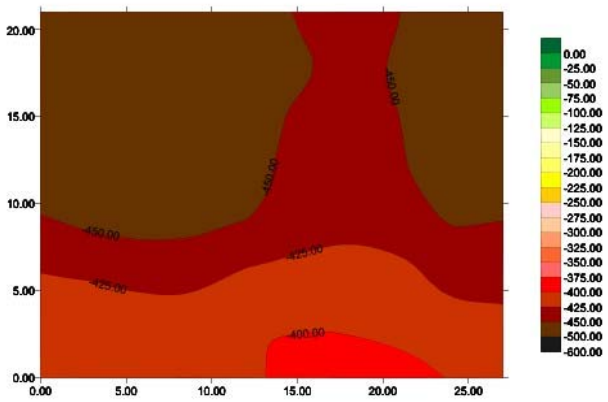

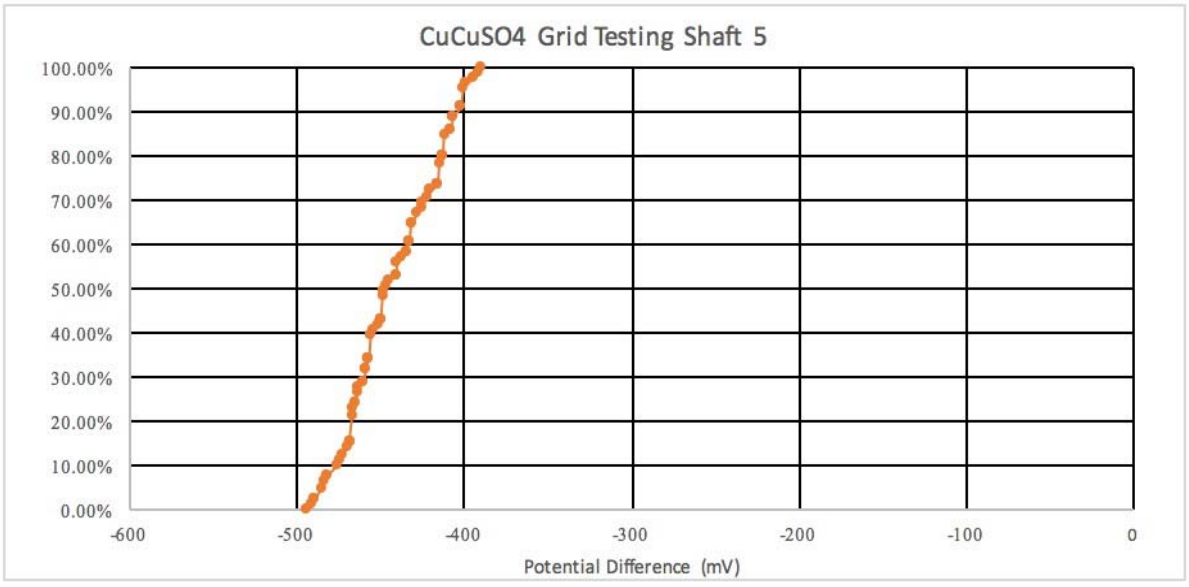

Figure C.5 Shaft 5

Summary Shaft #6	
Mix	4KDS
Slurry	H20
Avg. Pull out Strength	54.304 kips
E_{50}	-155mV

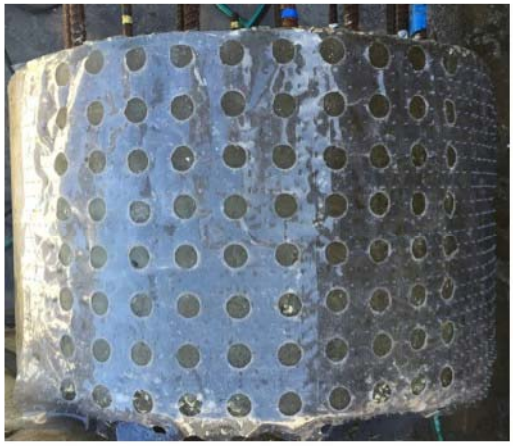

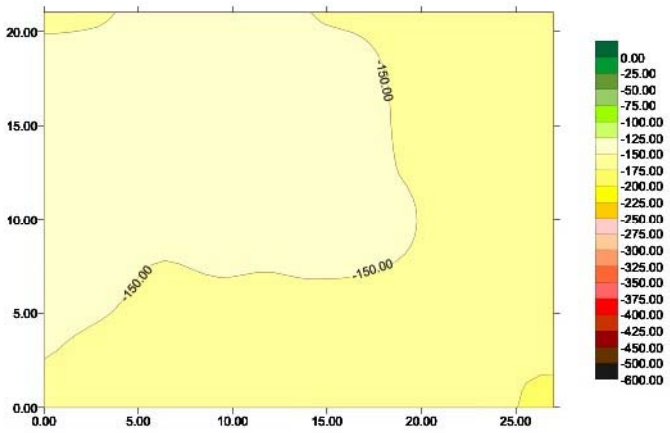

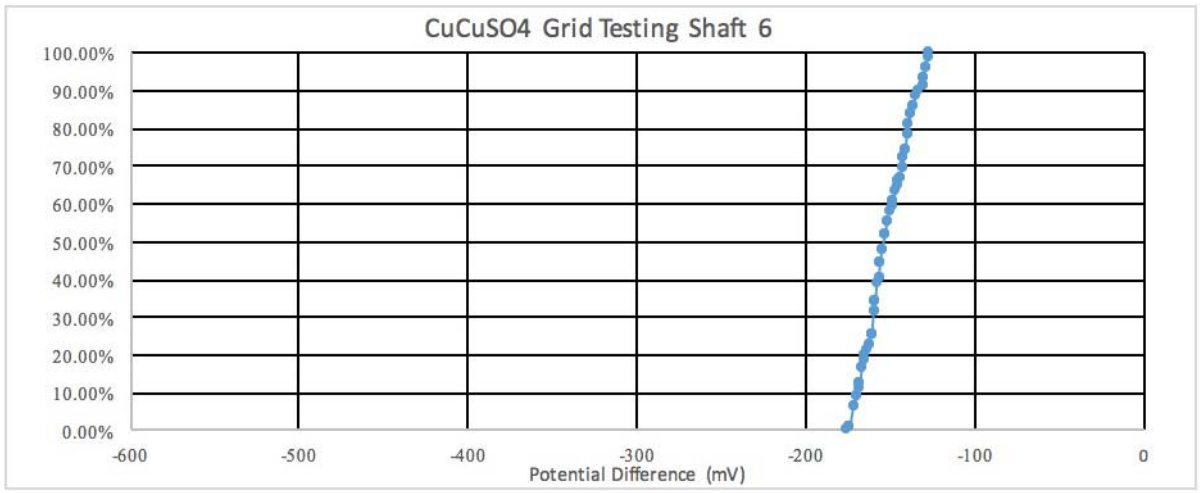

Figure C.6 Shaft 6

Summary Shaft #7	
Mix	4KDS
Slurry	B30
Avg. Pull out Strength	28.754 kips
E_{50}	-372mV

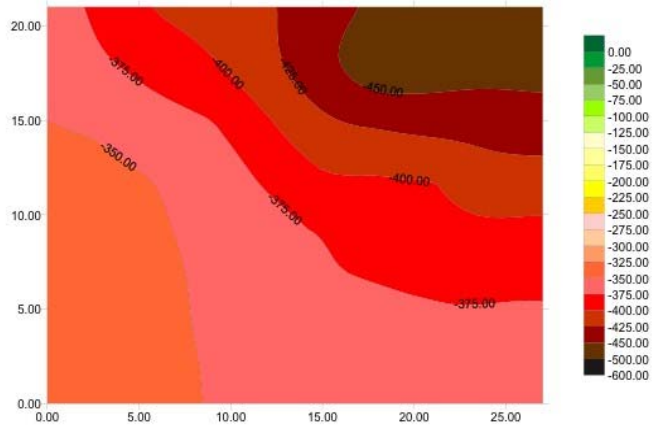

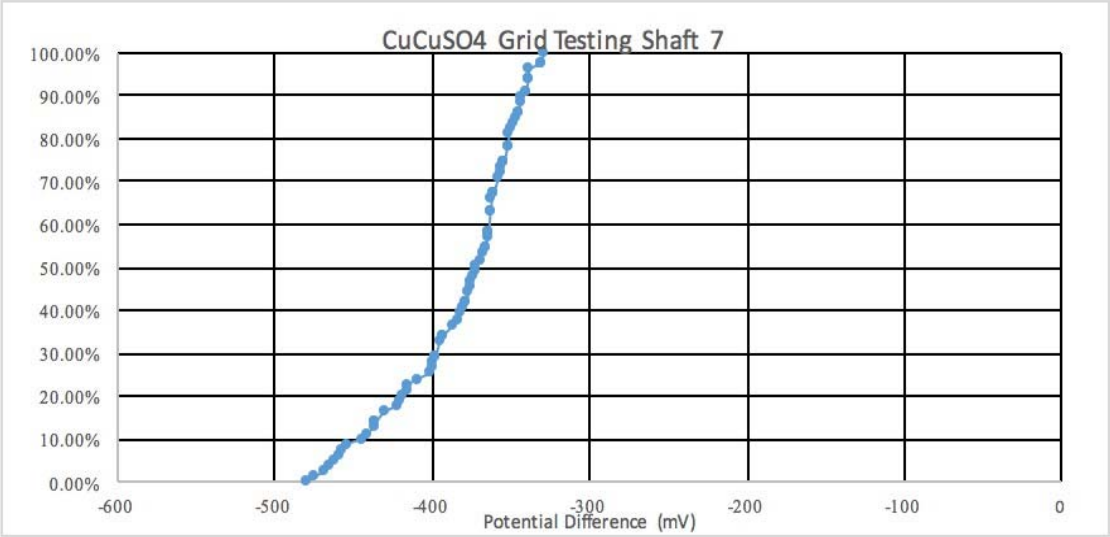

Figure C.7 Shaft 7

Summary Shaft #8	
Mix	4KDS
Slurry	B40
Avg. Pull out Strength	24.212 kips
E_{50}	-225mV

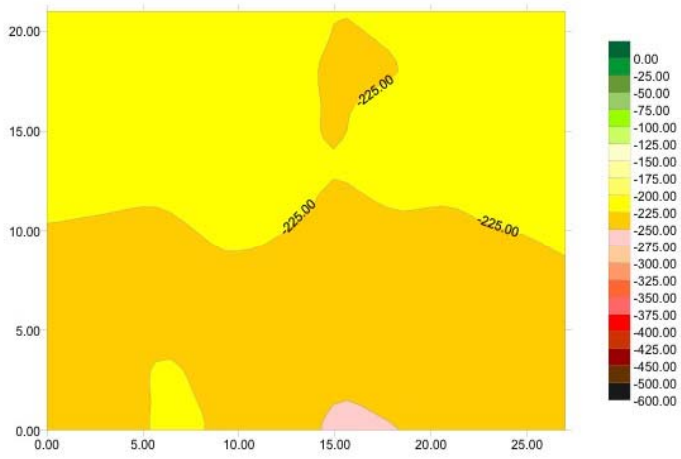

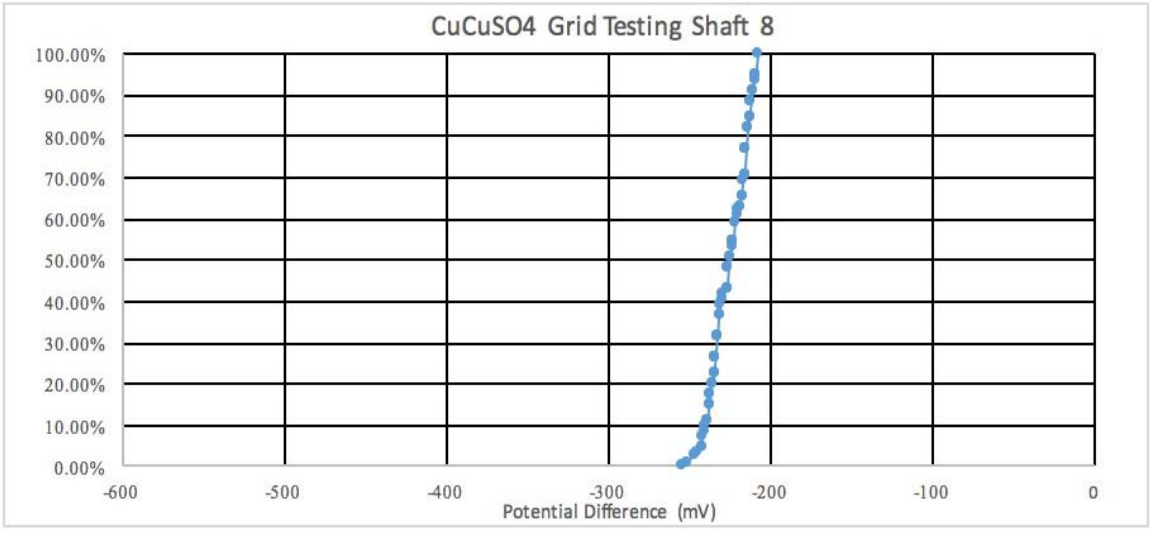

Figure C.8 Shaft 8

Summary Shaft #9	
Mix	4KDS
Slurry	B50
Avg. Pull out Strength	20.524 kips
E_{50}	-383

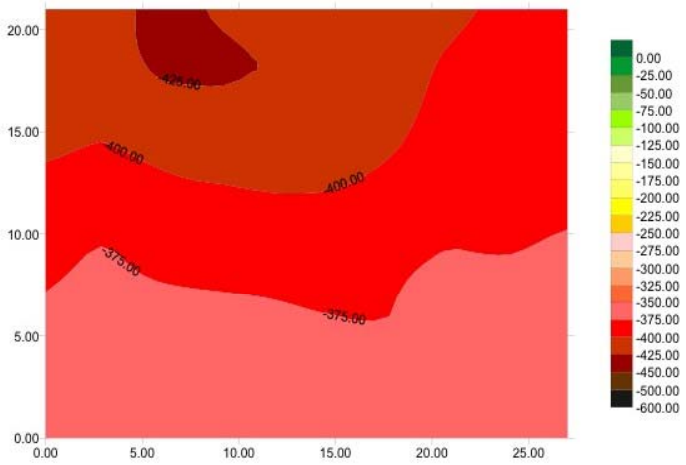

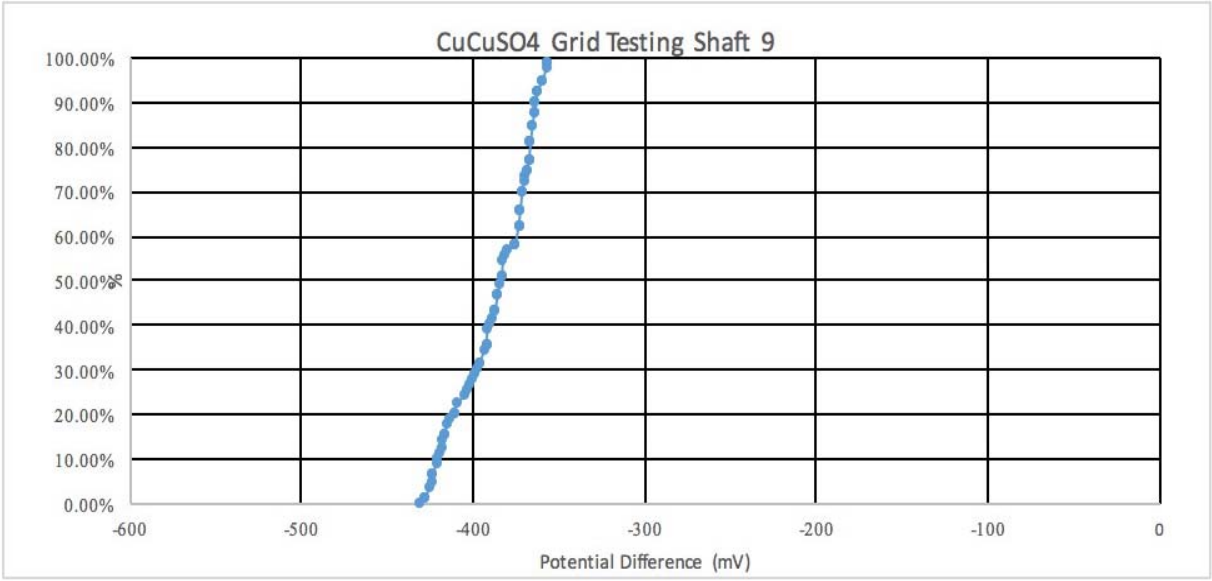

Figure C.9 Shaft 9

Summary Shaft #11	
Mix	4KDS
Slurry	P60
Avg. Pull out Strength	32.338 kips
E_{so}	-285 mV

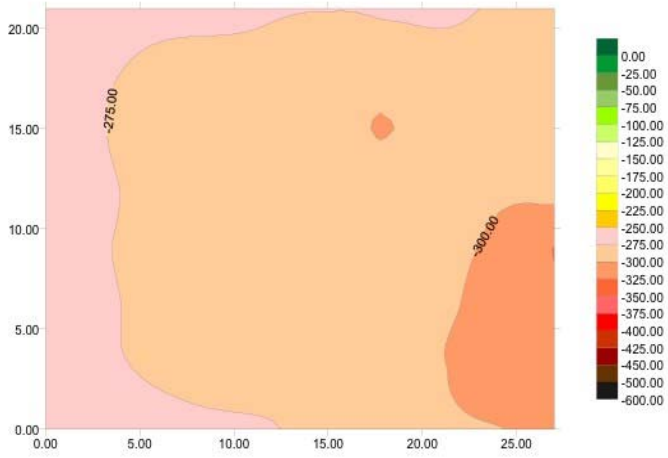

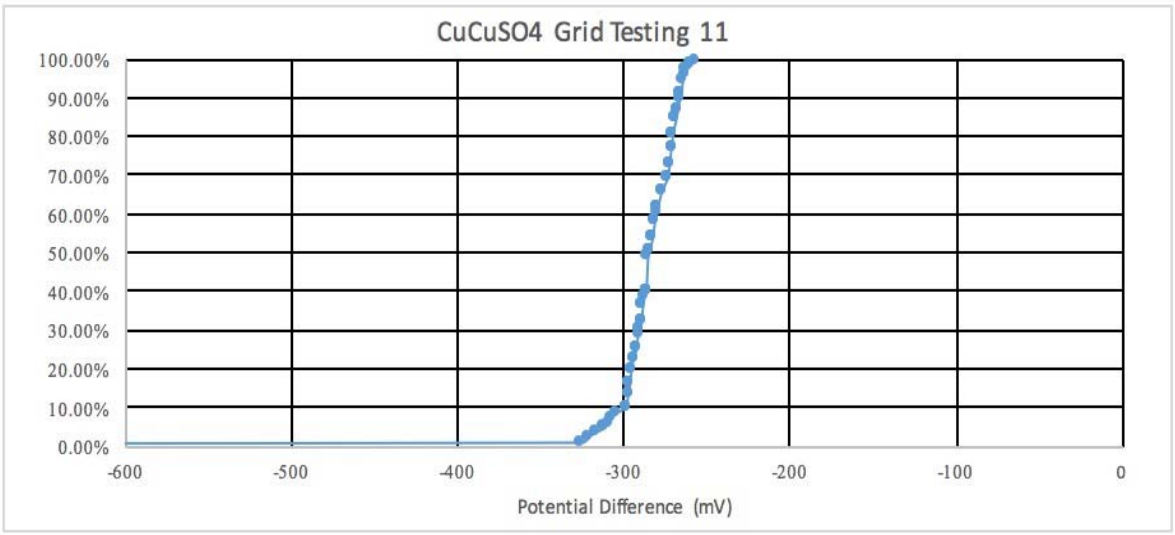

Figure C.10 Shaft 11

Summary Shaft #12	
Mix	4KDS
Slurry	P60
Avg. Pull out Strength	33.941 kips
E_{50}	-190 mV

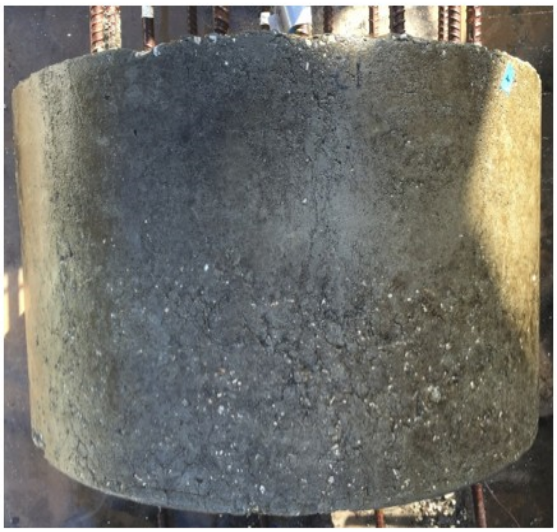

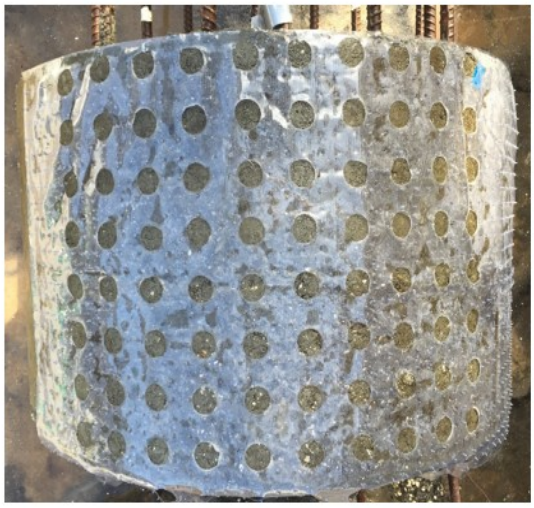

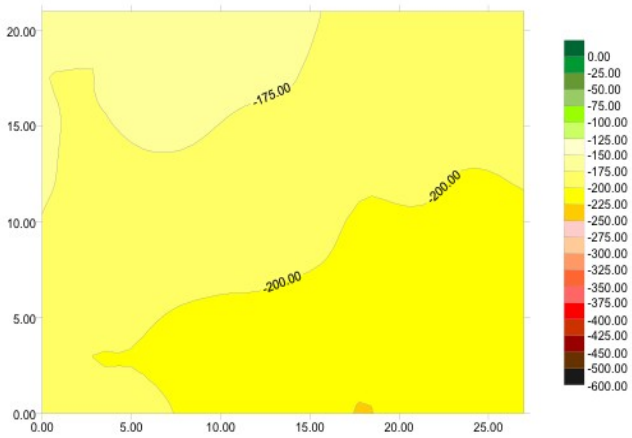

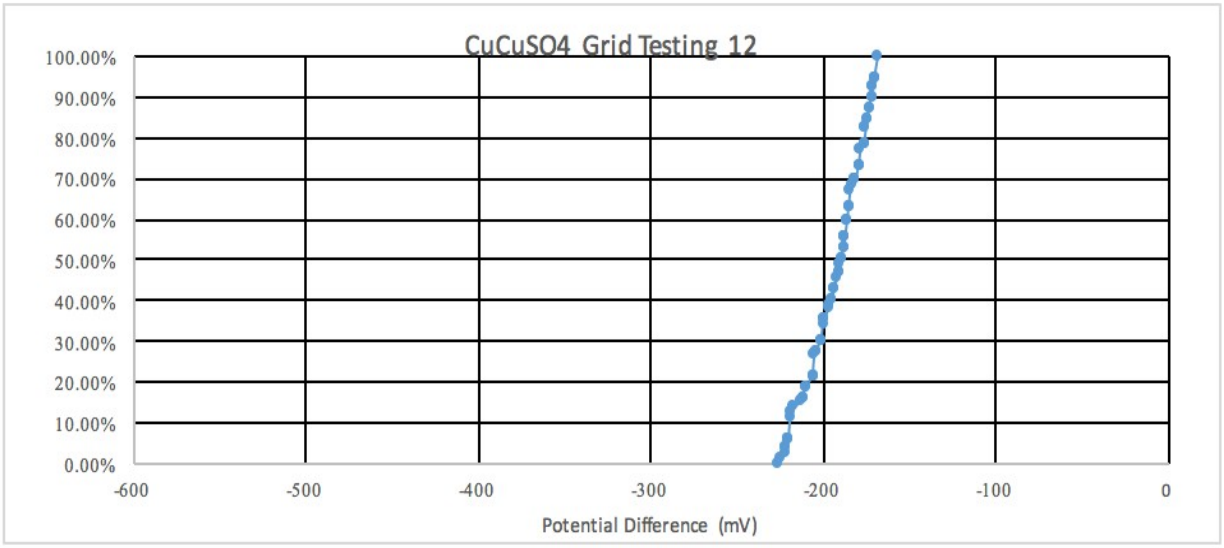

Figure C.11 Shaft 12

Summary Shaft #13	
Mix	4KDS
Slurry	B30
Avg. Pull out Strength	25.636 kips
E_{50}	-289 mV

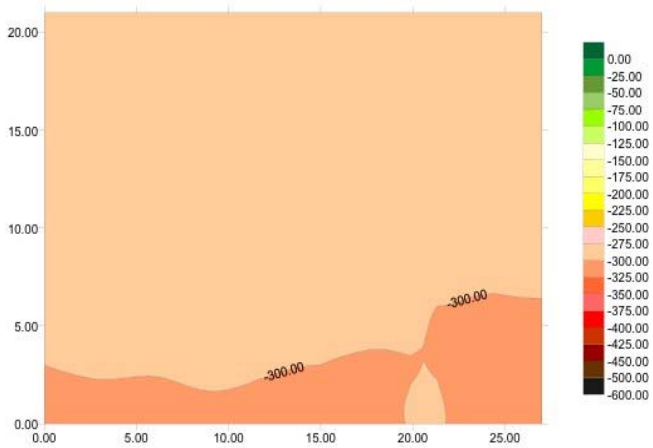

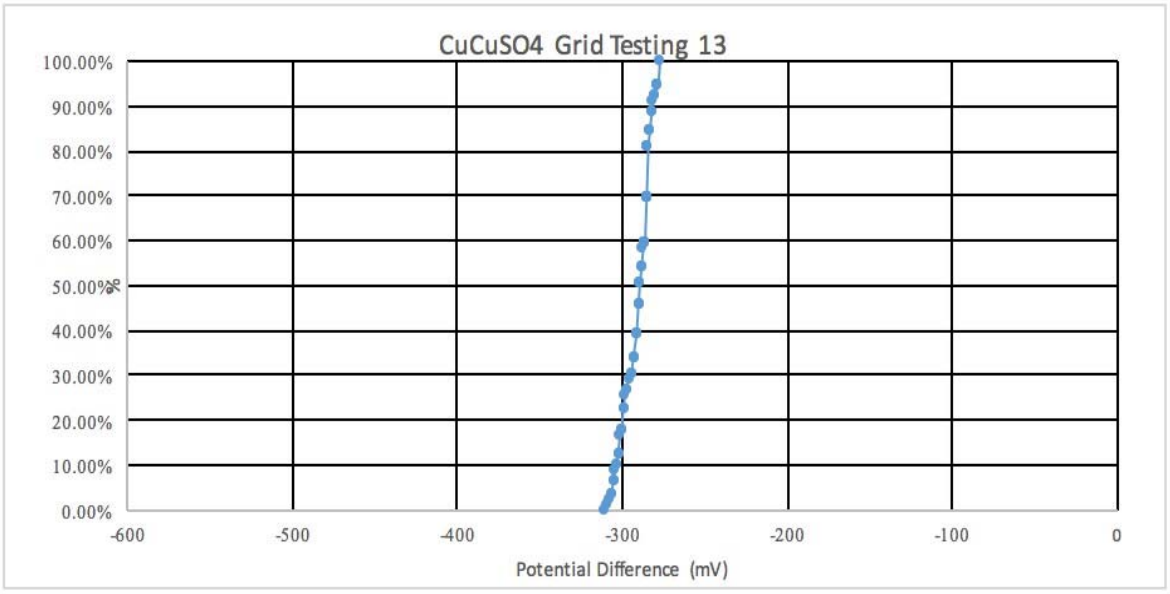

Figure C.12 Shaft 13

Summary Shaft #14	
Mix	4KDS
Slurry	B30
Avg. Pull out Strength	27.641 kips
E_{50}	-282 mV

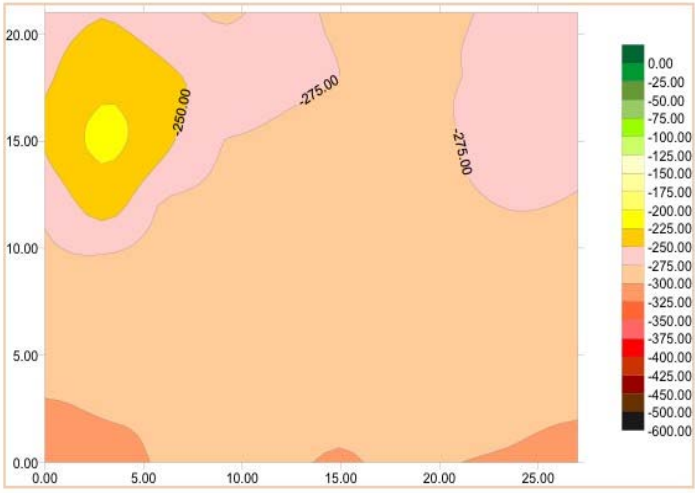

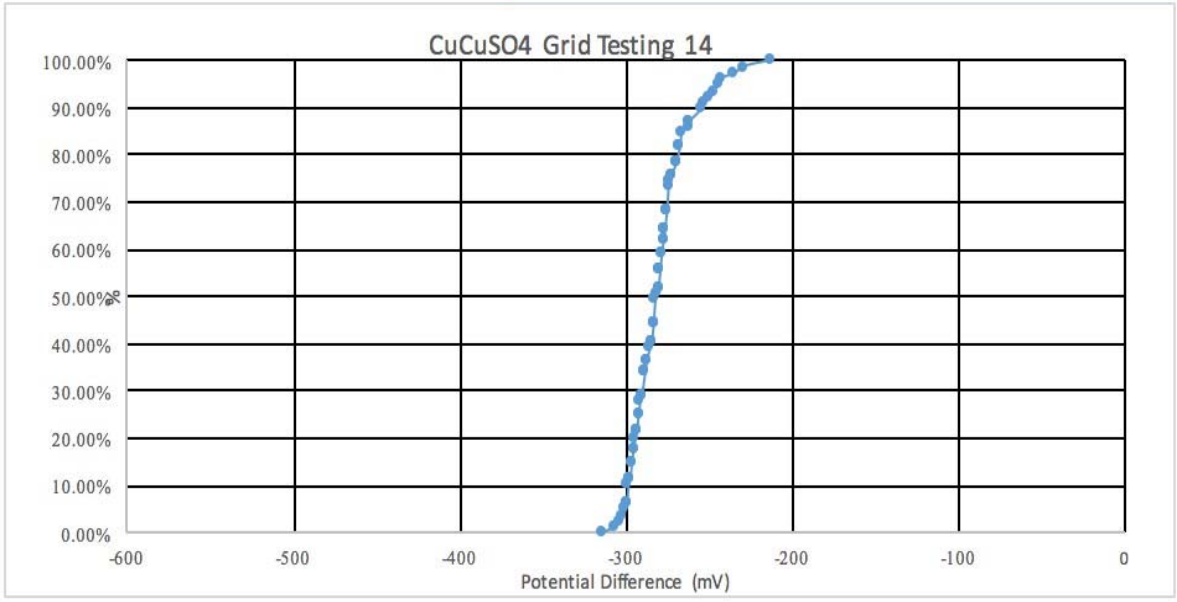

Figure C.13 Shaft 14

Summary Shaft #15	
Mix	4KDS
Slurry	B50
Avg. Pull out Strength	19.804 kips
E_{50}	-335 mV

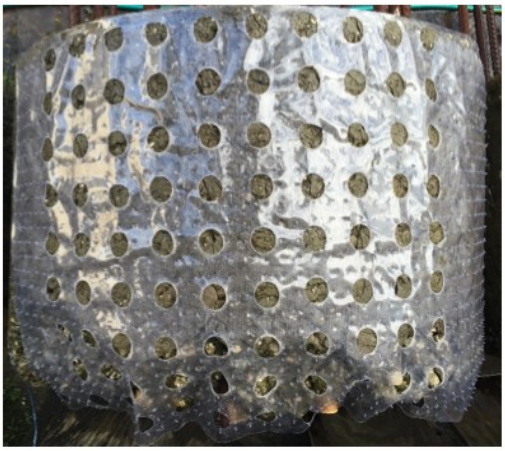

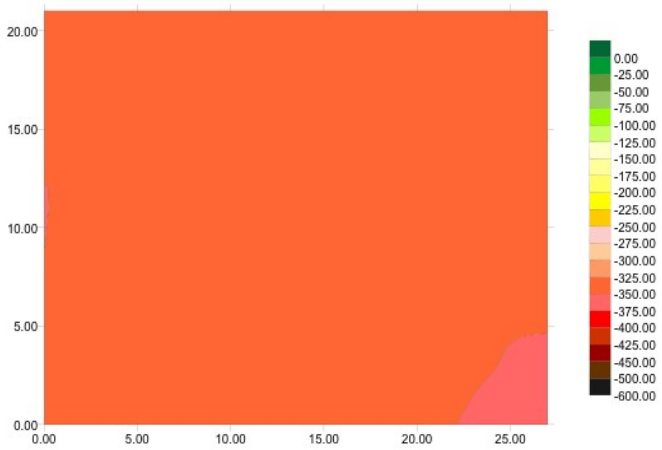

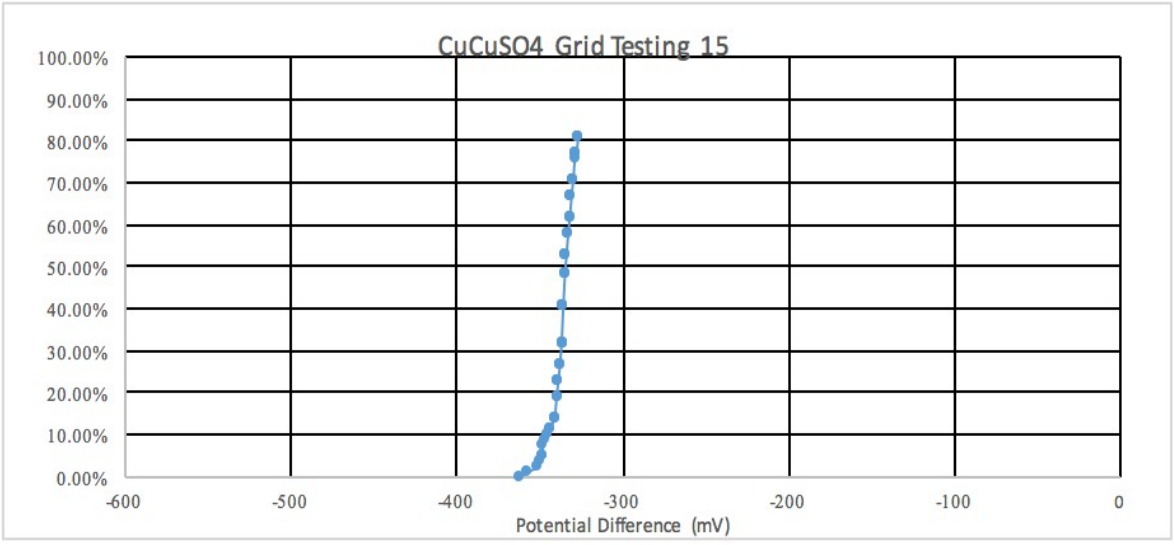

Figure C.14 Shaft 15

Summary Shaft #16	
Mix	4KDS
Slurry	P85
Avg. Pull out Strength	24.077 kips
E_{50}	-279 mV

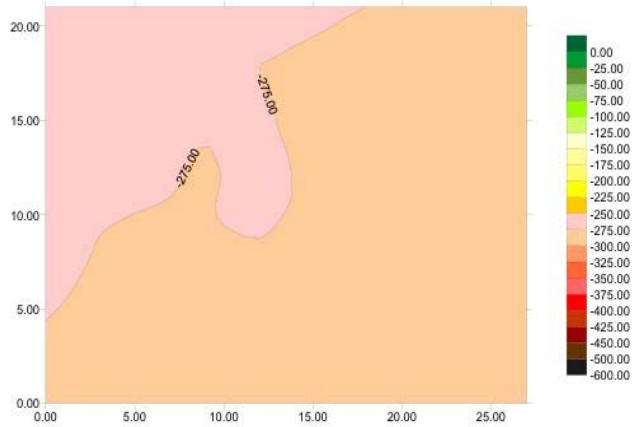

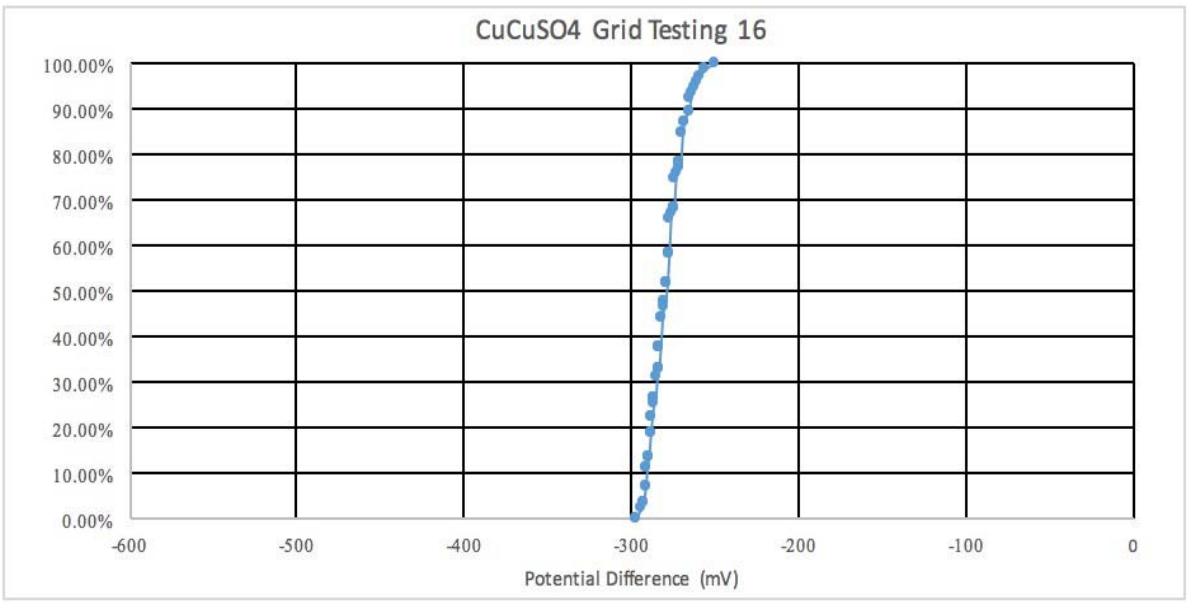

Figure C.15 Shaft 16

Summary Shaft #17	
Mix	4KDS
Slurry	P85
Avg. Pull out Strength	26.247 kips
E_{50}	-279 mV

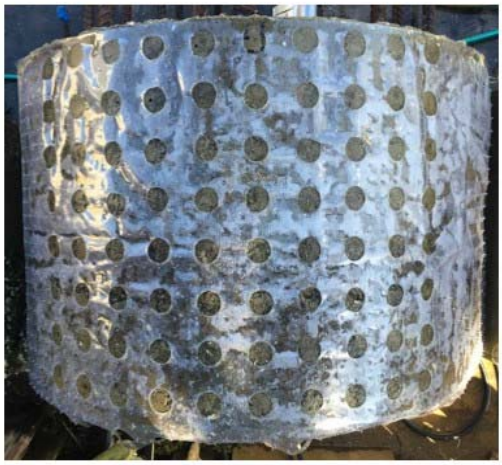

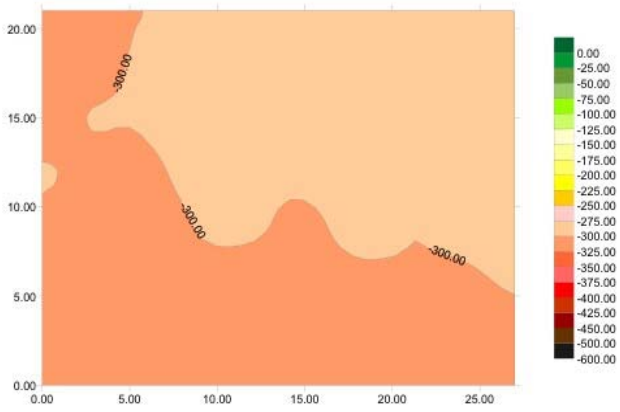

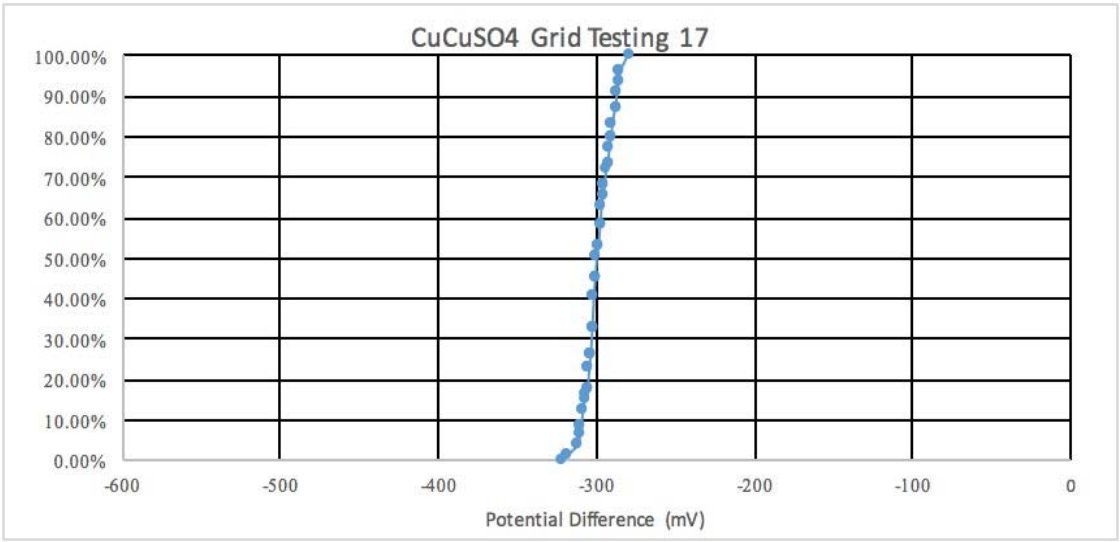

Figure C.16 Shaft 17

Summary Shaft #18	
Mix	4KDS
Slurry	H2O
Avg. Pull out Strength	34.042 kips
E_{50}	-293 mV

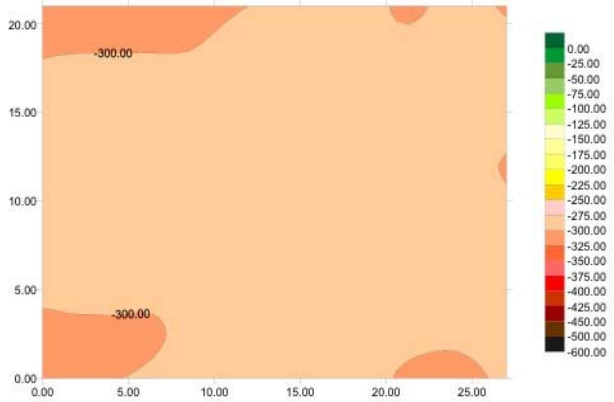

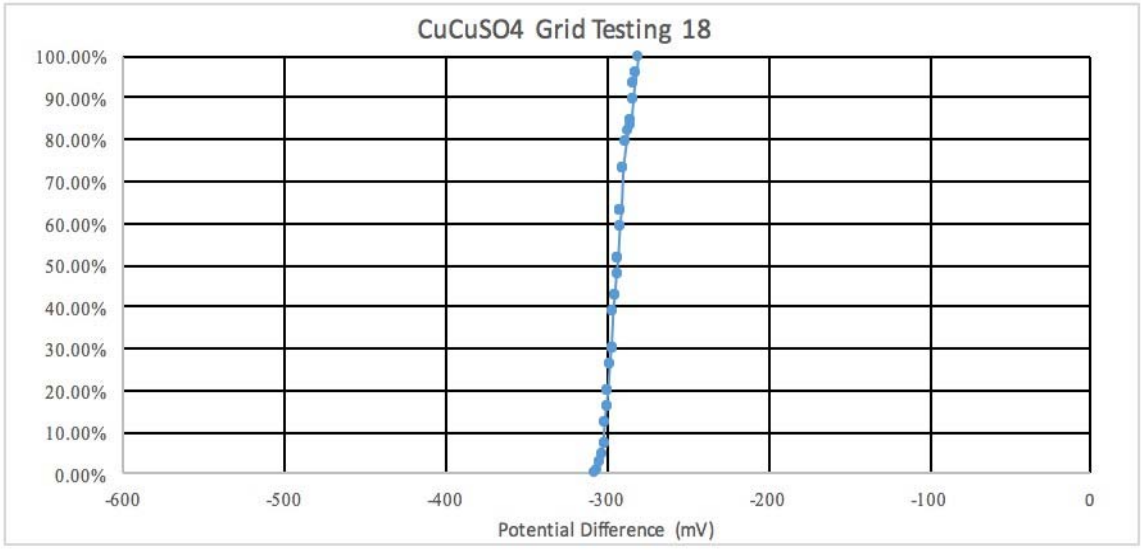

Figure C.17 Shaft 18

Summary Shaft #19	
Mix	4KDS
Slurry	P60
Avg. Pull out Strength	20.9 kips
E_{so}	-243 mV

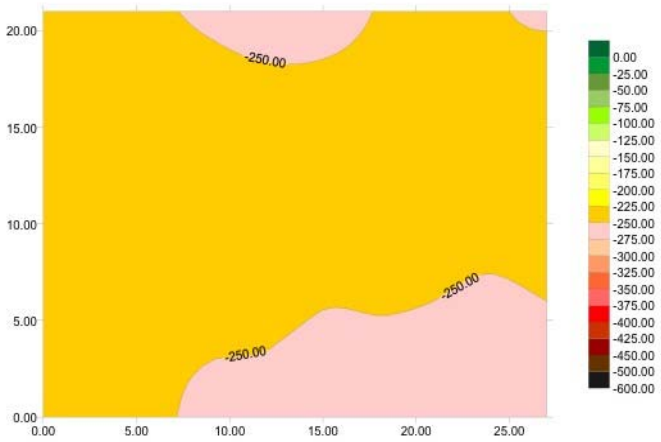

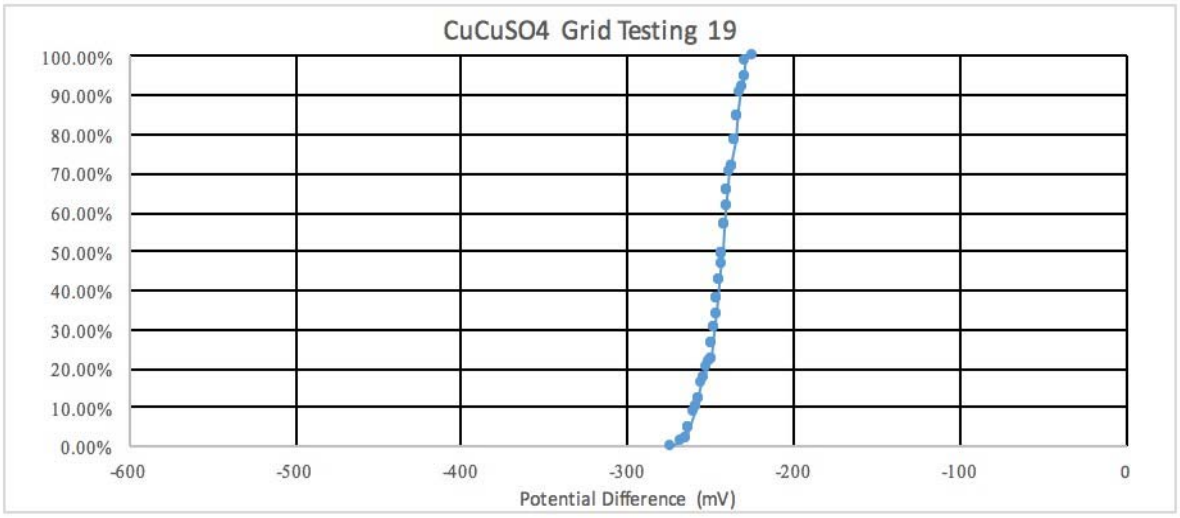

Figure C.18 Shaft 19

Summary Shaft #20	
Mix	4KDS
Slurry	P130
Avg. Pull out Strength	19.3 kips
E_{50}	-242 mV

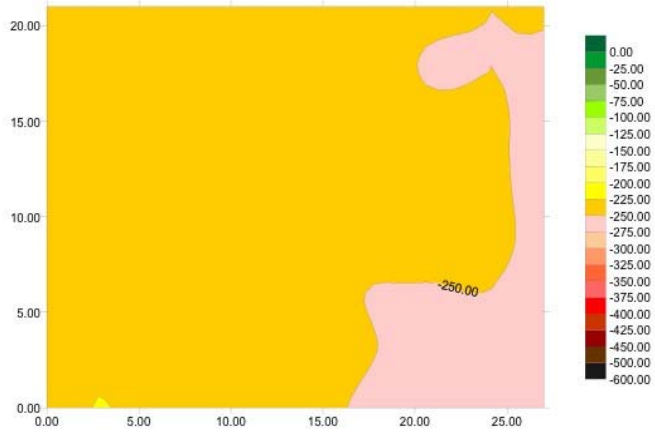

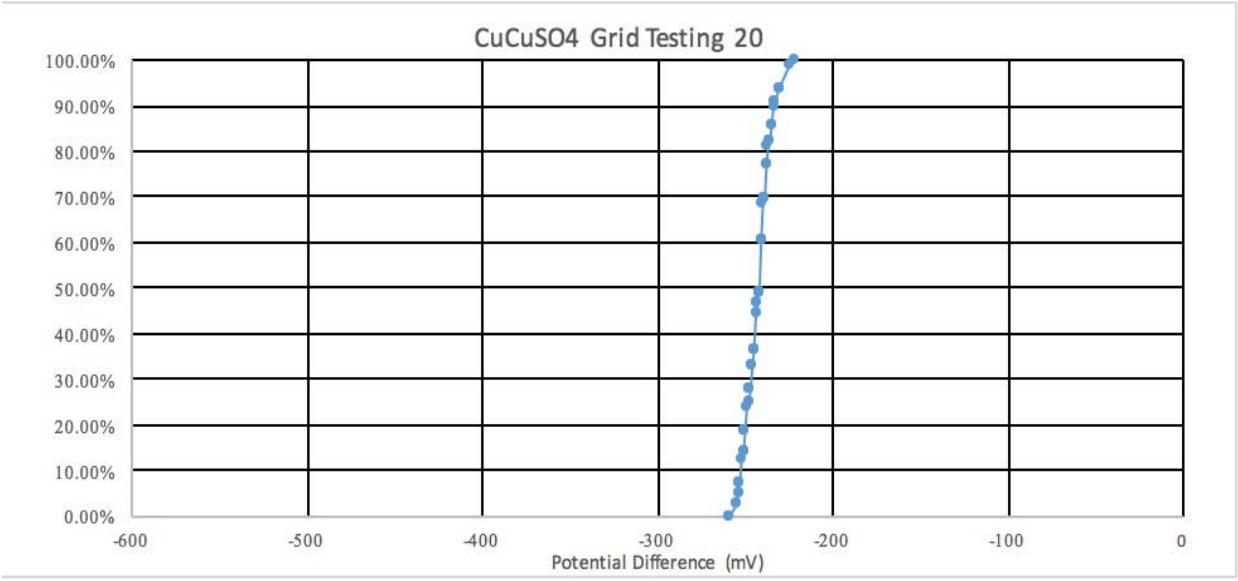

Figure C.19 Shaft 20

Summary Shaft #21	
Mix	4KDS
Slurry	B40
Avg. Pull out Strength	20.7 kips
E_{50}	-508 mV

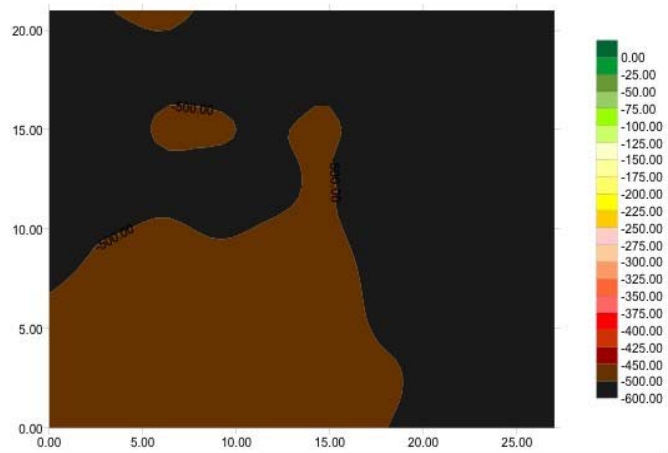

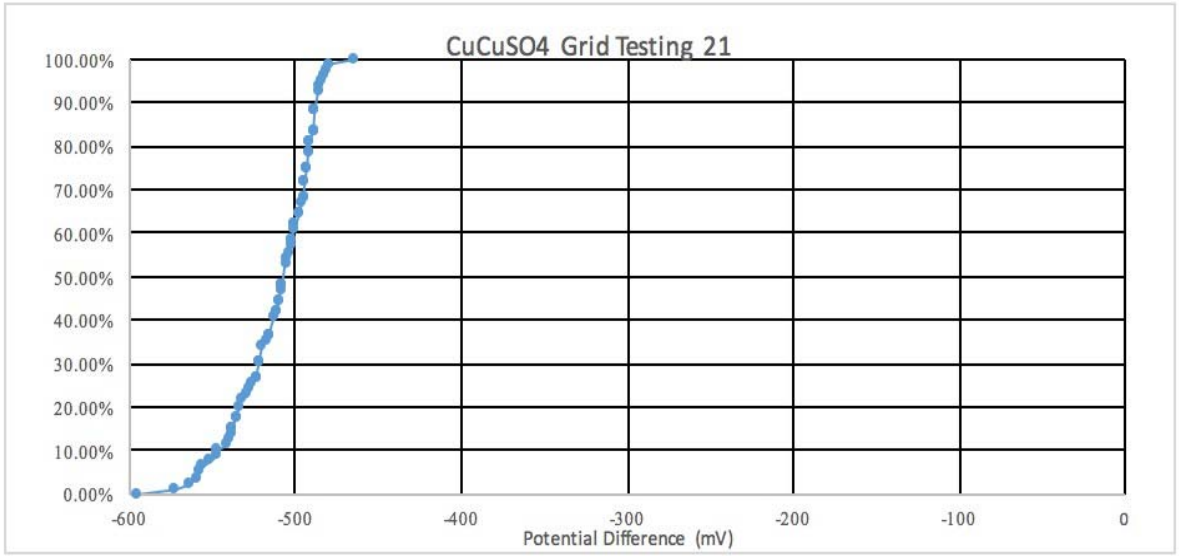

Figure C.20 Shaft 21

Summary Shaft #22	
Mix	4KDS
Slurry	H2O
Avg. Pull out Strength	26.5 kips
E_{50}	-250 mV

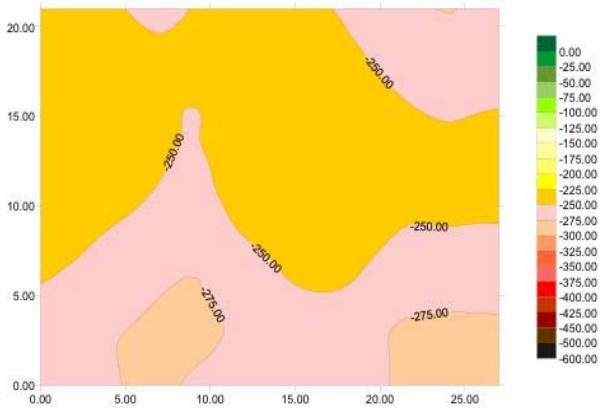

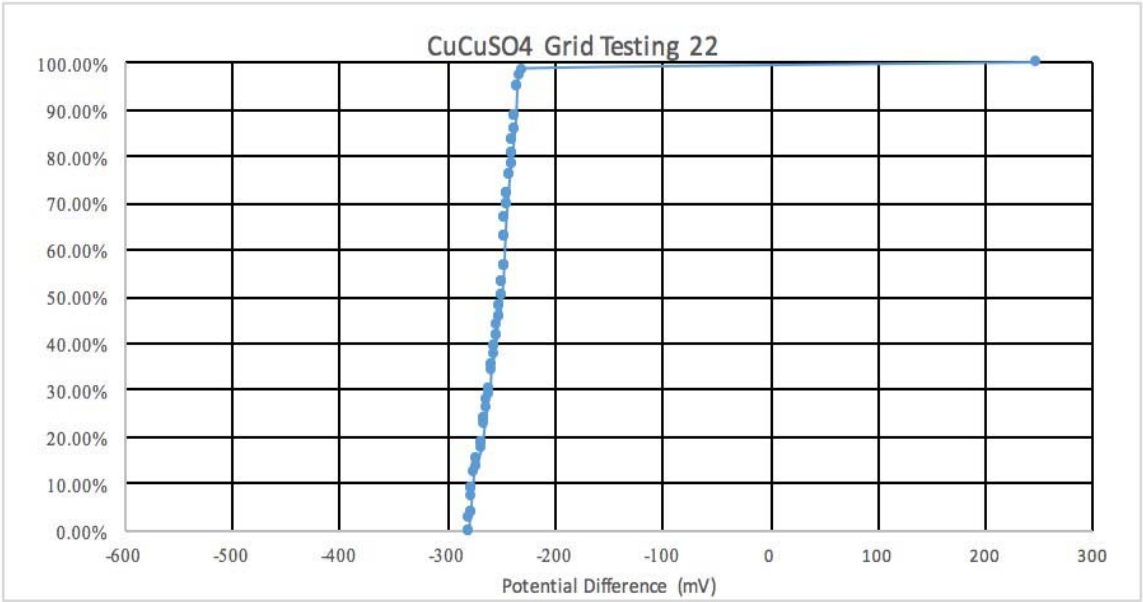

Figure C.21 Shaft 22

Summary Shaft #23	
Mix	SCC
Slurry	H2O
Avg. Pull out Strength	
E_{so}	-258mV

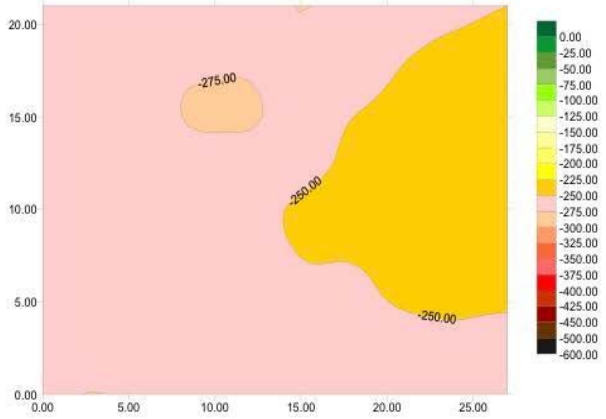

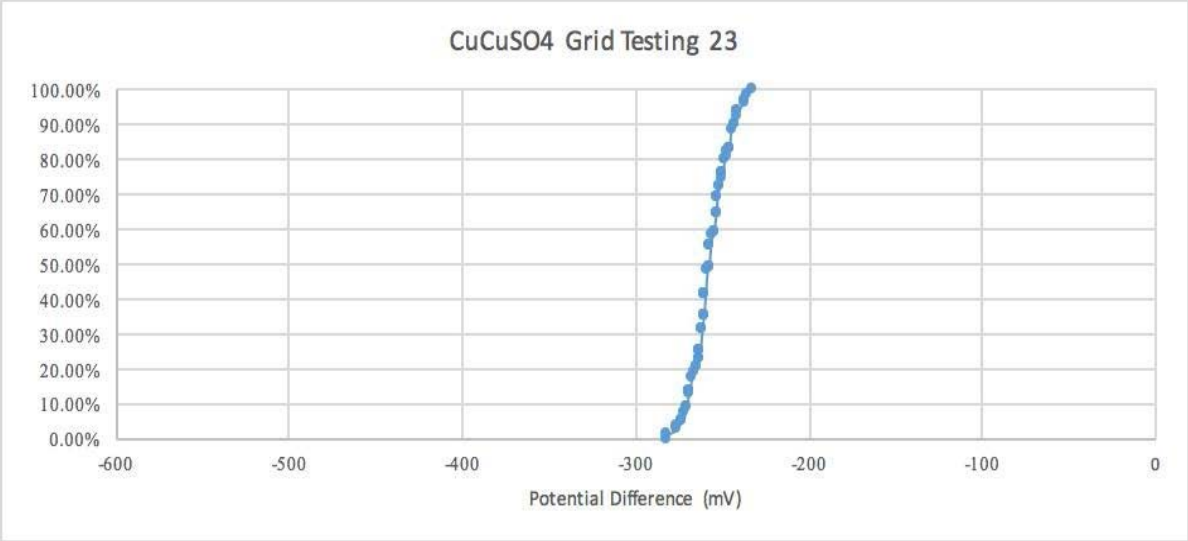

Figure C.22 Shaft 23

Summary Shaft #24	
Mix	SCC
Slurry	B40
Avg. Pull out Strength	
E_{50}	-425 mV

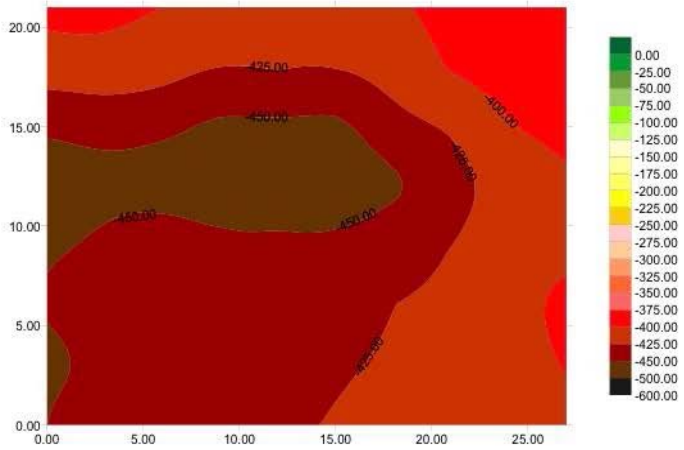

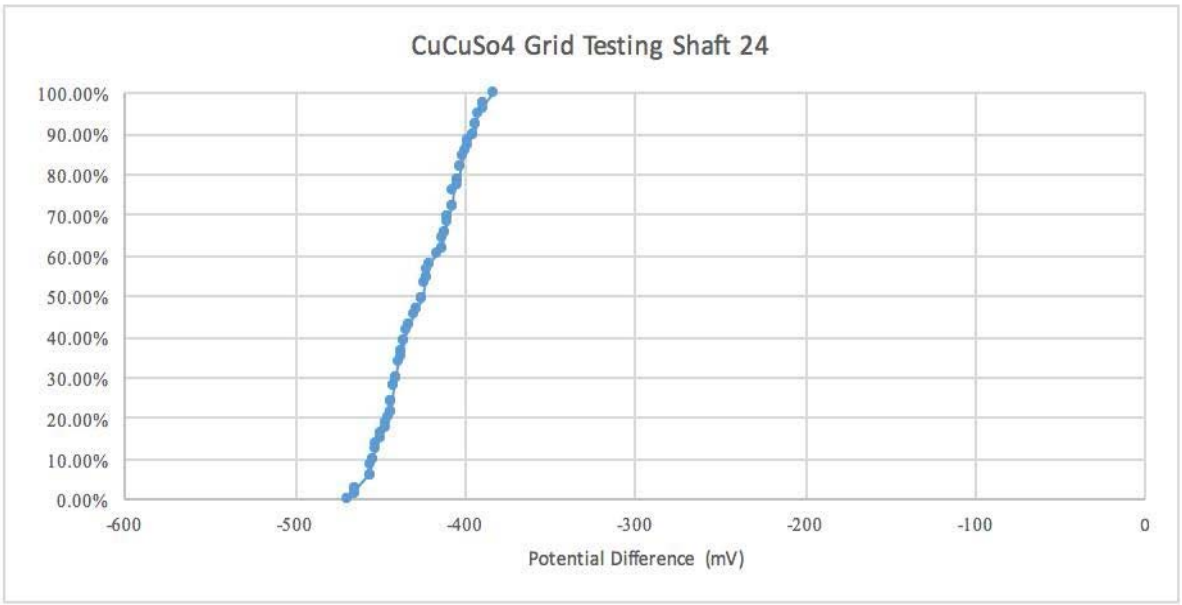

Figure C.23 Shaft 24